63-4-5

(5) 188 400

(1)

THE UNIVERSITY OF CHICAGO

DEPARTMENT OF METEOROLOGY

Scroll 3

(1) (7-5 NP

DESIGN OF A THREE-DIMENSIONAL MESO-METEOROLOGICAL NETWORK

(9)

Fourth Quarterly Technical Report (1 Apr)

1 January 1960 to 30 April 1960.

(14) NP
19-17
(20) 1

(1) IV
(13 NP

Sponsored by

U. S. Army Signal Engineering Laboratories
Fort Monmouth, New Jersey

(1)

Signal Corps Contract Nr. DA-36-039 SC-78901
Department of the Army Project Nr. 3A99-07-001-04-01

(11)

$6.60

(5) 155 400

DESIGN OF A THREE-DIMENSIONAL MESO-METEOROLOGICAL NETWORK

Fourth Quarterly Technical Report
1 January 1960 to 30 April 1960

To make a study and investigation into the capabilities of pre-existing and existing meso-meteorological networks and systems; to make analyses of these network data obtained; to revise and improve conventional meso-analysis techniques; and, based upon the data obtained, to submit a proposed design for a network system(s) best suited for the solution of three-dimensional meso-meteorological problems.

Signal Corps Contract Nr. DA-36-039 SC-78901
Department of the Army Project Nr. 3A99-07-001-04-01

(10) Prepared by

Tetsuya Fujita
Henry A. Brown

TABLE OF CONTENTS

PURPOSE

To study the capabilities of existing and pre-existing networks for serving as frameworks for mesometeorological studies, and to design a network best suited for the solution of mesometeorological problems involving three-dimensional space and time. In order to accomplish this task, research will be performed in two phases.

Phase 1. Networks will be examined through data and through prior investigations on the basis of their adequacy to resolve mesometeorological phenomena. At the same time, revisions and improvements of analytical techniques will be made.

Phase 2. The network design will be based on the network size, station spacing, and the instrumentation necessary to contain, resolve, and record mesometeorological systems or processes in three-dimensional space and time and over various terrains.

ACKNOWLEDGEMENTS

The authors of this report would like to extend their appreciation to the many agencies who supplied data for this research, to the many individuals with whom the authors had long and stimulating discussions, and in particular to the U. S. Army Signal Research and Development Laboratory for the sponsorship of the research and to Dr. D. M. Swingle, Dr. R. Schrott, and Prof. H. R. Byers for their encouragement and support.

The networks which supplied the fundamental data and the agencies who maintain them are:

New Jersey Microbarograph Network
U. S. Army Signal Research and Development Laboratory

Fort Huachuca (Arizona) Network
U. S. Army Electronic Proving Ground

Dugway (Utah) Automatic Network
U. S. Army Chemical Corps

Severe Local Storms Network (Texas-Oklahoma)
U. S. Weather Bureau

Montana Skyfire Network
U. S. Forest Service, Munitalp Foundation

Ohio Thunderstorm Network
U. S. Weather Bureau, U. S. Air Force, National Advisory Committee for Aeronautics, U. S. Navy

Muskingum (Ohio) Network
U. S. Soil Conservation Service

Lindenberg (Germany) Network
(under Dr. Koschmieder)

Japanese Thunderstorm Network
Japan Meteorological Agency

In addition to the networks, the progress of the design was greatly assisted by data acquired from groups who took observations of a specialized nature:

Illinois State Water Survey
Radar

A. & M. College of Texas
Radar

Geophysical Research Directorate and National Hurricane Research Project
Aircraft

Arthur D. Little, Inc.
Constant level balloon

The following should be commended for their time and efforts, which produced most valuable discussions on the variety of topics considered:

Dr. P. M. Austin and Mr. S. G. Bigler in the field of radar and east-coast mesometeorology.

Prof. J. Bjerknes on the basic problems of mesometeorology and mesoanalysis.

Dr. W. H. Clayton in the instrumentation required for a network.

Dr. Y. Sasaki for discussions in the relatively new field of numerical analysis and forecasting in mesometeorology.

Dr. V. J. Schaefer for advice in network installation in mountainous areas.

Dr. R. Stinson for new methods of analysis of the tropopause and severe storms.

ABSTRACT

Results of analyses of case studies of numerous networks in various locations are combined in a discussion of the observations necessary for the operation of a three-dimensional mesometeorological network. Four observational categories are considered: (1) surface, (2) upper air, (3) radar, and (4) photography. Each category is discussed in terms of the elements measured, optimum time and space resolution, accuracy required, and techniques for analysis.

A model network design incorporating the above results is then proposed. This is followed by a proposed practical design for three different areas in the United States characterized by coastal, plains, and mountainous environments.

PUBLICATIONS

1. Brown, H. A., 1960: Report on radar thin lines. Paper presented at the Eighth Weather Radar Conference, San Francisco, April 11-14, 1960. To be published in the Proceedings of the Conference.

2. Fujita, T., 1960: Mesometeorological study of pressure and wind fields beneath isolated radar echoes. Paper presented at the Eighth Weather Radar Conference, San Francisco, April 11-14, 1960. To be published in the Proceedings of the Conference.

LECTURES AND REPORTS

None

CONFERENCES

The following consultants met with project personnel in Chicago during the quarter:

Prof. J. Bjerknes of UCLA on January 17-18, 1960. Basic problems of mesometeorology and mesoanalysis.

Dr. P. Austin of MIT on February 2-3, 5, 1960. Radar and east-coast mesometeorology.

Dr. W. H. Clayton of Texas A. & M. on February 15-16, 1960. Network instrumentation.

Dr. V. J. Schaefer on February 23-25, 1960. Network installation in mountainous areas.

Dr. J. R. Stinson of St. Louis University on April 22-24, 1960. New methods of analysis of the tropopause and severe storms.

I. INTRODUCTION

Realizing that local weather changes are, to a large extent, produced by moving and continually changing weather systems whose linear dimensions range from a few miles to hundreds of miles (mesoscale) and which are in turn related to even to even larger scale features (i.e., fronts, cyclones, upper waves in the westerlies, etc.), it first behooves the meteorologist to strive for an understanding of the nature of the system, its origin, causes, life cycle, three-dimensional structure, and energy sources and sinks. Knowing local weather changes and the influence they have on army field operations, it then behooves the meteorologist to arrive at an understanding of the predictability of the system--of its origin, path, intensity variations, and of its effects on the surface.

Knowledge of mesosystems has been advanced through the establishment of special networks and by careful analysis of the data collected. The Thunderstorm Project networks in Florida and Ohio, in some respects the best of these networks, were sufficiently complete in time and three-dimensional space only over small areas for relatively short periods of time. Although designed for the study of individual thunderstorms, they still provide the most complete sets of data available for the study of mesosystems.

The present study was initiated to design a network specifically for the study of mesoscale systems in time and space. The design has been based on the results of previous network studies and on the analysis during the contract year of selected cases from eight different networks which are or have been in operation over various parts of the United States, Japan, and Germany. Included were:

New Jersey Microbarograph Network
Fort Huachuca (Arizona) Network
Dugway (Utah) Network
Texas-Oklahoma Severe Local Storms Research Network

Montana Skyfire Network
Ohio Thunderstorm Network
Muskingum (Ohio) Network
Lindenberg (Germany) Network
Japanese Thunderstorm Network

It should be emphasized that none of these networks had been designed with the above purpose in mind, but nevertheless the knowledge gained from them gave valuable support to the final network design in the following manner:

1. The areas covered by the networks and their capacity for containing a mesosystem at a given time pointed to the necessary areal coverage.
2. Their instrumentation indicated the types and response times of instruments needed.
3. The spacing of their instruments led to the selection of the optimum distances between stations.
4. The frequency of observations showed the time intervals required for the proper delineation of mesoscale features.

At the same time, analyses of the data obtained from the networks added to previous knowledge of the structure of mesosystems and suggested methods of revising and improving analytical techniques. The rate of change of mesoscale weather patterns and the scales and intensities of various mesosystems were also obtained.

II. OBSERVATIONS AND ANALYSIS TECHNIQUES

A. SURFACE

When we look back over the earlier history of modern synoptic charts, we see that the well-known Norwegian charts of the 1920's were carefully analysed surface charts. These charts were continuously improved in later years by adding upper-air observations, leading to the famous concepts of air masses and fronts.

Similar steps are now being followed by those who study three-dimensional mesometeorology. Their investigations begin and develop by understanding in full what is recorded and observed on the surface of the earth.

1. METHODS OF REPRESENTING ATMOSPHERIC MOTION

A synoptic chart can be constructed to represent motion of the atmosphere expressed by either the Eulerian or Lagragian equations of motion. In regular synoptic charts or macroscale charts it is more convenient to analyse weather in accordance with the Eulerian representation, in which motion of the atmosphere is entirely determined by knowing the weather elements at a fixed station. The charts are, therefore, fully examined by plotting station data at certain time intervals, thus representing the complete field of motion and its change with time.

In constructing a mesoscale chart, particularly where station density is low but where data are available as functions of time, Lagrange's method also becomes useful for expressing atmospheric motion. Individual disturbances, which usually are not identifiable in macroscale charts, are important in mesoscale analysis and can be followed for hours in mesoscale charts. These individual disturbances or active portions of the atmosphere may be termed, for instance, A, B, C,...s, and their motion expressed by

$$r = f(i, t) \qquad \text{II.A.1}$$

where r is the position vector of an individual disturbance of the atmosphere (a small portion of fluid in Lagrangian expression). The individual velocity of disturbances is, therefore, obtained by differentiating their position vectors by

$$v = \left(\frac{\partial r}{\partial t}\right)_i \qquad \text{II. A. 2}$$

Figure II. A. 1 is prepared to show how a Lagrangian mesoscale chart can be plotted. First, the surface stations in the area affected by an individual disturbance, i, are numbered 1, 2, 3,...n, the position vectors of which are r_1, r_2, r_3,...r_n, etc. Based upon the Eulerian concept, the field of motion at time t is described by plotting the meteorological elements at each station. After the passage of time Δt, the field is again represented by plotting a group of data observed at $t = t + \Delta t$.

The Lagrangian approach permits us to follow individual disturbances from time t to $t + \Delta t$. If Δt is assumed to be so short that the disturbances and their accompanying field remain unchanged, two charts for t and $t + \Delta t$ can be combined by superimposing them in such a position that A and B in Fig. II. A. 1 coincide. The position vector of stations on the chart at t after superposition becomes

$$\Delta r_{n-i}(t + \Delta t) \qquad \text{II. A. 3}$$

where $\Delta r_{n-i}(t + \Delta t)$ is the vector connecting station n with the disturbance at $t + \Delta t$. The equation, then, can be transcribed as

$$r_n(t + \Delta t) = r_i(t + \Delta t) + [r_n - \{r_i(t) + \left(\frac{\partial r}{\partial t}\right)_i \Delta t\}]$$

$$= r_n - \left(\frac{\partial r}{\partial t}\right)_i \Delta t$$

or $$= r_n - v_i \Delta t \qquad \text{II. A. 4}$$

This equation shows that a Lagrangian mesoscale surface chart may contain station data observed at both time t and between t - Δt and t + Δt (if time Δt is short enough to assume that disturbances affecting the station remain unchanged). An example of data plotting is shown in Fig. II.A.2.

2. CONVERSION OF TIME SECTIONS INTO SPACE SECTIONS

As seen in the previous discussion, a Lagrangian mesoscale synoptic chart includes not only station data observed at the map time but also their time change. Time-section charts, either recorded or plotted ones, are converted into a space section simply by changing the time scale into a proper space scale. This conversion technique, described and developed by Fujita, appears in his articles (1; 2; 3).

3. PRINCIPLE AND TECHNIQUE OF MEAN-VALUE ADJUSTMENT

Absolute measurements are always more difficult and expensive than relative measurements. An aneroid barometer may indicate change in pressure from 1010.1 to 1012.2; however, this does not always mean that these barometer readings have a 0.1 mb absolute accuracy. Absolute accuracy is required whenever the readings of two or more instruments are compared. So long as we take differences in readings of a single instrument, the difference 1012.2-1010.1 = 2.1 mb will have 0.1 mb relative accuracy.

In analysing network data, it always becomes necessary to compare meteorological data measured by different instruments at different stations. This necessitates high accuracy in absolute measurement.

Techniques were developed by Fujita, Brown, and their associates for attempting analysis of high absolute accuracy by using data of only relative accuracy.

Mean-Value Adjustment

Change in a meteorological element at a single station is expressed by a

sine series,

$$A = f(t) = A_0 + A_1 \cos \omega t + B_1 \sin \omega t + A_2 \cos 2\omega t + B_2 \sin 2\omega t + \cdots$$

$$= A_0 + \sum_{n=1}^{a} (A_n \cos n\omega t + B_n \sin n\omega t) + \sum_{n=a}^{b} (A_n \cos n\omega t + B_n \sin n\omega t) + \sum_{b}^{\infty} (A_n \cos n\omega t + B_n \sin n\omega t)$$

(MACRO) (MESO) (MICRO) II.A.5

where a and b represent the limits of frequency of mesoscale disturbances affecting the station under consideration. Taking the mean value of A between time t_1 and t_2, we have

$$\overline{A} = A_0 + \frac{1}{t_2 - t_1} \int_{t_1}^{t_2} \sum_{1}^{a} (A_n \cos n\omega t + B_n \sin n\omega t)\, dt \quad \text{(MACRO)}$$

$$+ \frac{1}{t_2 - t_1} \int_{t_1}^{t_2} \sum_{a}^{b} (A_n \cos n\omega t + B_n \sin n\omega t)\, dt \quad \text{(MESO)}$$

$$+ \frac{1}{t_2 - t_1} \int_{t_1}^{t_2} \sum_{b}^{\infty} (A_n \cos n\omega t + B_n \sin n\omega t)\, dt \quad \text{(MICRO)} \qquad \text{II.A.6}$$

By increasing $t_2 - t_1$, the averaging period, all three terms will decrease; however, by selecting a proper averaging period it is feasible to minimize the last two terms on the right side of the equation. The mean value is thus reduced approximately to

$$\overline{A} \doteq A_0 + \frac{1}{\Delta t} \int_{t}^{t+\Delta t} \sum_{1}^{a} (A_n \cos n\omega t\, dt + B_n \sin n\omega t\, dt) \qquad \text{II.A.7}$$

where Δt is the averaging period.

For Lagrangian mesoanalysis, Δt can be chosen to be between 12 and 36 hours so that none of the micro and few of the mesoscale disturbances contribute to the mean value.

Figure II.A.3 represents an example of mean wind and pressure values from hourly-reporting stations for which high absolute accuracy in pressure (0.1 mb) and wind are expected.

Let us assume that the box in the figure indicates a mesometeorological network with stations indicated by dots. It is now possible to read off the mean pressures at each network station. The absolute accuracy of these mean values would be as high as 0.1 mb. Using this result, pressures at network stations i, j, k, ... are expressed as

$$P_i = \overline{P}_i + \sum_{n=1}^{b} (P_{in}\cos n\omega t + P_{in}\sin n\omega t) + \sum_{n=b}^{\infty} (P_{in}\cos n\omega t + P_{in}\sin n\omega t) = f_i(t)$$

$$P_j = \overline{P}_j + \sum_{n=1}^{b} (P_{jn}\cos n\omega t + P_{jn}\sin n\omega t) + \sum_{n=b}^{\infty} (P_{jn}\cos n\omega t + P_{jn}\sin n\omega t) = f_j(t)$$

$$P_k = \overline{P}_k + \sum_{n=1}^{b} (P_{kn}\cos n\omega t + P_{kn}\sin n\omega t) + \sum_{n=b}^{\infty} (P_{kn}\cos n\omega t + P_{kn}\sin n\omega t) = f_k(t)$$

II.A.8

where $\overline{P}_i$, $\overline{P}_j$, $\overline{P}_k$, ... are mean pressures at stations i, j, k, ...

It is evident that all terms in equation II.A.8 possess accuracy high enough to obtain a satisfactory absolute accuracy of P_i, P_j, P_k, ..., the time variations of pressures which are used in mesoanalysis. With this technique we can use relatively low-cost instruments with high relative accuracy as if they had high absolute accuracy.

4. RELATIVE ACCURACY AND FREQUENCY OF METEOROLOGICAL DATA COLLECTION

It is extremely important to determine how much more frequently meteorological data should be collected in order to perform mesometeorological analysis

for research purposes than for operational purposes alone.

Pressure

Atmospheric pressure obtained by either a mercury or an aneroid barometer is one of the most important elements analysed in mesoscale charts. Figure II.A.4 gives an example of data collection at continuous, 2.5-minute, 5-minute, and 10-minute intervals. A similar example is presented by Stout, et. al. (4) in a final report to the Signal Corps. It is, of course, desirable to obtain microbarograph traces from instruments with 0.1 mb accuracy and less than 10-second time constant. However, digitized data at reasonable intervals will also serve research purposes. The following table indicates the frequency and the accuracy required.

Type of Disturbance	Frequency	Relative Accuracy (mb)
Pressure Surge Line	1 min	0.05
Pressure Jump Line	1 min	0.1
Pressure Nose	30 sec	0.1
Thunderstorm High (dome)	5 min	0.1
Sea-Breeze Front	continuous	0.05 ?
Diurnal Press Variation	30 min	0.1
Tornado Cyclone	1 min	0.2
Tornado	continuous	1.0
Dust Devil	continuous	0.2
Warm & Cold Front	5 min	0.1
East-Coast Rain & Hurricane Rainband	1 min	0.05 ?
Tropical Squalls	1 min	0.05 ?
Inversion Wave	continuous	0.05
Explosion Wave	continuous	0.02

Table II.A.1. Observation frequency and accuracy required to investigate meso-meteorological pressure structure of various disturbances.

Assuming that observations at 10-minute intervals are begun at four different times (0.0, 2.5, 5.0, and 7.5 minutes after each 10-minute section), four time-sections of pressure were digitized from the continuous microbarograph trace in the previous figure. The result appears in Fig. II.A.5. It should be noted that the slope and the phase of pressure variation change due to the difference in observation times even though their interval remains the same.

Temperature and Humidity

Because of the face that air temperature and humidity (dew-point temperature, relative humidity, or absolute humidity) are less representative than atmospheric pressure, their analysis on a mesoanalysis chart should be interpreted carefully. It is sometimes extremely difficult to determine whether or not a particular temperature or humidity disturbance is accompanied by one or several mesometeorological systems.

Type of Disturbance	Frequency	Relative Accuracy Temp. ^{o}F	Relative Accuracy Dew-point Temp. ^{o}F
Pressure Jump Line	1 min	0.5	1
Humidity Dip	continuous	0.1	0.5
Warm & Cold Front	10 min	0.5	1
Sea-Breeze Front	3 min	0.5	1
Diurnal Variation	30 min	0.5	1
Tornado	continuous	0.1	1
Dust Devil	continuous	0.05	0.3
Precipitation	continuous	0.1	0.5
Advection Fog	continuous	0.05	0.1
Radiation Fog	1 min	0.5	0.3

Table II.A.2. Observation frequency and accuracy of temperature and relative humidity required for the investigation of mesometeorological systems.

Figure II.A.6 reveals a series of temperature drops accompanied by precipitation occurring in a mesoscale area. The continuous trace at the top was

digitized at 2.5, 5.0, and 10-minute intervals. These time sections of temperature indicate that less frequent observations are required for temperature than for pressure. Table II.A.2 presents frequency and accuracy of temperature and humidity measurements which are to be used for basic data in mesometeorological research.

Precipitation

Precipitation measurement in a mesoscale area is very important in connection with the meteorological interpretation of radar echoes. Our experience in mesoanalysis shows that the number of raingauges (accumulative or recording types) is more important than their individual accuracy.

Before plotting precipitation on analysis charts, the recorded amounts of precipitation are differentiated with time. The top curve in Fig. II.A.7 is an example of a precipitation rate thus obtained. Accumulative amounts of precipitation are also given for comparison. Examination of the figure leads to the conclusion that accumulative amounts are not sufficient for our mesometeorological requirements. Even 2.5 or 5.0-minute accumulative amounts do not represent true rainfall characteristics.

At the present time it is extremely difficult to interpolate the precipitation rate occuring between two recording stations. Figures II.A.8 and 9 present the case of the Illinois Tornado, when its intense associated echo did not produce the surface rainfall expected. As shown in the figures, the eastern half of the echo moved eastward over the Goose Creek raingauge network (Illinois State Water Survey). The stations, about one mile apart, did not receive rain until the western half of the echo had arrived.

The figure also indicates that precipitation stations must be dense enough to permit the analysis of surface-rainfall-rate patterns comparable to the associated radar echoes. It is also suggested that non-recording raingauges and hailgauges be distributed within the mesometeorological network.

Wind

A gust-recording type wind instrument is recommended for each surface network station. A recorded wind-speed trace would appear like the top curve in Fig. II.A.10. Our experience in mesosystem analysis shows that the one-hour distance on the recorded chart is preferably about two inches. It is not necessary to accelerate the chart in an attempt to record individual wind gusts. Any fluctuation of wind lasting over one minute would be recorded very clearly on a two-inches-per-hour chart. The dimensions of such a disturbance drifting at the rate of, for example, 30 mph, would be only 1/2 mile. Its characteristics would be different by the time it arrived at the next station.

As a basic principle it may be stated that we do not need time resolution for any systems which would be picked up by only two network stations. That is, if the system in which we are interested is very small, we should in the planning stage accelerate the recording charts and increase the number of network stations in the area of interest.

		Relative Accuracy		
Type of Disturbance	Frequency	Direction (degrees)	Speed (mph)	Component (mph)
Pressure Surge Line	continuous	5	2	3
Pressure Jump Line	2 min	10	3	5
Sea-Breeze Front	1 min	10	2	2
Diurnal Variation	30 min	5	1	1
Advection Fog	continuous	5	2	2
Dust Devil	continuous	3	2	5
Tornado	continuous	3	5	10
Tropical Squalls	1 min	5	1	2
Low-intensity Meso-systems	15 min	3	1	2

Table II.A.3. Frequency and relative accuracy of wind measurement required for mesometeorological network.

A series of 2.5- and 5.0-minute average wind speed plotting appears in the second and third wind charts, respectively. As expected from such a running mean, wind gusts are smoothed out. Meanwhile, the leading edges of the wind system become less distinct. Table II.A.3 shows the frequency and relative accuracy of wind measurement at the mesometeorological network stations.

Digitized one-minute mean wind speeds measured at 10-minute intervals are given in Fig. II.A.10. It is of interest to see that the phase of wind variation apparently shifts when the time of observation is changed, even though the observation interval remains unchanged. The use of gust-recorder type wind instruments (direction and speed) at each mesometeorological network station is thus recommended.

Other Direct Measurements

Microbarovariographs which record $\frac{P}{t}$ directly on a sheet of paper or a photographic film can be placed at a number of stations. The exposure of the pressure variograph is very critical, however, since it tends to record the suction effect of gusty wind, especially when the time constant of the instrument is very short.

Atmospheric electricity measurements within a limited area inside a mesometeorological network will be helpful in understanding the electrical structure of convective clouds and precipitation.

Related Studies

Since any major mesometeorological network will be both costly and unique, maximum advantage should be taken of the opportunity to simultaneously investigate other phenomena which may be significantly affected by the mesoscale. This would include studies of sound propagation for sound ranging and other purposes, radio-radar propagation from low frequencies through millimeter waves, ballistic meteorology, low-level winds for missiles, the deposition of radioactive fallout, the dispersal of CBR materials, etc. These and many other investigations can be greatly benefitted by mesometeorological data collected by network stations.

5. DISTRIBUTION OF SURFACE STATIONS

The next important problem is to determine the distribution of surface stations forming the mesometeorological network. The solution should depend on the types of mesometeorological systems to be investigated.

Table II. A. 4 summarizes the dimensions of meteorological systems to be investigated by mesometeorological analysis. The table is based upon the knowledge accumulated during and prior to the research carried out under the present contract and is subject to revision as our knowledge increases. Nevertheless, it seems reasonable to design a network consisting of three different station densities.

Network

This network consists of surface meteorological stations separated by about five miles. It will be seen in Table II. A. 4 that such a station density is suitable for investigating various individual systems which may be called small mesoscale disturbances. The horizontal extent of these systems in their post-mature stage is 30 to 100 miles, so that the proposed network must cover an area at least 30 miles square. Taking into consideration the uncertain location of systems with respect to the network, it is strongly suggested that a network of 81 surface stations arranged on a 5 x 7.5 mile grid be established to cover an area of 40 x 60 miles.

As shown in Fig. II. A. 11, the area of this network can be elongated in the direction of the movement of individual systems. This alteration will permit us to cover a much larger area without increasing the number of stations. The capability of representing features of a mesosystem would not be affected by increasing the station distance in this manner because space sections of the station data will fill up the space in the vicinity of each network station.

If we assume that a system traveling over the network at the rate of, for instance, 30 mph, remains unchanged for about 2.5 minutes before and after the map time, the space section would extend one and a quarter miles on each side of the station. Under such a circumstance, the space section entered in the map would be equivalent to the data obtained simultaneously at stations located on the short

Systems (* = Microscale)		Max. Horizontal Dimensions at the Surface (miles)	Suitable Distance of Network Stations (miles)
* Fair Weather Cumulus	inflow	2 ?	1/2
* Swelling Cumulus	inflow	5 ?	1
Low-intensity Mesosystems		100	5
Cellular Thunderstorm	rain	10	1
	outflow	30	2
	inflow	30	5
Squall-line Thunderstorms	rain	10 x 300	2
	outflow	500	10
	inflow	700	30
Tropical Squalls	rain	10 x 20 ?	1
	outflow	100 ?	5
Hurricane Rainband	rain	10 x 500	2
	outflow	unknown	5 ?
Tornado Cyclone	circulation	20	2
Tornado	circulation	3	1/4 or less
	inflow	10	1
* Dust Devil	circulation	1	1/10 or less
Mesolow	inflow	100	5
Microlow	inflow	10	1
Land & Sea Breeze	front		3
Mountain-Valley	circulation	10	1
Advection Fog	front		5
Mountain Phenomena	wave	20	2

Table II.A.4. Horizontal dimensions of micro to mesometeorological systems and the distance of network stations required for their investigation.

vectors attached to each network station.

Once a network is set up, it is not possible to reorient its long side every day in an attempt to have systems move in the direction of the long side. The time section will, therefore, be oriented in a slightly different direction determined by the movement of the individual system, which may vary with time and space. Figure II. A. 12 presents an example of a thunderstorm cell which would appear in a network analysis.

Network

For the purpose of revealing mesometeorological conditions surrounding the network, a surface-station network with a larger station distance becomes of vital importance. This network for linking the network with an existing macroscale station network may be called the network.

The station distance of this network will be 30 and 40 miles as indicated in Fig. II. A. 13. In view of the horizontal dimensions of mesosystems, the area of this network will be 300 x 400 miles. Based upon an idea similar to that used in designing the network, the network area is elongated in the direction of movement of compound mesoscale systems consisting of a cluster of individual or cellular systems. The velocity of such compound systems is called group velocity, which is usually considerably different from the velocities of individual systems in the group. It should be emphasized, therefore, that the elongated directions of the and networks are different.

Network

This is a smaller mesoscale network which may be established inside the network. The station spacing of this network would be determined according to the mesometeorological phenomena which are to be investigated. Generally a network of 121 surface stations arranged on a 1 x 1.5 mile grid to cover an area of 10 x 15 miles should permit investigation of the smaller mesoscale phenomena.

REFERENCES

1. Fujita, T., 1955: Results of detailed synoptic studies of squall lines, Tellus, 7, 405-436.

2. Fujita, T., 1956: Mesoanalysis: an important scale in the analysis of weather data. Res. Paper No. 39, U. S. Wea. Bur.

3. Fujita, T., 1958: Mesoanalysis of the Illinois tornadoes of 9 April 1953, J. Meteor., 15, 288-296.

4. Stout, G. E., R. H. Blackmer, Jr., J. B. Holleyman, and H. M. Gibson, 1958: Mesometeorological analysis of atmospheric phenomena. Final rep. to USASRDL.

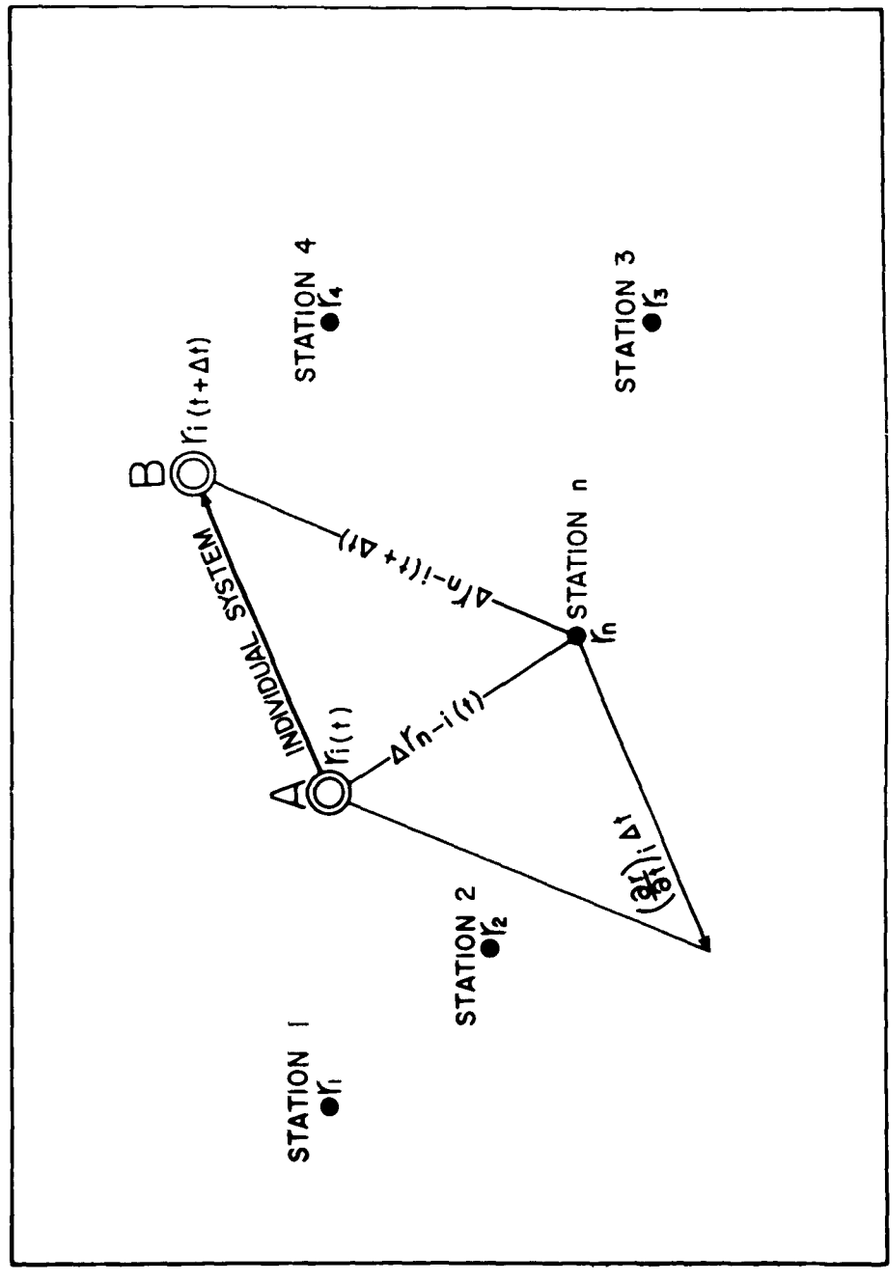

Fig. II.A.1. An individual system moving over a mesometeorological station network.

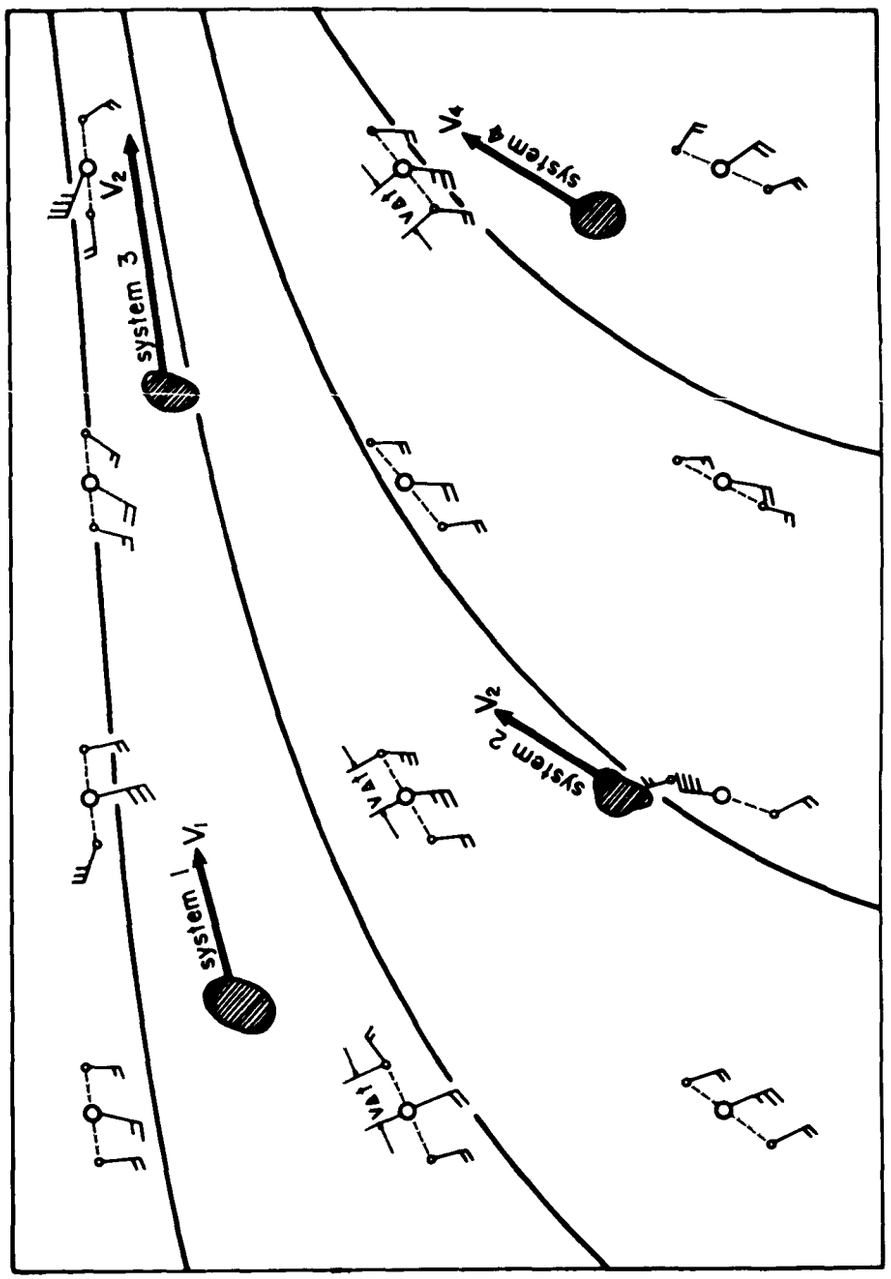

Fig. II.A.2. An example of meteorological data plotting in an area of complicated system movement.

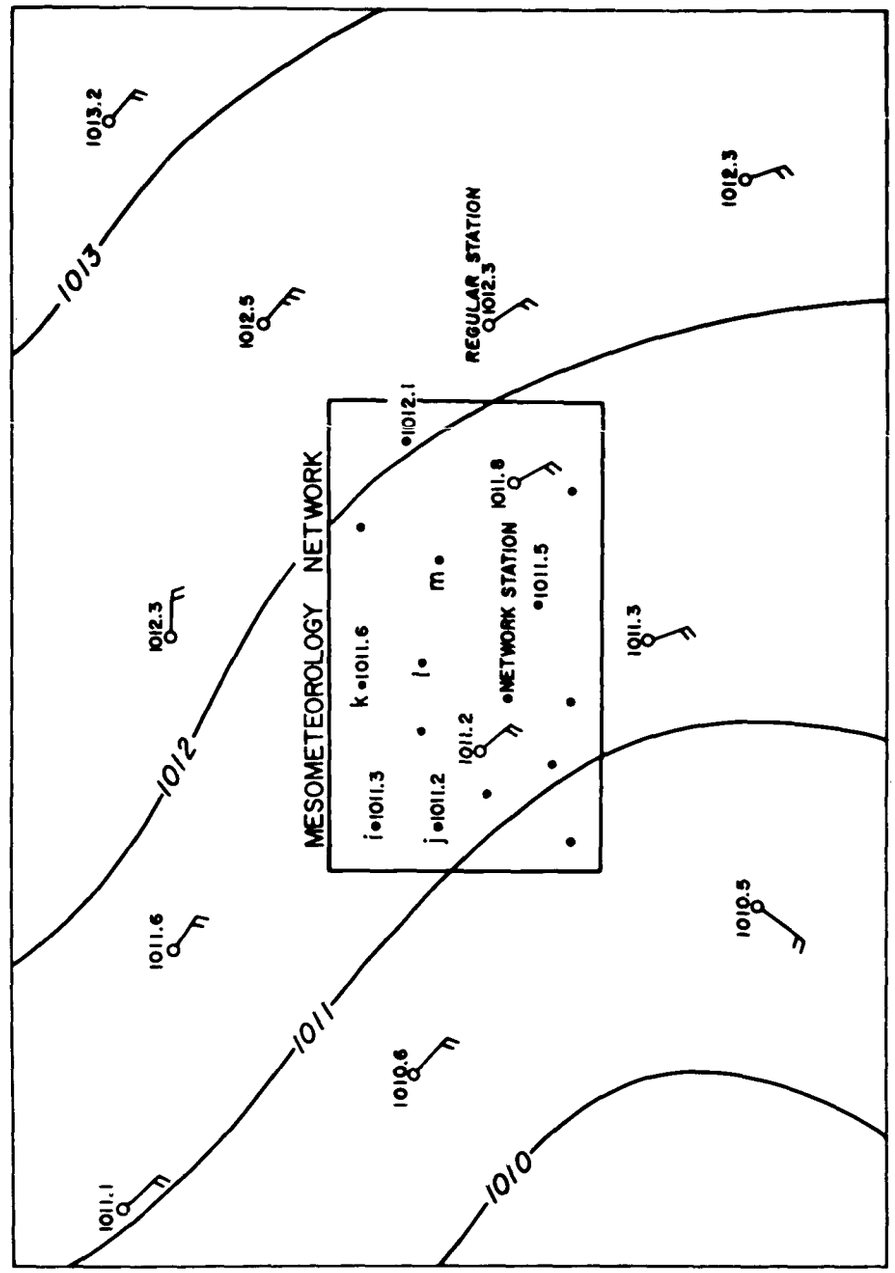

Fig. II.A.3. For the determination of mean pressure values of each mesometeorological station.

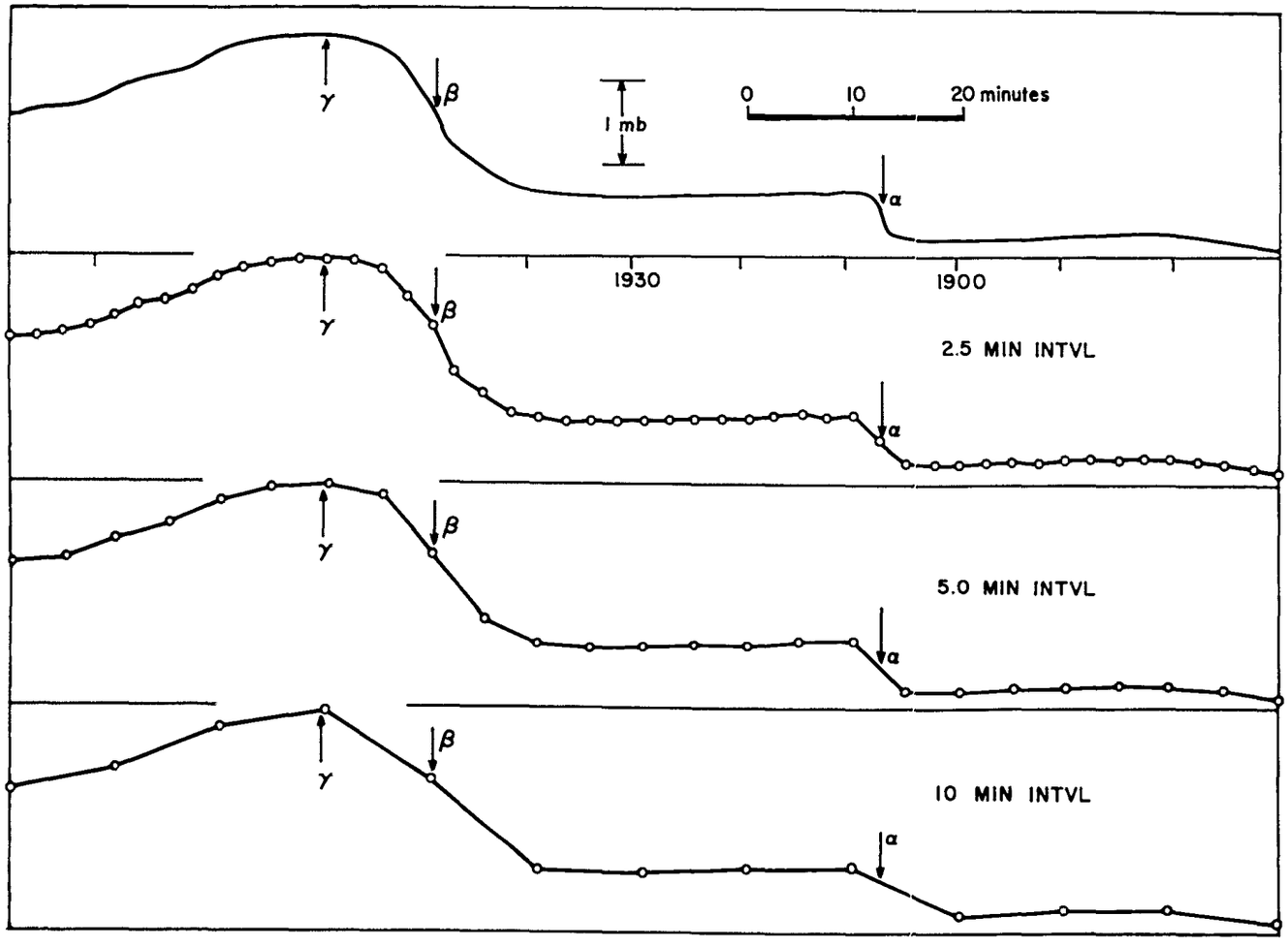

Fig. II.A.4. Change in pressure at a single station, assuming data are collected continuously or at various time intervals. Time on the chart runs right to left.

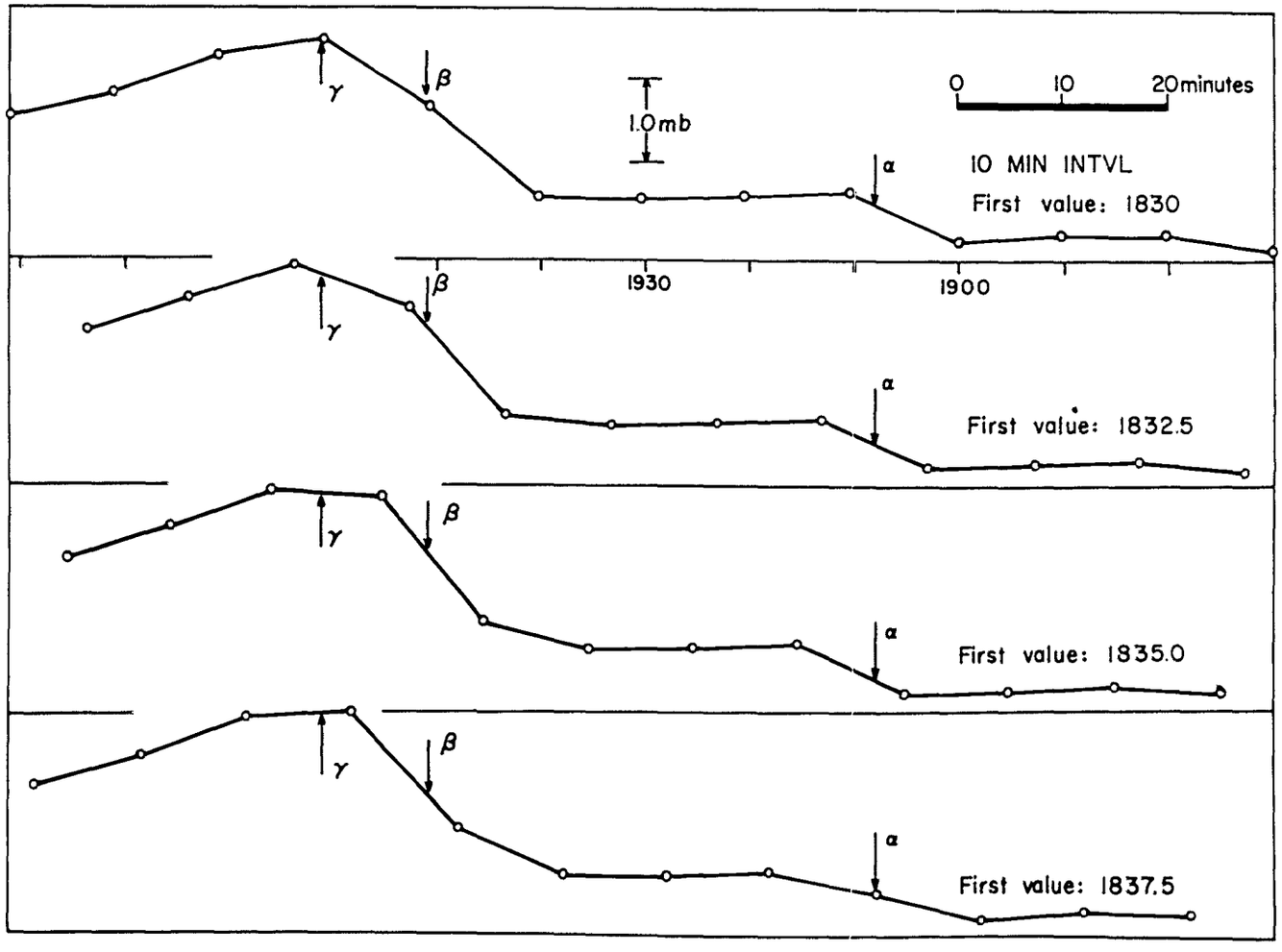

Fig. II.A.5. The difference in station pressure when data are collected at 10-minute intervals beginning at four different times: CST. Time on the chart runs right to left.

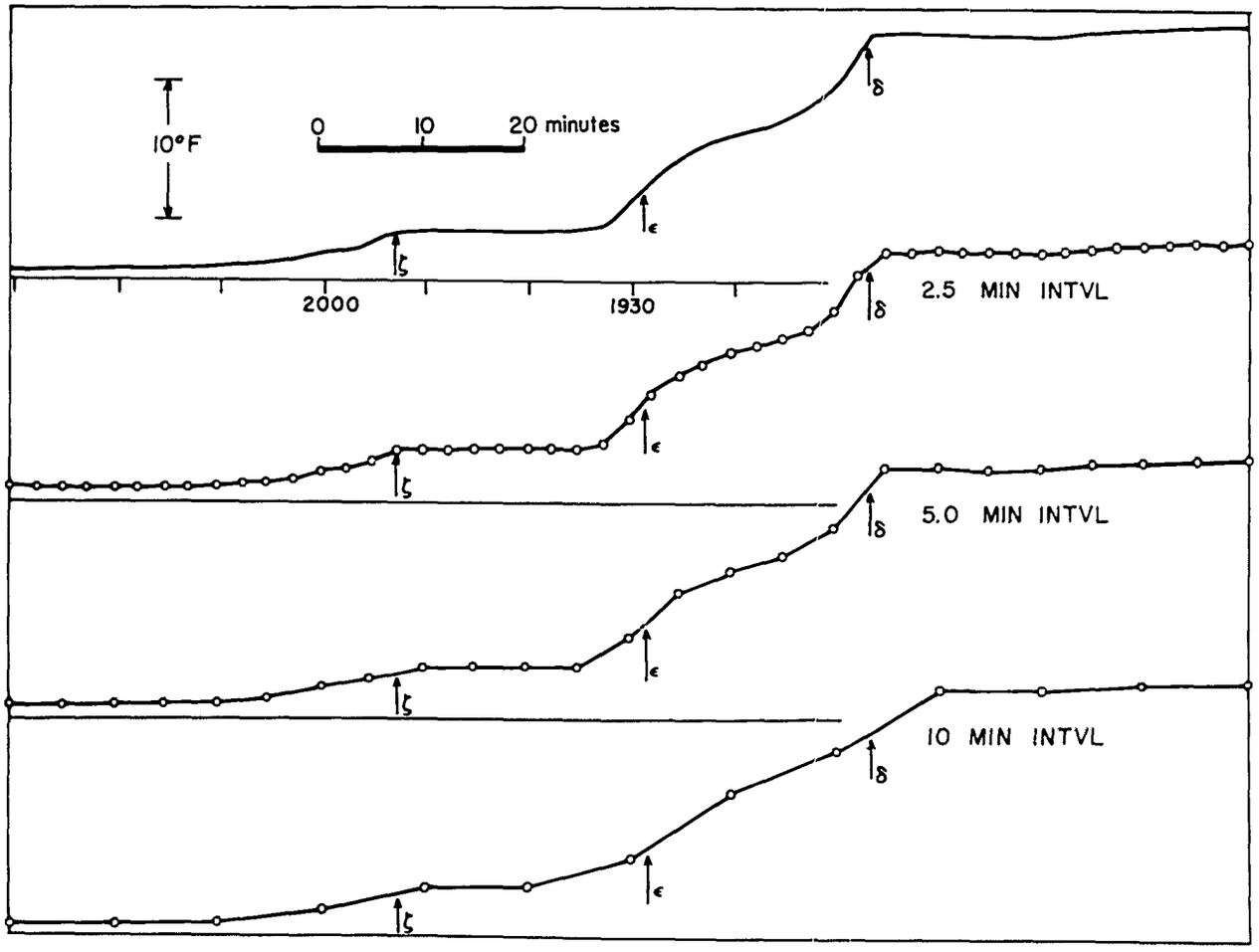

Fig. II.A.6. Comparison of continuous and digitized temperature values associated with squall line activity. *Time on the chart runs right to left.*

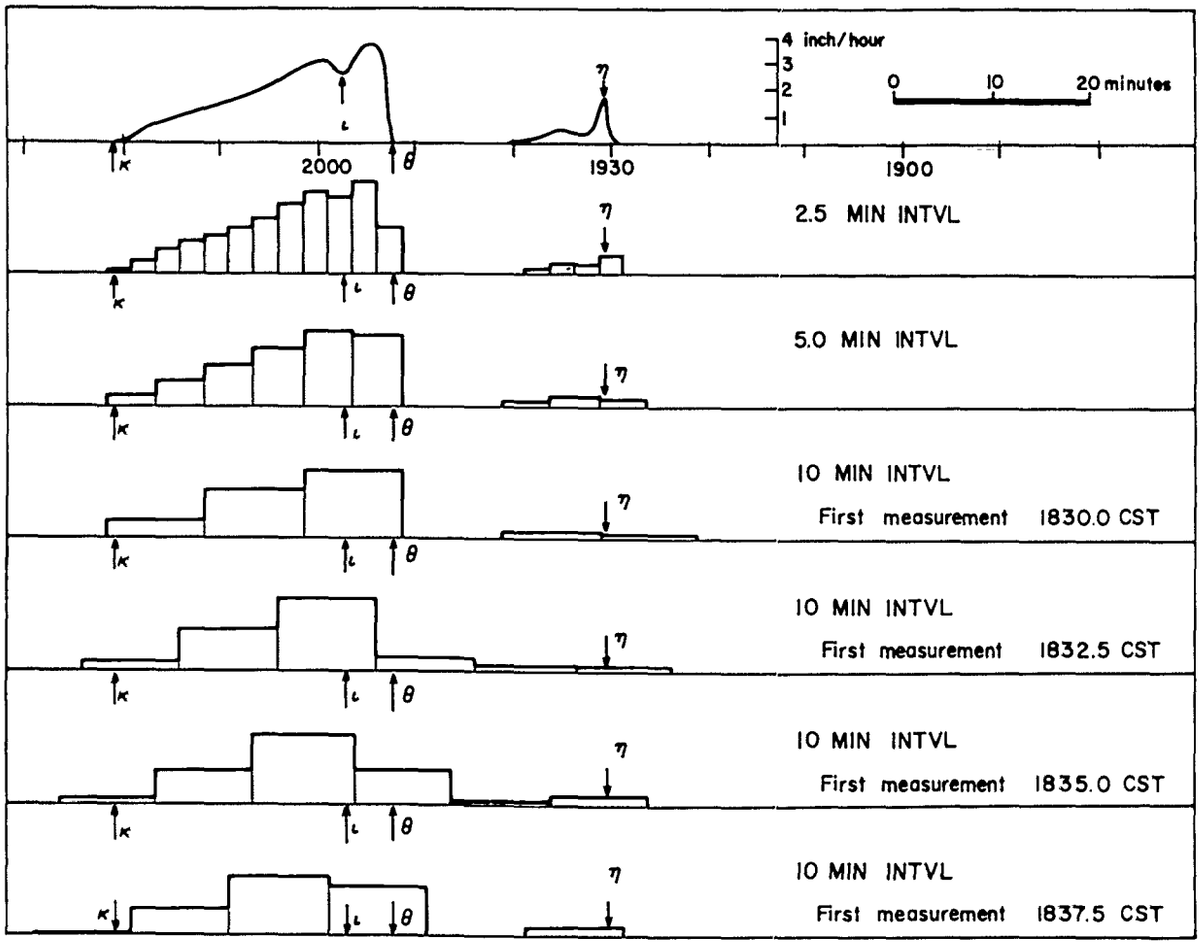

Fig. II.A.7. Precipitation rate (top) and accumulative amounts of precipitation measured at 2.5, 5.0, and 10.0-minute intervals. Time on the chart runs right to left.

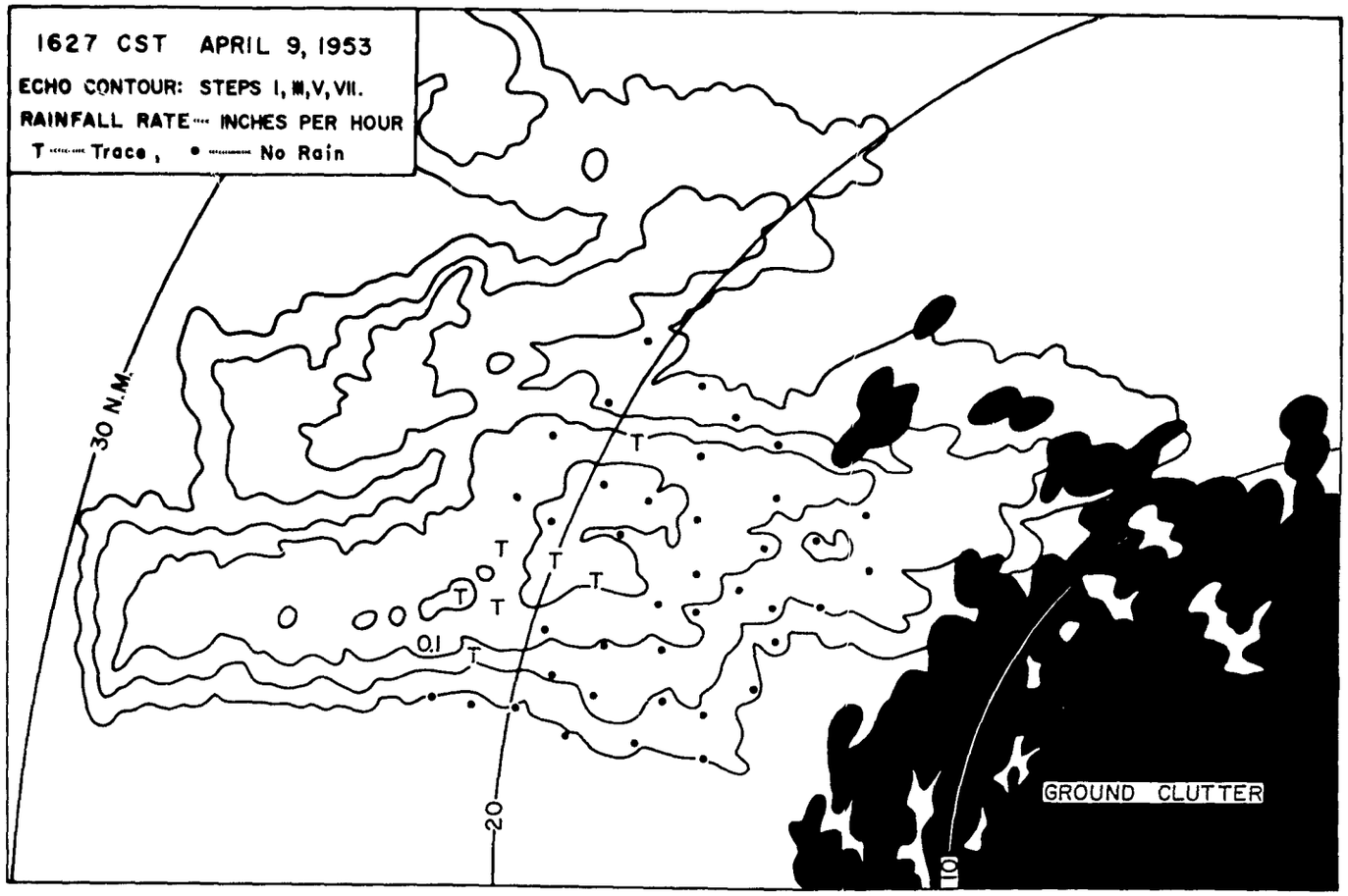

Fig. II. A. 8. Rainfall rates beneath the tornado-related echo of April 9, 1953. The rates were obtained from Goose Creek raingauge network.

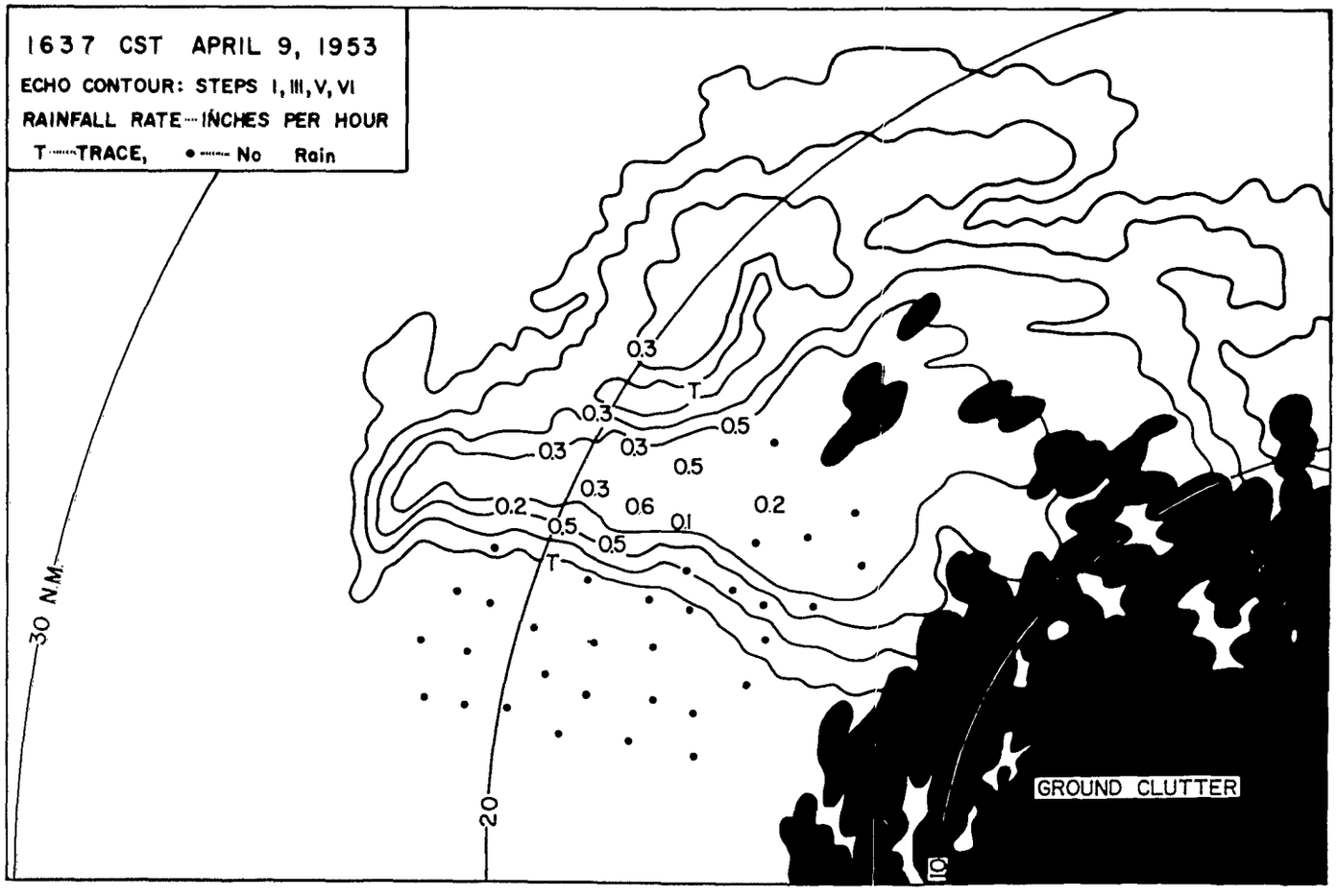

Fig. II.A.9. Rainfall rates beneath the tornado-related echo of April 9, 1953. Echo contours were obtained from Champaign radar pictures.

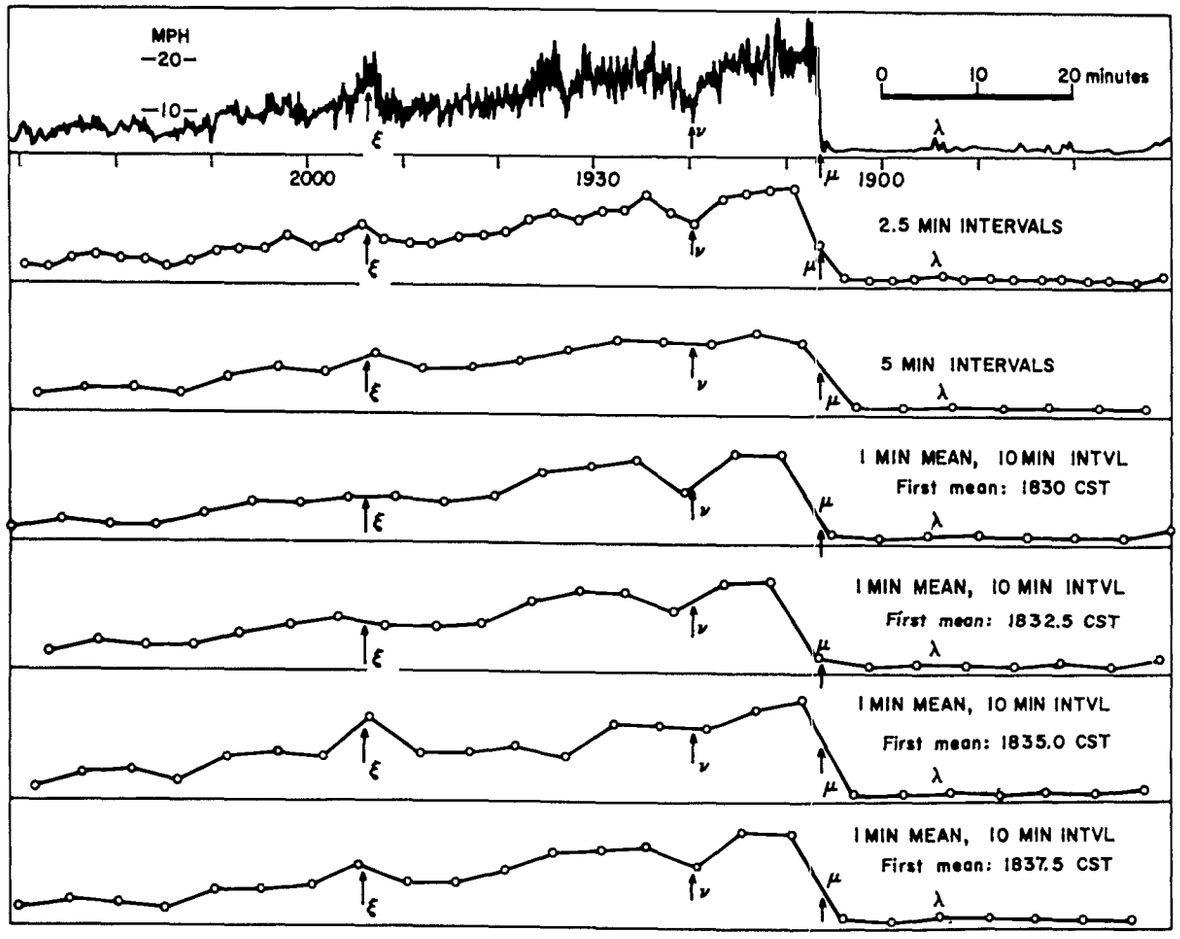

Fig. II.A.10. Various representations of thunderstorm gust. Time on the chart runs right to left.

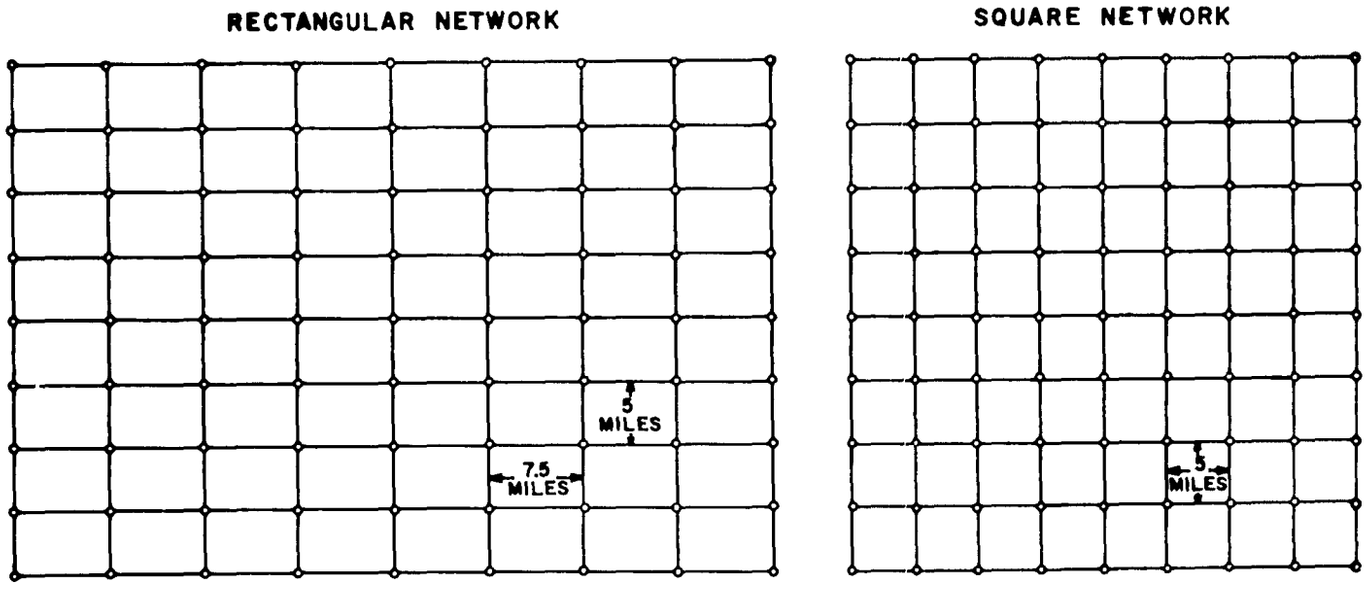

Fig. II.A.11. Rectangular grid network ideal for the study of individual mesoscale systems.

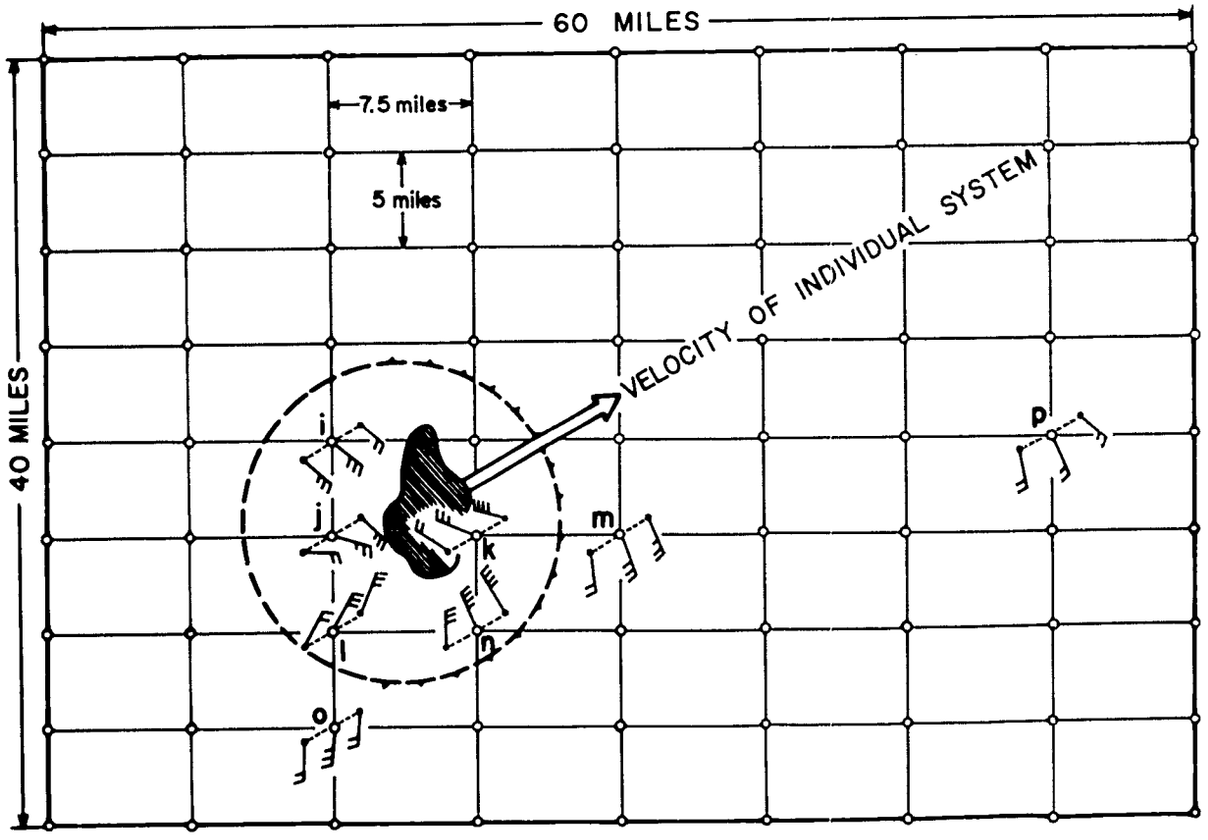

Fig. II. A. 12. An example of an individual thunderstorm system as represented by the β network stations.

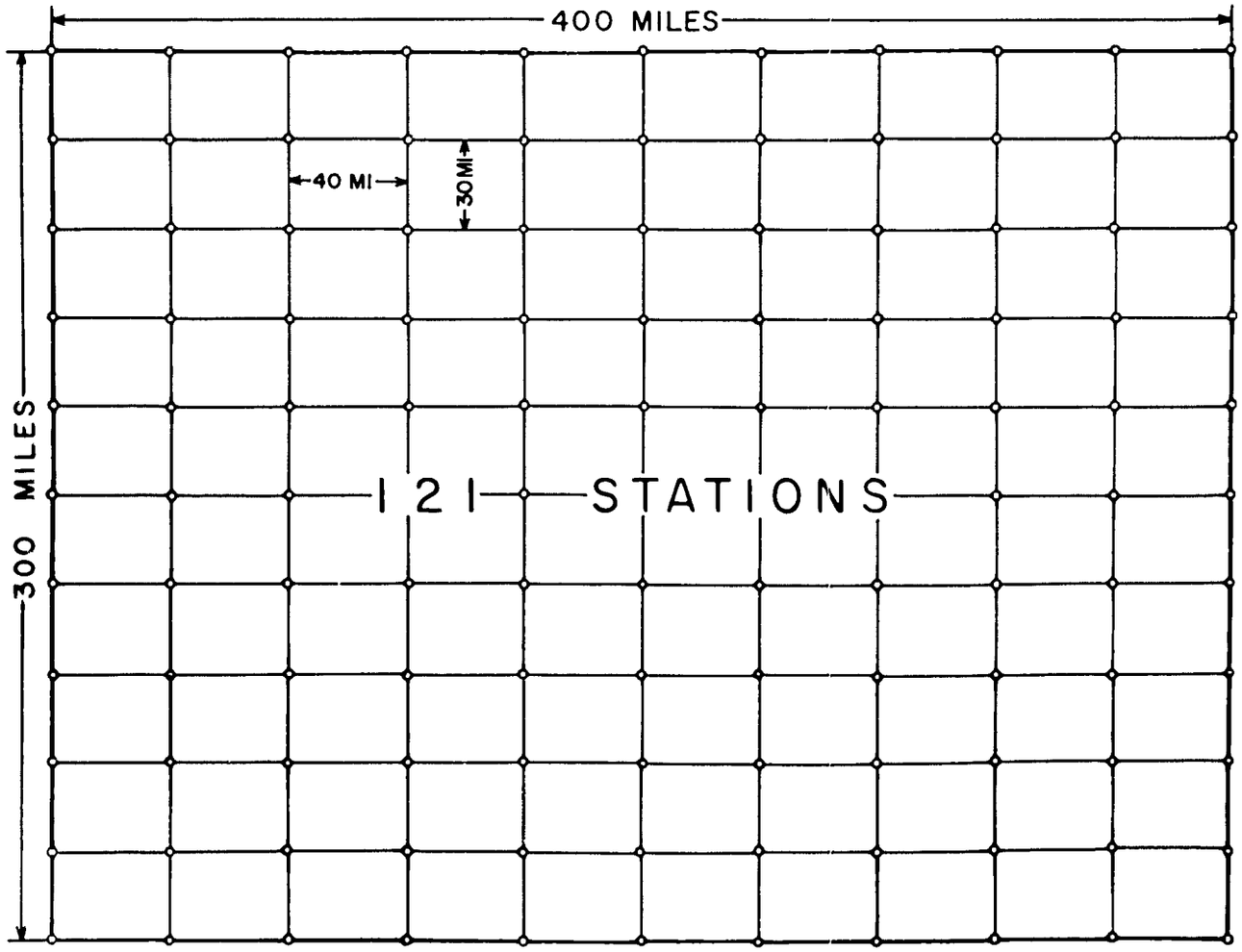

Fig. II.A.13. a network. This is a rectangular network serving for the investigation of compound mesometeorological systems.

B. UPPER AIR

The problem of time and space adjustment of observed data is of minor importance so long as they are used for macrometeorological studies. For instance, rawinsonde data may be entered in a macroscale chart at the station where the balloon was released even though it drifts away while climbing to higher levels. Usually the difference in time of release, if about one hour or less, does not affect the results of analysis. Similarly, reconnaissance flight data taken during several hours along a flight path may be plotted in a macrosynoptic chart without considering minor time differences.

Once we reduce to mesoscale, however, the situation becomes completely different, and the proper adjustment of time and space is of vital importance. For a reasonable design of a mesometeorological network, problems of this adjustment must be considered in detail.

1. METHOD OF UPPER AIR MEASUREMENTS

Methods of upper air measurement may be classified into two categories:

Measurements at Fixed Points on Elevated Ground or Artificial Structure

When a meteorological element or parameter is measured at a fixed point relative to the surface of the earth, the quantity measured is given by

$$A_n (x_n, y_n, z_n, t) \qquad \text{II.B.1}$$

where x_n, y_n, z_n are the space coordinates of the instrument. If measurements are made in a mountainous area, the wide range of elevation will permit us to study the vertical structure of mesoscale disturbances. An example of wind

measurement at various altitudes along the slope of San Francisco Mountain, Arizona, is shown in Fig. II.B.1.

Over flat terrain, however, it is difficult to fix a meteorological instrument at a given x, y, and z. An artificial tower, such as Cedar Hill Tower (1430 feet), is a useful platform for measuring vertical and time changes in meteorological elements. Telescopic poles reaching 100-150 feet above the ground are also useful in measuring micro to mesoscale disturbances.

When we desire to remain fixed for a considerable length of time at higher levels, we encounter tremendous difficulties. If FAA regulations permit and appropriate cables and balloons can be designed, a captive balloon fixed by three cables might be used as a platform. Or, an instrumented helicopter with an automatic position control system could stay in the air at a fixed point measuring the required parameter for a certain period of time; of course, it should have a long probe extending into the undisturbed atmosphere. The capability and limitations of such a helicopter for studying mesometeorological disturbances should be investigated from a practical point of view.

Measurement from Moving Vehicles

Difficulties encountered in maintaining a fixed platform can be overcome by the use of a moving vehicle for upper air measurements. The values obtained by such moving platforms are

$$A_m (x, y, z, t) \qquad \text{II.B.2}$$

which may be reduced to

$$A_m (x_o, y, z_o, t)$$

or

$$A_m (x, y_o, z_o, t) \qquad \text{II.B.3}$$

if the aircraft flies at a constant height toward the north or east, where x_o, y_o, z_o represent the initial coordinates of the aircraft.

A semi-vertical sounding

$$A_m (x_o, y_o, z, t) \qquad \text{II.B.4}$$

may be made by using a rocket or a high-ascension-rate balloon. In any respect, the observed value contains both time and space changes.

2. AIRCRAFT MEASUREMENTS

Instrumented aircraft measure various meteorological parameters continuously or semi-continuously while flying along given flight paths. The advantages of using weather reconnaissance aircraft over the area of a mesometeorological network are their mobility and continuous sampling capability.

Recent developments in airborne instruments permit us to obtain various data useful to three-dimensional mesometeorological research. Following is a brief statement concerning airborne measurements and the accuracy required.

Position Fix

About one-half mile accuracy in horizontal position fix is required. Omni and airborne radar fix over land or coastal areas will meet this requirement; however, if possible, a Doppler navigation system as used by Project Jet Stream (APN-66) or the National Hurricane Project (APN-82) is much more convenient in fixing position semi-continuously.

Since the weather aircraft under discussion will be flying over continents covered by surface network stations, it is not absolutely necessary to have an airborne radio altimeter. The rough surface topography even over the well charted Midwest does not under normal conditions permit us to compute the absolute altitude from radio altitude. A 200-foot contour map covering the Texas-Oklahoma border is presented in Fig. II.B.2. The radio-altitude chart of any flight path in such an area will show appreciable noise. Figure II.B.3 shows a hypothetical radio-altitude measurement. It is evident that there will be no way of comparing absolute values

of pressure and radio altitude. Since D-values cannot be computed, the use of the pressure altimeter is limited to height determination. Therefore, about half a millibar accuracy will be sufficient.

Airborne Radar

Since the aircarft will fly over a mesometeorological network covered by the effective range of ground radars, it need not be equipped with PPI radar unless necessary for navigation. For research purposes it is preferable to use RHI radar for making cross sections of approaching precipitating clouds.

Temperature

A vortex thermometer with a resolution of $0.1^{o}C$ and a range of $+40^{o}$ to $-80^{o}C$ will be satisfactory for measurement over the network area. As shown in examples in Fig. II.B.4 and 5, the data should appear either in a continuous trace or in digital form at intervals of less than 10 seconds. Otherwise, temperature gradients might not be measured properly. In-cloud temperature is not always measured accurately because of the wet-bulb effect experienced when flying through a cloud. An in-and-out cloud indicator recording on the temperature trace will be highly valuable. We can obtain the horizontal temperature gradient at constant levels by eliminating the vertical variation of temperature.

Wind

Semi-continuous measurement of wind direction and speed is required. When the Doppler wind measuring system is used, an accuracy (less than 2^{o} in direction and 2 knots in speed) sufficient for mesometeorological research purposes is obtained. So far, it has been difficult to determine the wind structure of meso-scale squall lines because weather reconnaissance aircraft equipped with the Doppler system have avoided the active portions. One penetration reported by the Air Force (1) was made accidentally by an instrumented B-47 on mission 32, April 23, 1957. Figure II.B.6 was plotted from "Flight Data Pertaining to Jet Streams" (2).

Evidently the aircraft flew south between two squall lines about 15 miles apart and into one of them; after flying through it, the plane turned back into the squall line again and extraordinary measurements were made. It will be found in the chart that a strong mesoscale outflow existed inside the squall lines in an area 30 x 30 miles in the vicinity of Bryan, Texas.

Other Airborne Measurements

In connection with other research which will normally be undertaken inside a mesometeorological network, it will be desirable to add other instruments to measure humidity, liquid water content, drop-size distribution, vertical acceleration, turbulence, vertical and horizontal potential gradients, radioactive fallout, etc.

3. RAWINSONDE OBSERVATIONS

There have been only a few instances when frequent rawinsonde observations were made in special networks. During the course of the network investigations previously reported (3; 4; 5), attempts were made to reveal the three-dimensional structure of mesoscale systems using available upper air soundings. It was found, however, that only the Thunderstorm Project network made rawinsonde observations sufficiently close in time and space for mesometeorological investigation.

In view of this, it is highly desirable to operate a rawinsonde network in combination with an ideal surface mesometeorological network as presented in this report.

Position Adjustment

Properly analysed rawinsonde data are extremely useful in studying mesoscale disturbances. Figure II.B.7, showing trajectories of balloons released at close intervals from Thunderstorm Project stations 19 and 47, reveals that balloon movement cannot be neglected in mesoscale studies.

Let us express a value measured by a balloon as

$$F\,(P,\ x,\ y,\ t) \qquad \text{II.B.5}$$

where P denotes the pressure level penetrated by the balloon at t. If several balloons are available over the network area at the level of pressure P, the values measured by each balloon are

$$F_1\,(P,\ x_1,\ y_1,\ t_1)$$

$$F_2\,(P,\ x_2,\ y_2,\ t_2)$$

$$F_3\,(P,\ x_3,\ y_3,\ t_3) \qquad \text{II.B.6}$$

In order to carry out mesosynoptic analysis, differences in time t_1, t_2, t_3, ... should be adjusted to t. This adjustment may be made by moving the balloon along the pressure surface P for a reasonable distance, determined by time differences $t\text{-}t_1$, $t\text{-}t_2$, $t\text{-}t_3$, ... etc. In shifting the balloon to a new position, it is assumed that the values measured are conserved. There is a question, then, how far the balloon should be moved along the constant pressure surface. A number of test analyses showed that an adjustment as great as $V_n\,(t\text{-}t_n)$ can be made, where V_n denotes wind velocity measured by the balloon at pressure level P; and t_n, the time when the balloon reached the level. We also reached the conclusion that the time difference $(t\text{-}t_n) = \Delta t$ should not exceed 10 minutes, which is reasonably short for mesoscale upper air analysis.

Such an adjustment may be expressed by

$$F_n\,(P,\ x_n,\ y_n,\ t_n) = F_n\,(P,\ x_n + V_{nx}\ \Delta t,\ y_n + V_{ny}\ \Delta t,\ t) \qquad \text{II.B.7}$$

where V_{nx} and V_{ny} are respectively the x and y components of wind observed by balloon n.

A schematic figure showing such a position adjustment appears in Fig. II.B.8. It can be seen in the figure that the balloons are moved in either a downwind or an upwind direction, depending upon the positive or negative sign of $(t-t_n)$.

Selection of Analysis Times and Levels

Since we are able to make position adjustments of rawinsonde balloons for time differences up to $\pm$10 minutes, most of the balloons released simultaneously can be utilized during this 20-minute period.

Figure II.B.9 shows a z-t diagram of ascents made by the Thunderstorm Project and analysed by Fujita (6). It should be noted that the time difference between balloon passage of a constant pressure level increases with time. Even if their release is simultaneous, we must expect to find about a 20-minute time variation by the 200 mb level. During a storm, when up and downdrafts prevent smooth ascents, the time variation at the 200 mb level may reach over 30 minutes. This example will be seen in the 2030 EST ascent made shortly after a mesoscale front passed over the network. The balloon from station 19 reached the 200 mb level about 30 minutes after the one from station G.

The circled numbers in the figure indicate the balloons available at a given height within $\pm$10 minutes from the 10-minute interval analysis times. If the rate of ascent is about 800 feet per minute, it will be convenient, when analysing 10-minute interval charts, to treat two successive levels separated by 100 mb as occurring at the same time.

4. UPPER AIR NETWORK

Spacing of Rawinsonde Stations

This is one of the most difficult and critical problems in designing a three-dimensional mesometeorological network. Of course, if it were possible to include an unlimited number of stations in the network design, we could make various tests

for determining the proper station distance. This, however, is obviously out of the question.

It was found in the course of our research toward the network design that the spacing in question should differ somewhat, according to the meteorological parameters to be measured. Among these elements--such as temperature, pressure, humidity, and wind--humidity was found to be the most variable in the horizontal.

Shown in Fig. II.B.10 is a typical distribution of dew-point temperature measured by an infra-red hygrometer during Cook's P-38 flight from Dallas to Kansas City by way of Gage, Oklahoma. The dew-point temperature diagram plotted for every three-mile flight distance seems to show meso to microscale disturbances fairly well. When these dew-point temperatures are plotted at 15 and 30-mile intervals as shown in the lower curves, they are not frequent enough to show microscale humidity disturbances.

Usually upper air temperature fluctuates much less than dew-point temperature. Therefore, as shown in Fig. II.B.11, temperature values at 15-mile intervals will give a fairly good description of mesoscale temperature disturbances except where tight gradients exist.

Based upon analyses of data from the Thunderstorm (7), Jet Stream (1), and National Hurricane Research Projects (8), a reasonable separation of upper air stations was determined to be about 20 miles. Figure II.B.12, showing a portion of mission 32 appearing in Fig. II.B.6, is a wind field described by 3, 15, and 30-mile station spacing. The less than five-mile spacing of the Thunderstorm Project is definitely too dense for mesometeorological study. This was noted in our upper air analyses involving both undisturbed and disturbed cases (4; 6).

With regard to atmospheric pressure, there is, at the present time, no way of measuring changes in hydrostatic pressure in the free atmosphere. The D-value defined as the difference between radio and standard pressure altitudes, gives us some idea of pressure change at the flight level. Figure II.B.13 represents D-values, pressure and radio altitude of a hurricane flight. It is evident that the D-value change is much less than the aircraft altitude change, which is produced by up and down drafts even in a constant-pressure-level flight. Our experience with D-value analysis

of hurricane data reveals that about one-mile intervals of observation are required to investigate the structure of rainbands. For the study of mesoscale structure a 10-20 mile interval will be sufficient.

Finally, Table II.B.1 summarizes the maximum station spacing for the study of four different weather elements by a rawinsonde network. The table also shows intervals of aircraft sampling ideal for small scale research.

Element	Rawinsonde Station Spacing	Aircraft Sampling Interval
Pressure	10-20 miles	1/2 mile
Temperature	20 miles	1/2 mile
Dew Point	10 miles	continuous
Wind	20 miles	1 mile

Table II.B.1. Maximum rawinsonde station spacing and aircraft sampling interval.

This table indicates that a much denser network is required for the study of humidity, which is more variable than any other element. It should be mentioned, however, that this rawinsonde spacing is ideal for investigating smoothed mesometeorological disturbances rather than for sharp changes in weather elements. In order to measure the change in a horizontal dimension, reconnaissance aircraft would be used even though their measurement capability is limited to their flight path.

Distribution of Upper Air Stations

It was stated in the previous sections that a 20-mile spacing is ideal for describing smoothed mesometeorological disturbances. This does not mean that we should cover the entire three-dimensional mesometeorological network by upper air stations of such a high density. Since our intention is to design a research network, it will be satisfactory if a small portion of the α network (300 x 400 miles) is covered by a dense rawinsonde network.

A schematical distribution of upper-air stations inside the surface network appears in Fig. II.B.14. It should be noted that the center of the upper air network is located about 20 miles to the west (upwind) of the center of the surface network.

This design derives from the fact that balloons drift a considerable distance east of their release points before they reach heights at the 200 or 100 mb level.

Thus we have a total of 57 rawinsonde stations. It should be emphasized that this number is still conservative for investigating the three-dimensional structure of mesoscale disturbances, whose physical and dynamical characteristics are practically unknown.

Frequency and Period of Soundings

In determining the maximum frequency of the rawinsonde releases, consideration should be given to the speed of the systems, the spacing of the stations, and the height to which observations are desirable. It has already been considered that a spacing of twenty miles is desirable over a small area within the [illegible] network. The necessity of extending observations to the tropopause and the desirability of achieving simultaneous releases require, with an ascension rate of about 800 feet per minute, that observations from the individual stations be spaced at 1.5-hour intervals.

The maximum time for a full scale operation during a one-day period will depend on the area of the network and the speed and lifetime of the systems. Since the network will be 500 miles on the diagonal and the speed of the squall line systems will average approximately 30 mph and last an indeterminate time, an operational time of up to 16 hours will be necessary. Maintaining a standby status during the remaining 8 hours could be more than justified for the collection of vital data during an unexpected outbreak of mesoscale weather systems.

REFERENCES

1. Endlich, R. M., and R. M. Rados, 1959: The meteorological measurements and field program of Project Jet Stream from 1956 to 1958. Geophys. Res. Papers, No. 64, AFCRC.

2. Project Jet Stream Staff, 1959: Flight data pertaining to jet streams: Jet No. 32, April 23, 1957. AFCRC and Univ. of Dayton.

3. Fujita, T., H. A. Brown, and Y. Omoto, 1959: Design of a three-dimensional meso-meteorological network. First Quarterly Tech. Rep. to USASRDL, Contract No. DA-36-039 SC-78901.

4. _____ Second Quarterly Tech. Rep. to USASRDL.

5. _____ Third Quarterly Tech. Rep. to USASRDL.

6. Fujita, T., 1958: Three-dimensional mesoanalysis of a squall line. Rep. of Investigation 36, Ill. State Water Survey (Appears also as Res. Rep. 1 to USASRDL, Contract No. DA-36-039 SC-64656.)

7. Byers, H. R., and R. R. Braham, Jr., 1949: The Thunderstorm. Govt. Print. Off.

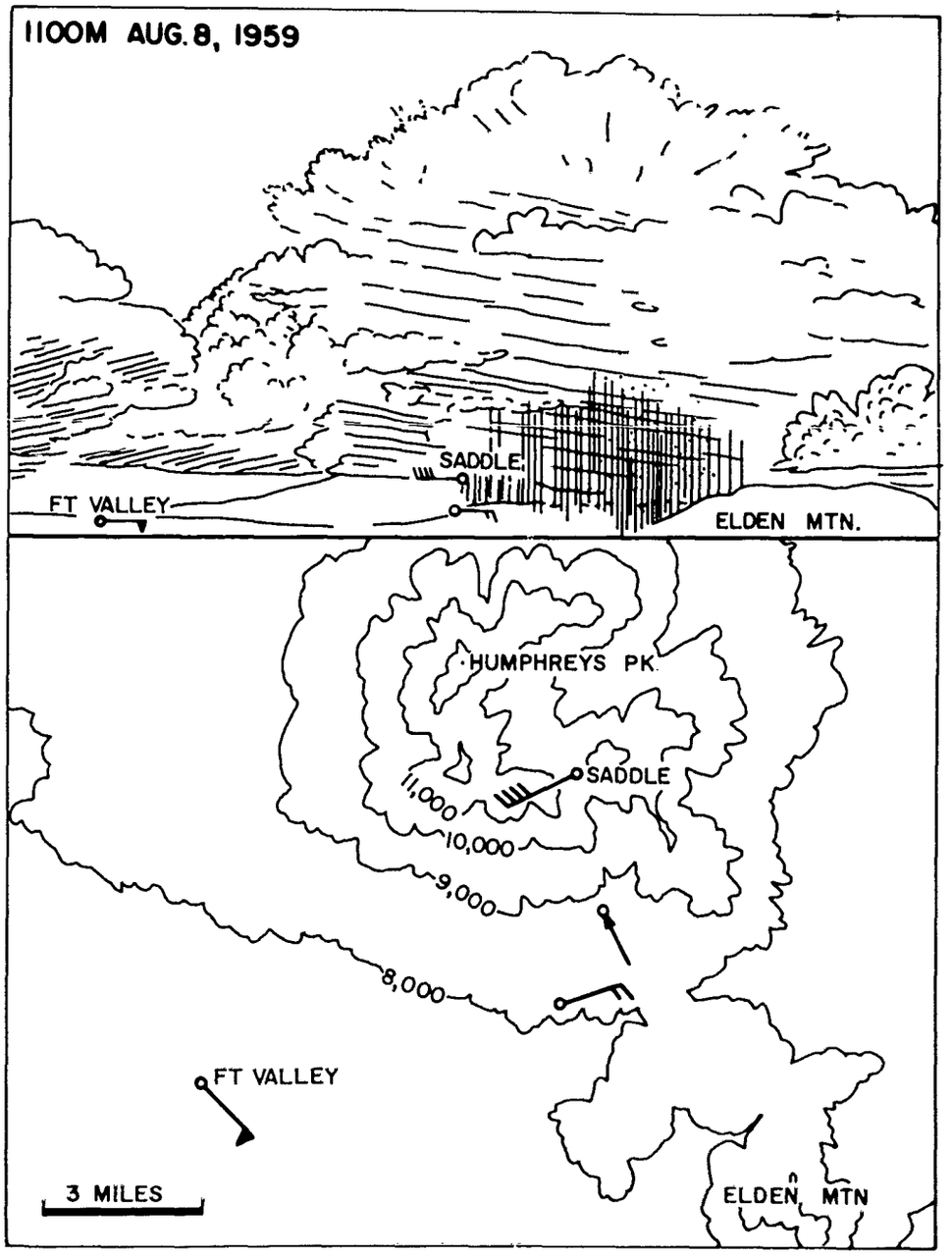

Fig. II.B.1. Example of wind distribution over the slope of San Francisco Mountain, August 8, 1959.

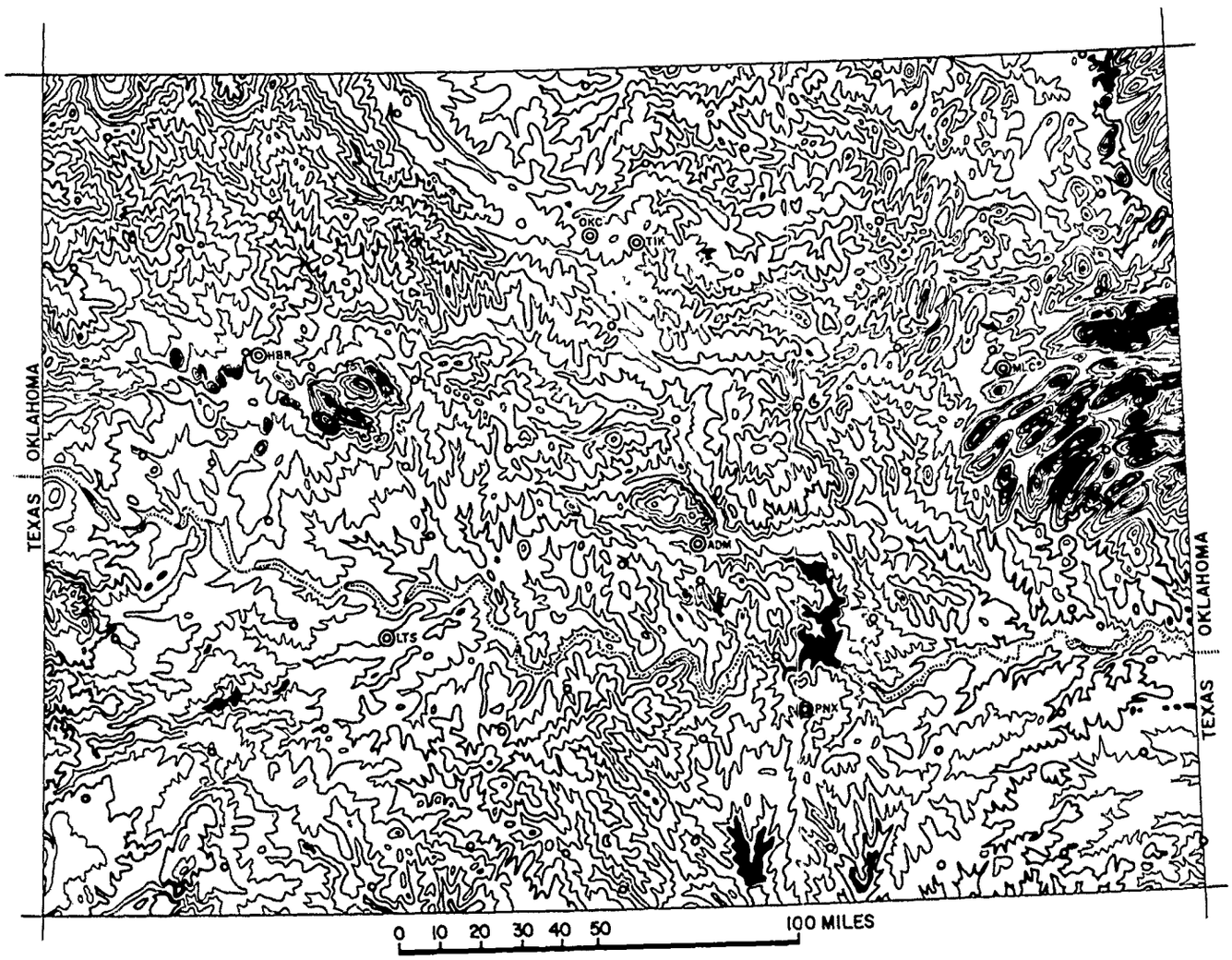

Fig. II.B.2. Topographic map of Texas-Oklahoma border area contoured at 100-foot height intervals.

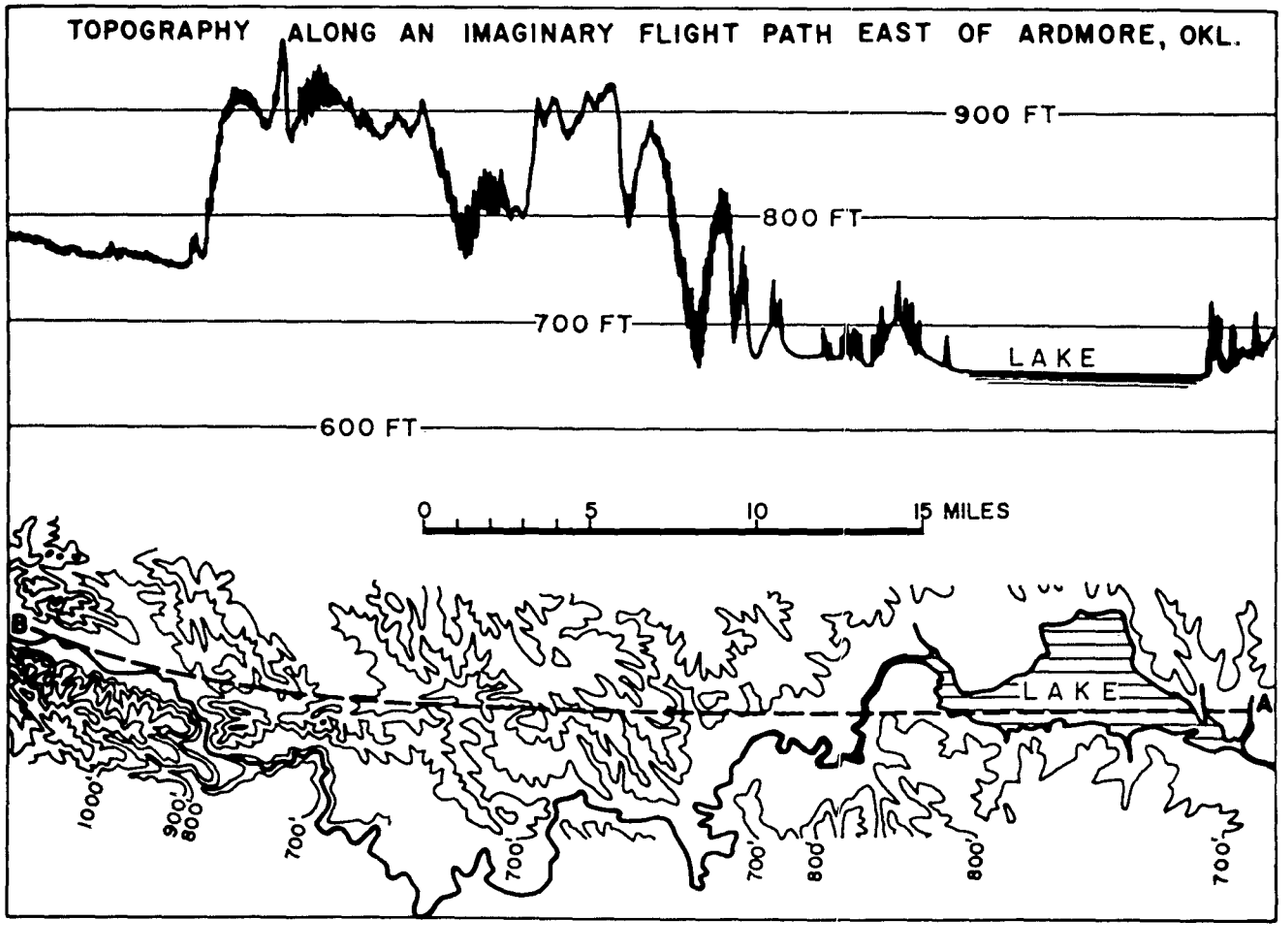

Fig. II.B.3. Variation in radio altimeter reading for a hypothetical flight over the Midwest.

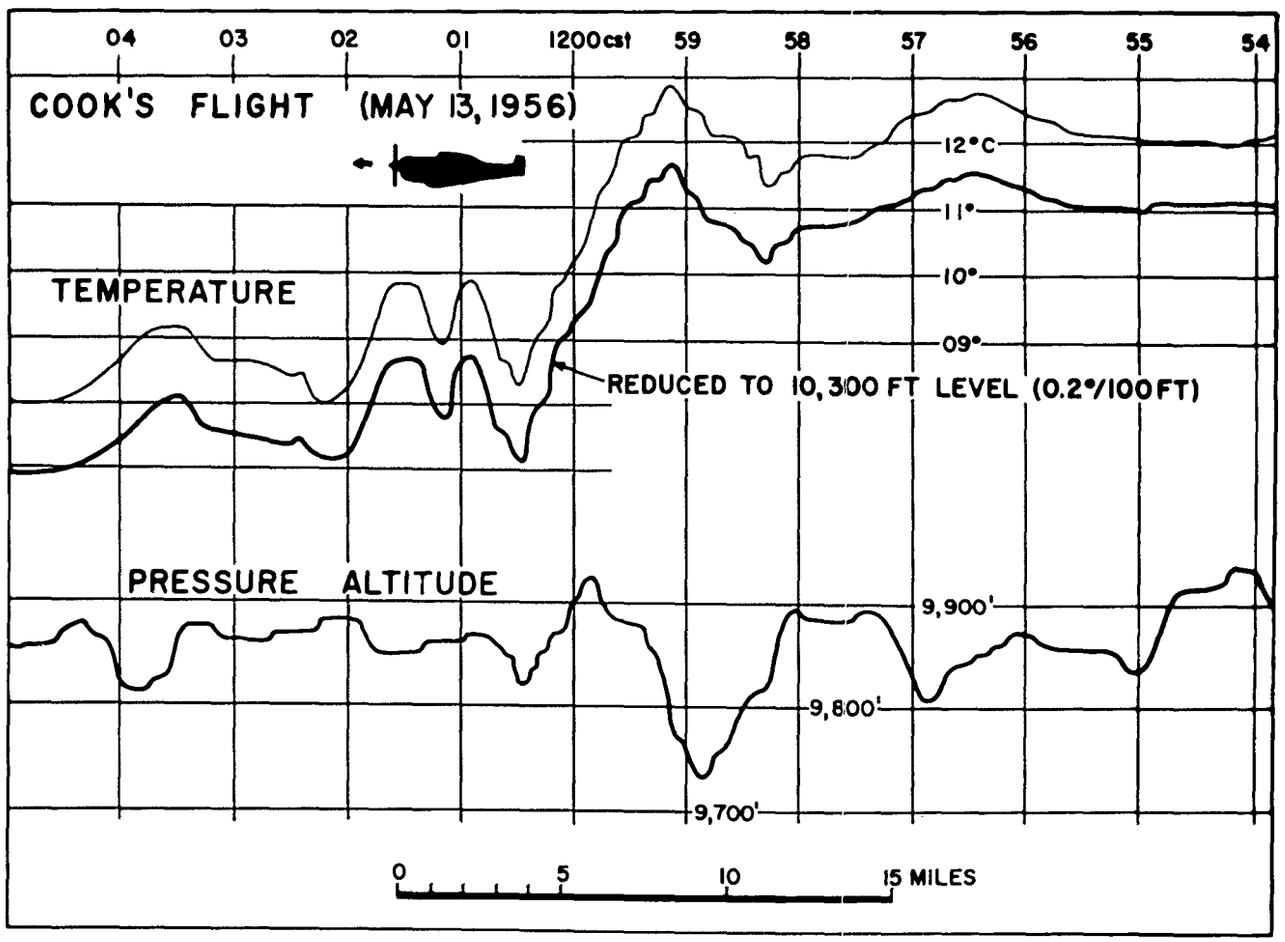

Fig. II.B.4. Continuously recorded air temperature reduced to 10,300 foot level.

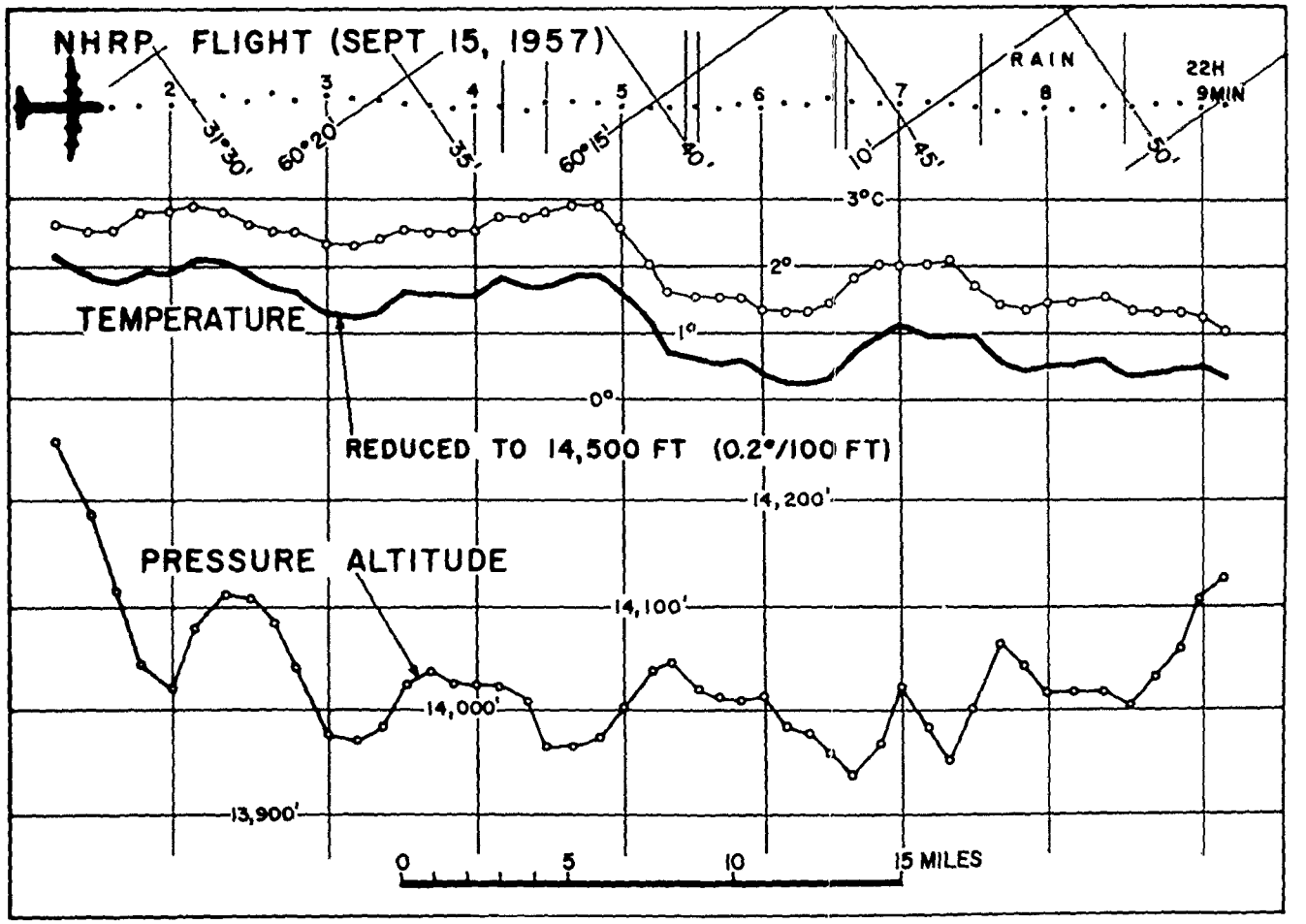

Fig. II.B.5. Temperature digitized at 10-second intervals.

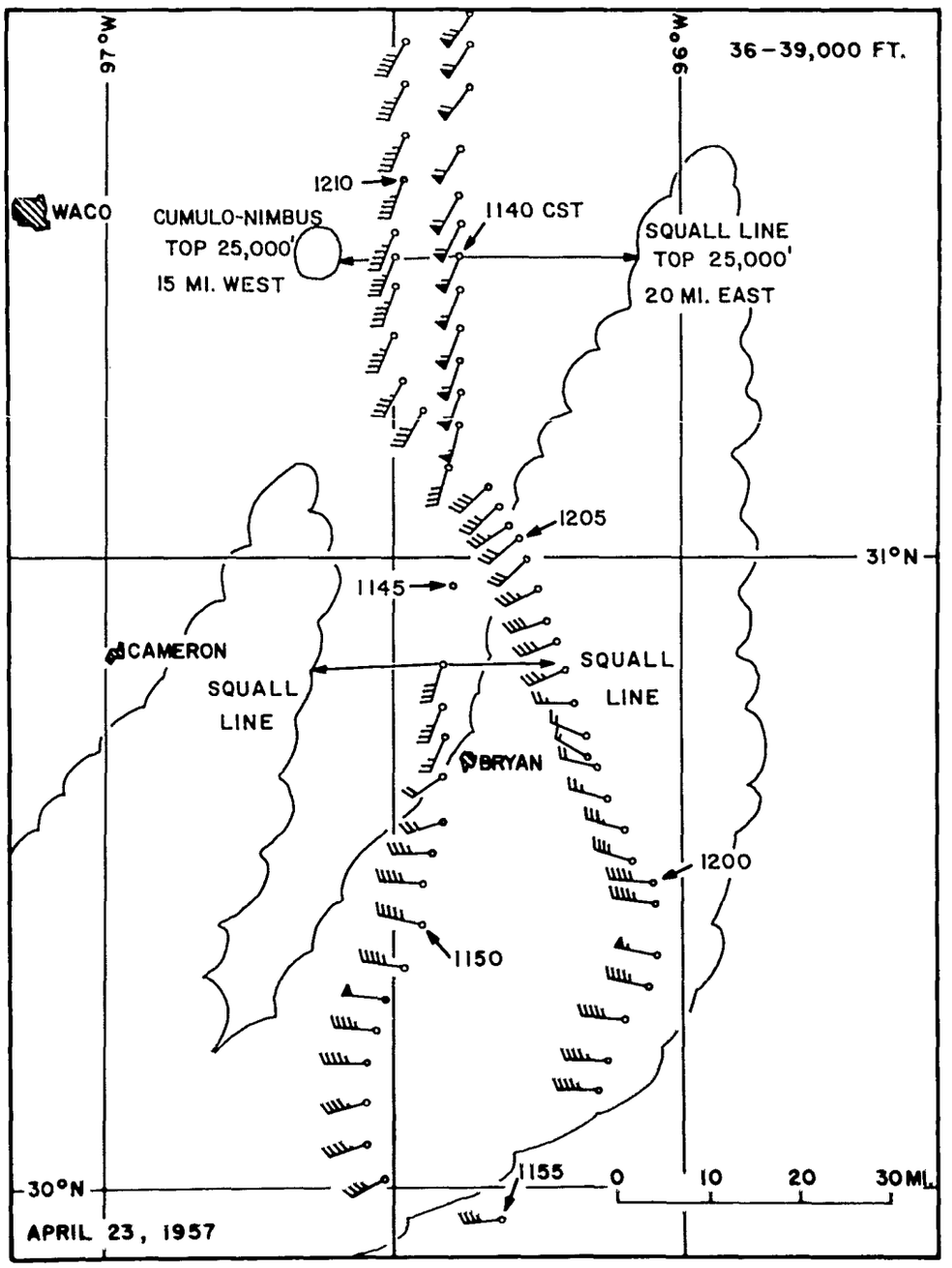

Fig. II.B.6. Semi-continuous wind measurement made by an instrumented B-47, Project Jet Stream.

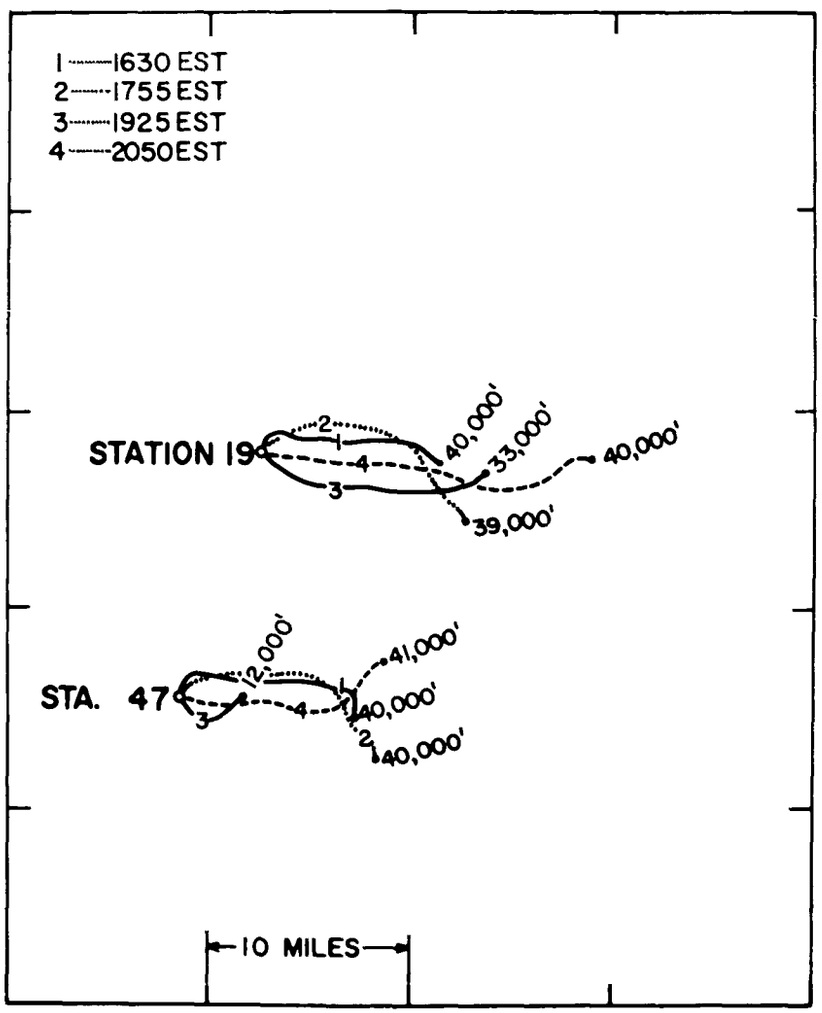

Fig. II.B.7. Paths of balloons released from two upper air stations, Thunderstorm Project, 1947.

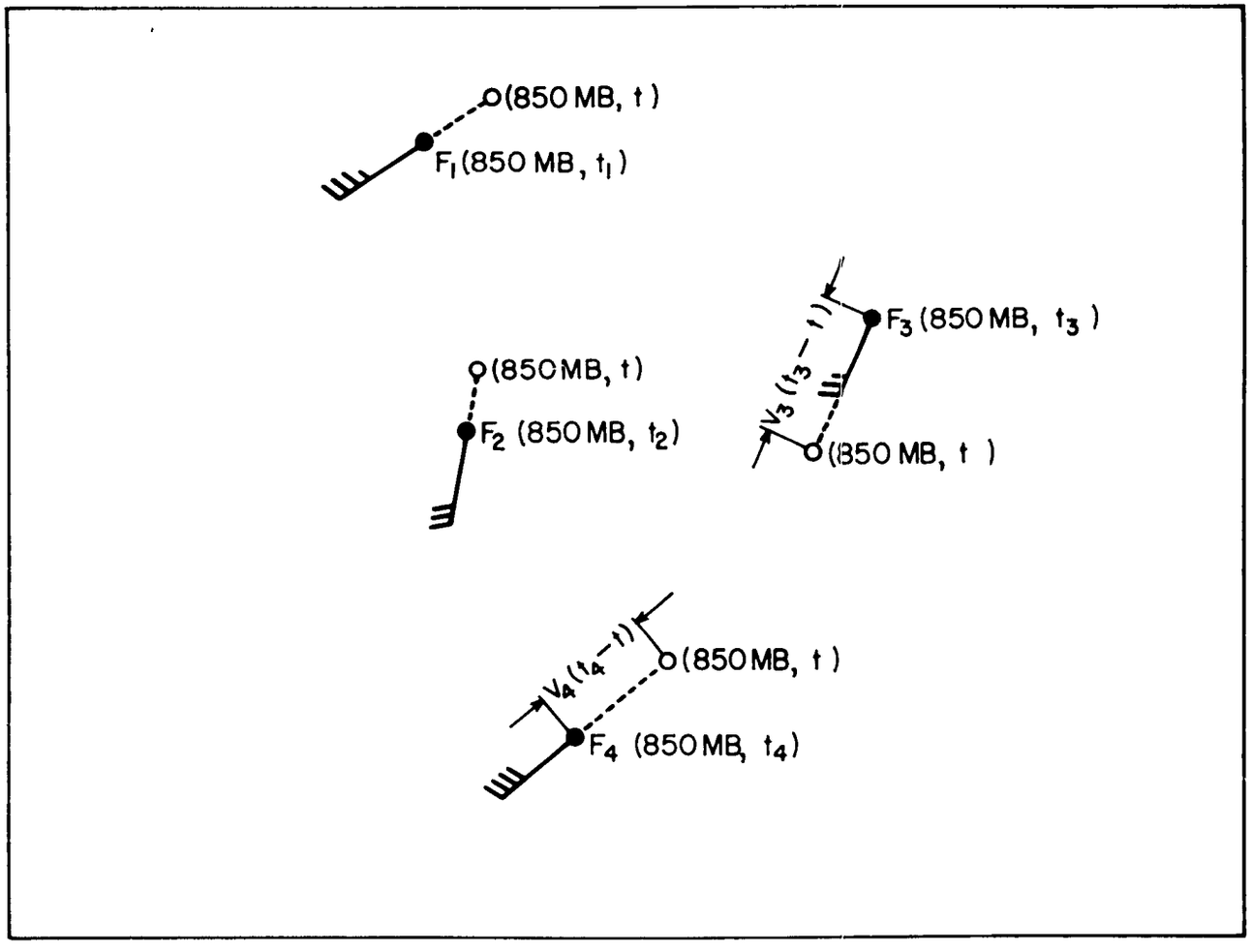

Fig. II. B. 8. Adjustment of balloon location for compensating t.

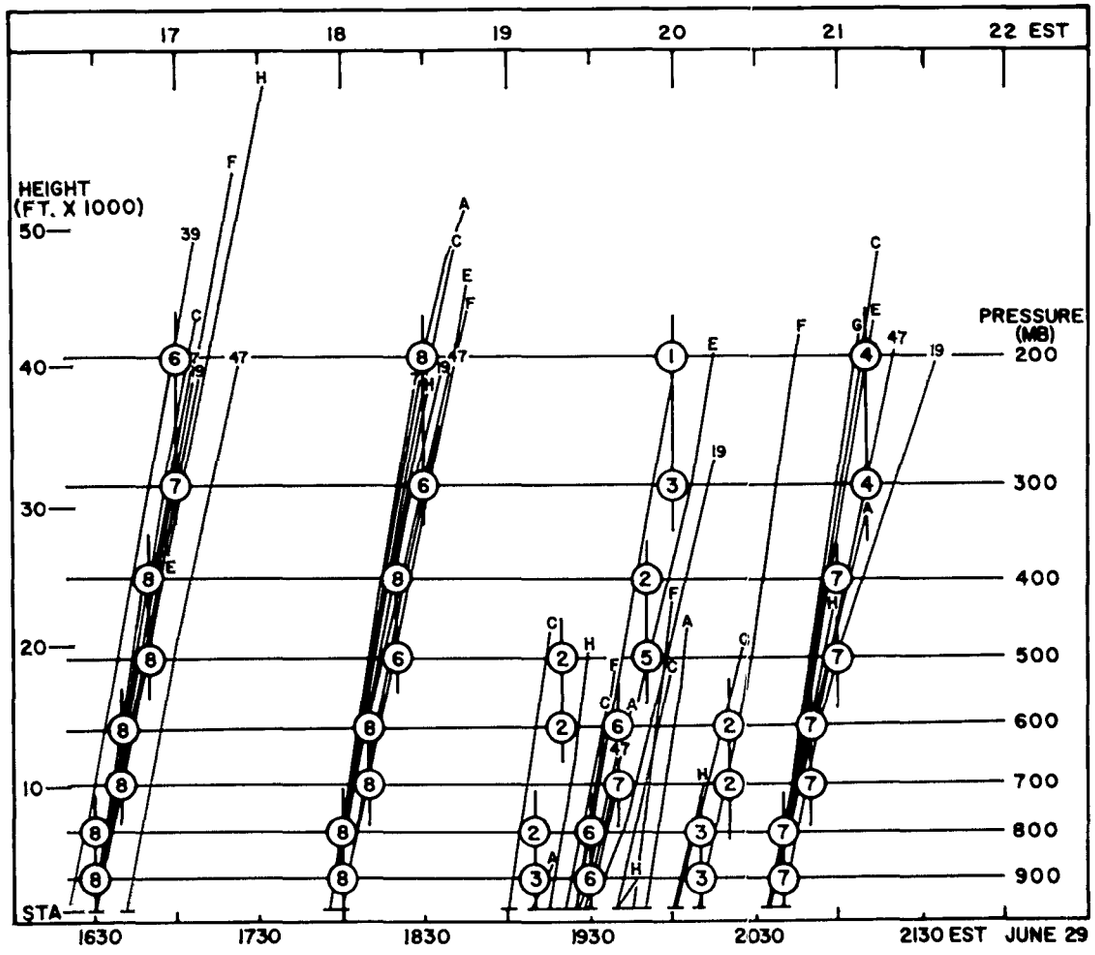

Fig. II.B.9. z - t diagram of upper air sounding balloons on June 29, 1947, Thunderstorm Project.

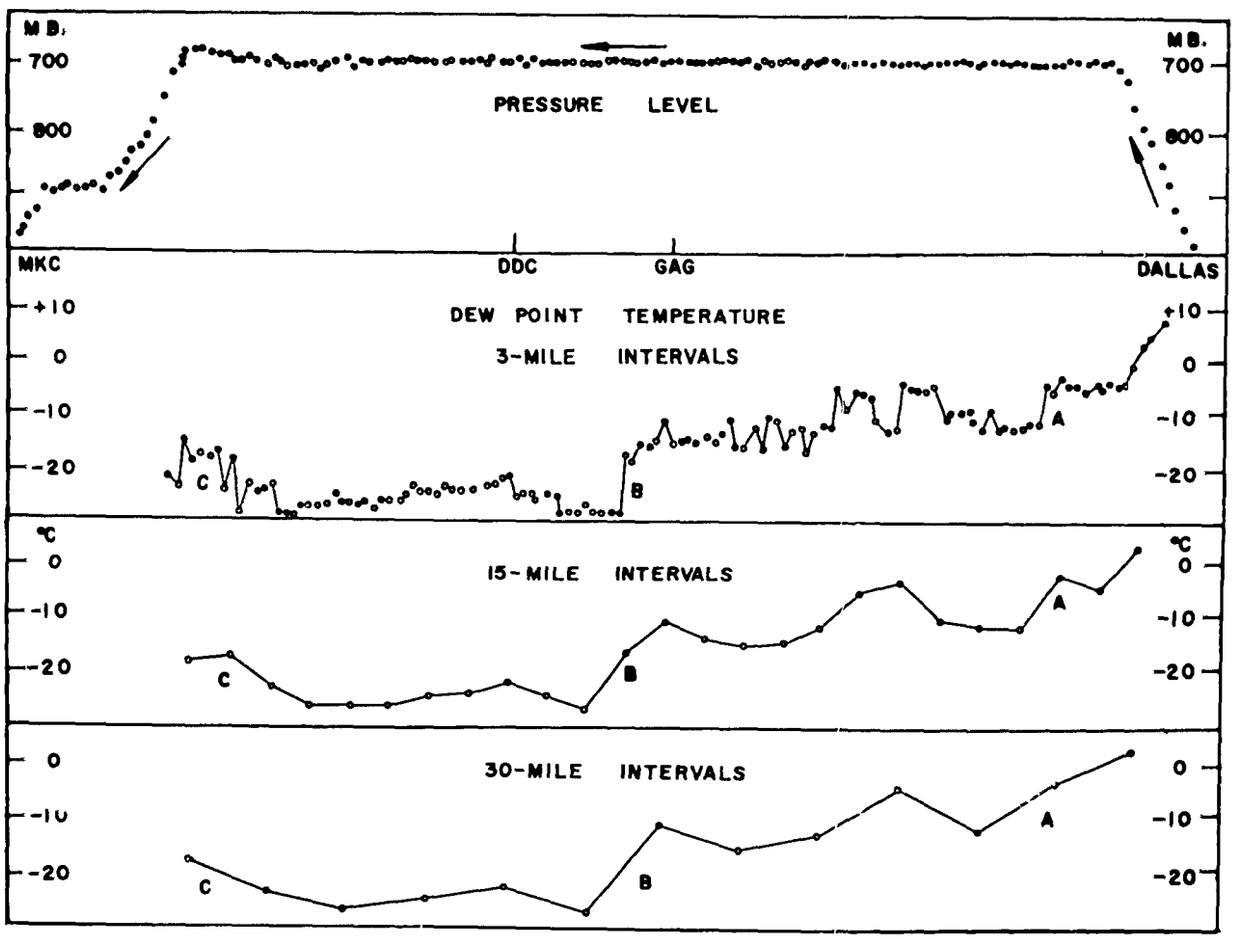

Fig. II.B.10. Dew-point temperature distribution at 700 mb as described by values at 3, 15, and 30-mile intervals.

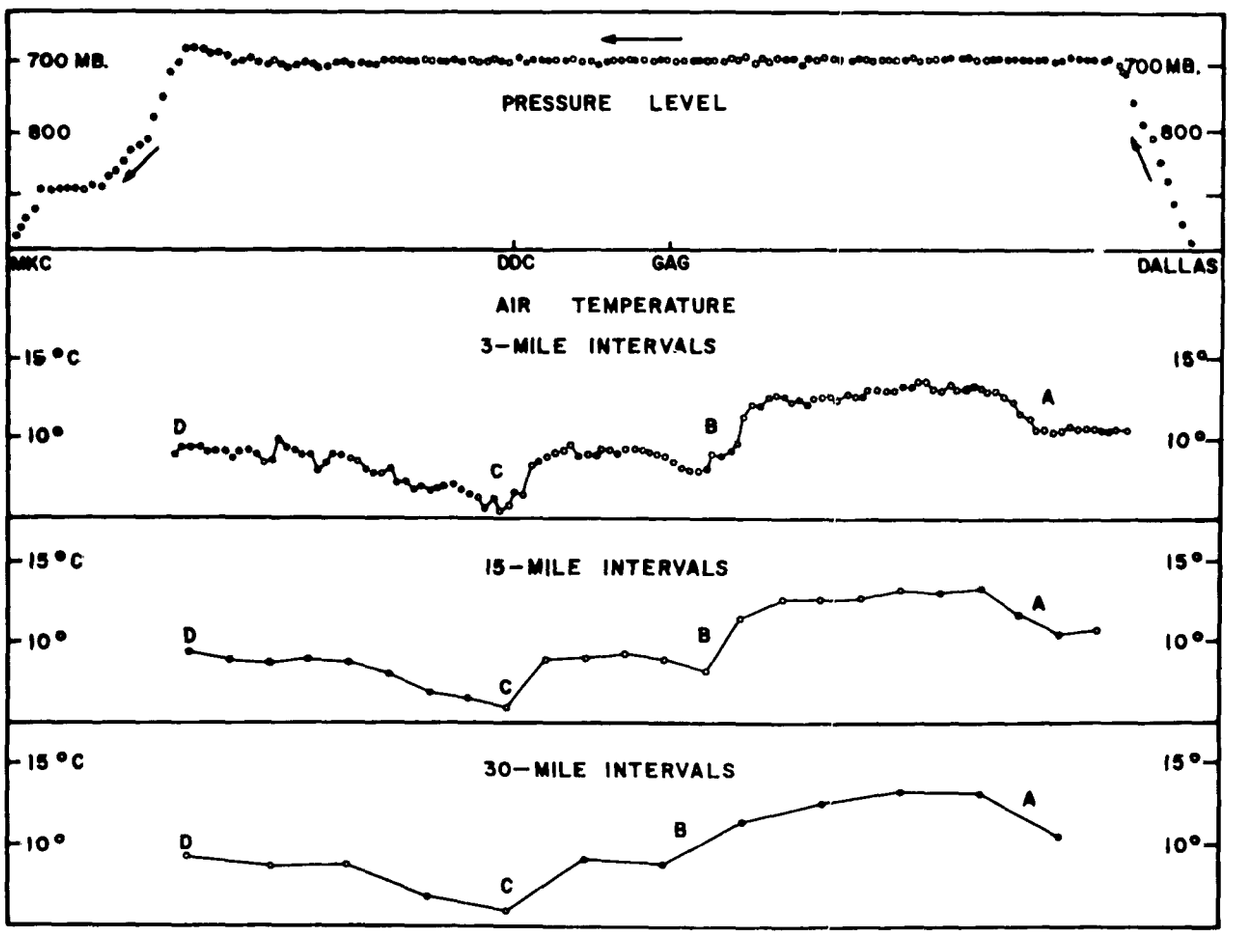

Fig. II.B.11. Temperature distribution at 700 mb represented by values at 3, 15, and 30-mile intervals.

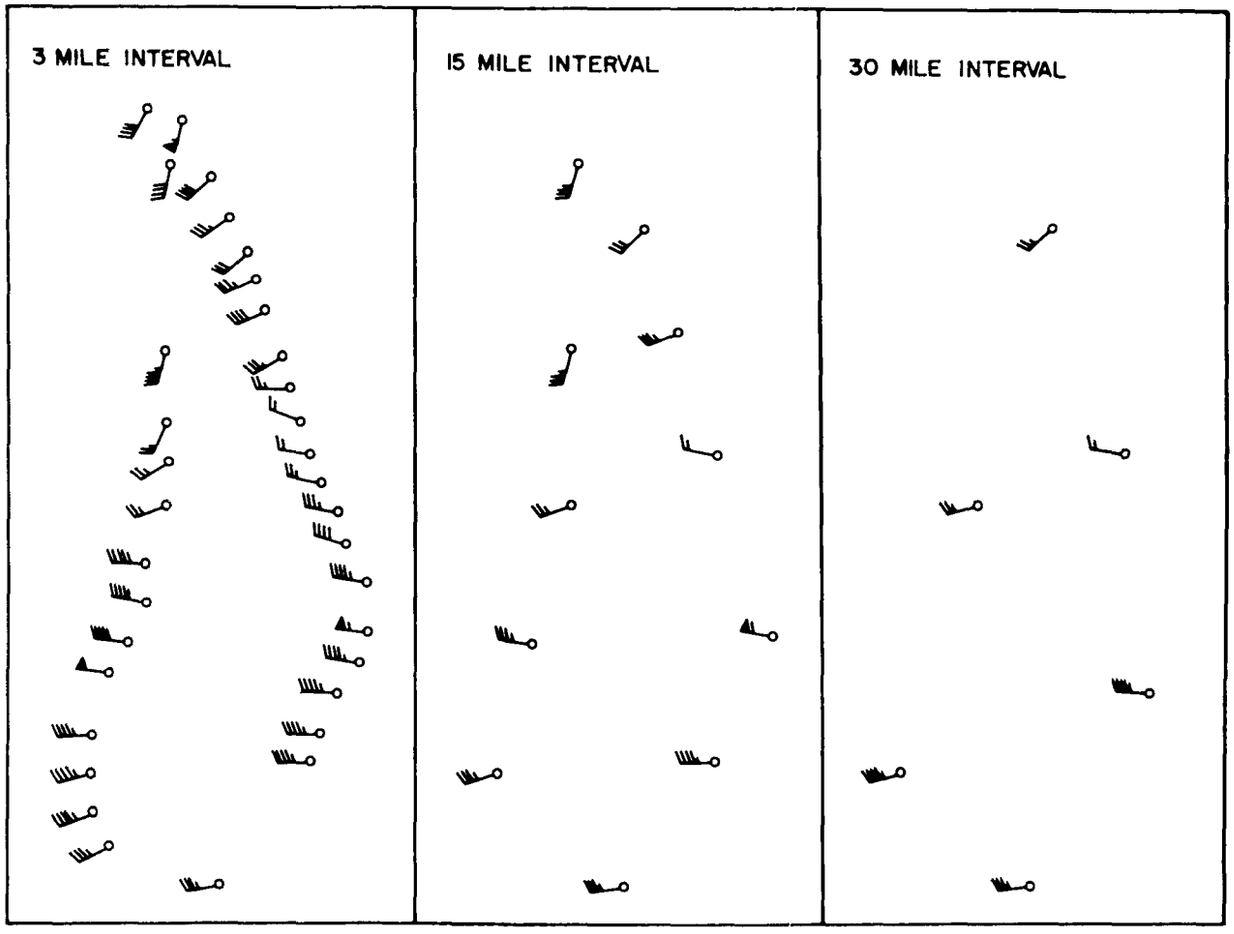

Fig. II.B.12. Wind distribution at 36,000-40,000 foot level represented by values at 3, 15, and 30-mile intervals.

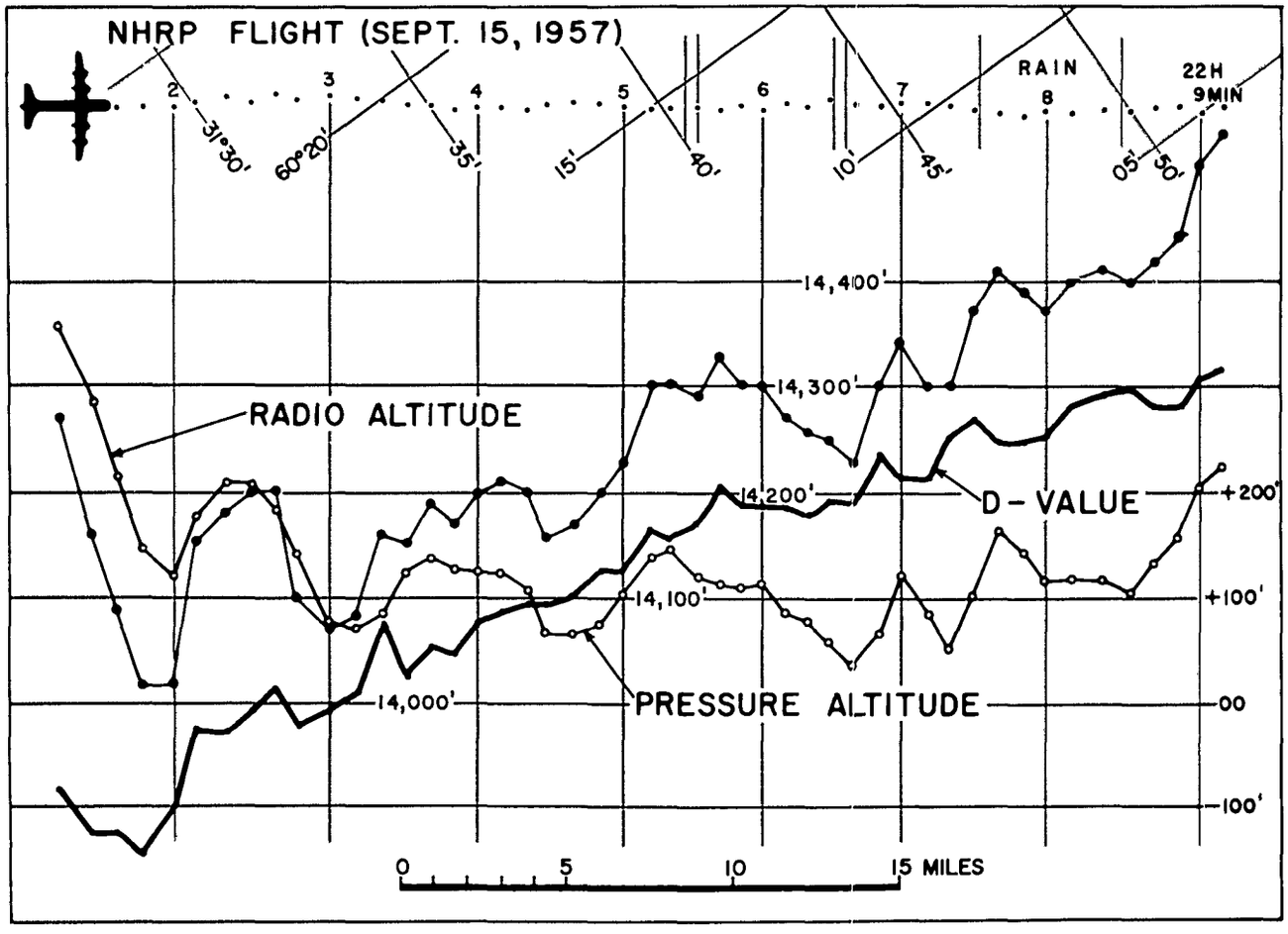

Fig. II.B.13. D-value, pressure and radio altitude measured at 10-second intervals.

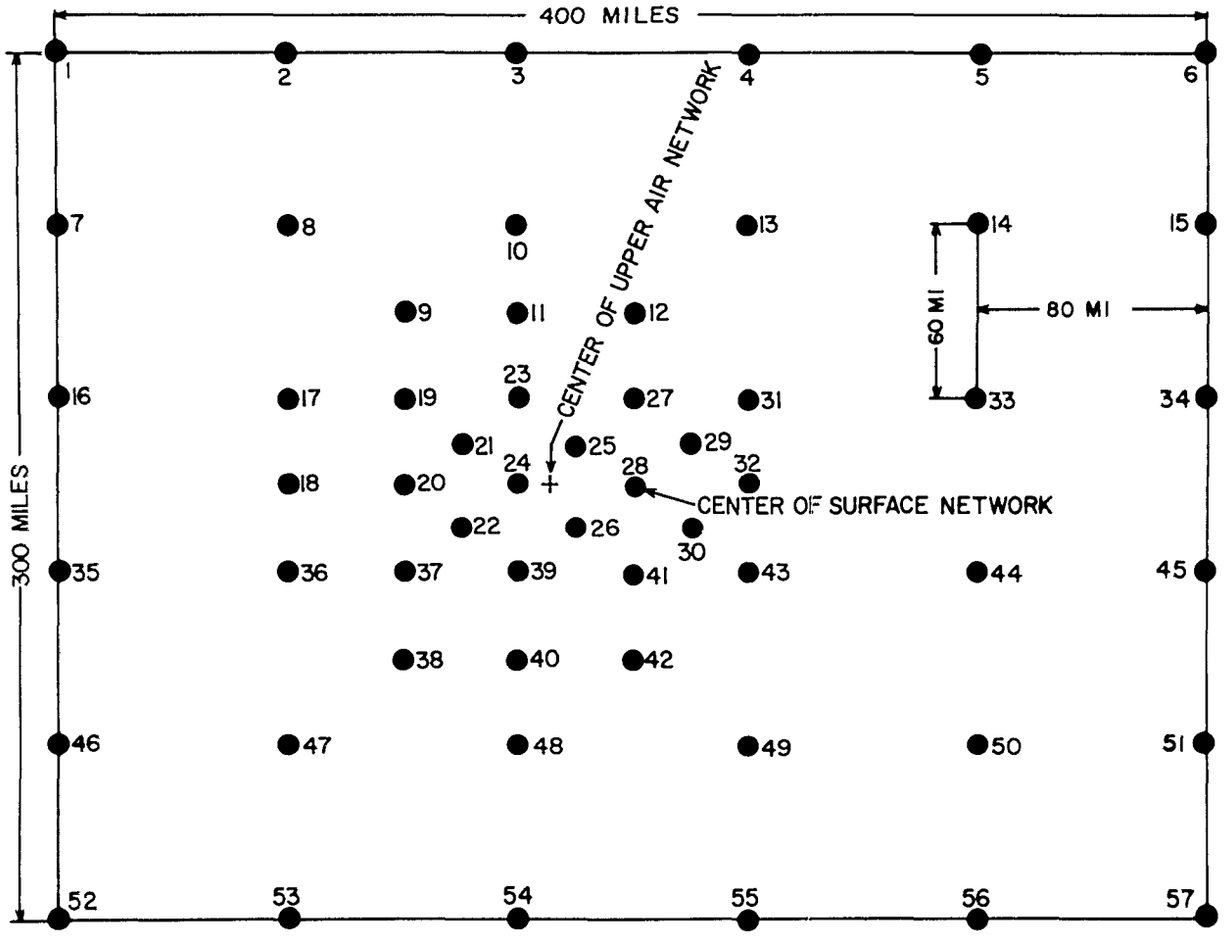

Fig. II.B.14. Distribution of rawinsonde stations within a 300 x 400-mile surface network area.

C. RADAR

The tremendous potential of ground-based radar as a meteorological instrument, especially in the mesoscale, has been emphasized for several years by numerous writers (1; 2). It has been conclusively shown that echoes can be obtained from tornadoes, hail, snow, and lightning, and from precipitation associated with layer-type clouds, convective clouds, thunderstorms, and hurricanes. Non-precipitating echoes (e.g., thin lines) may with further research provide information as valuable as precipitation echoes.

The value of knowing the distribution and type of precipitation over areas of the order of 120,000 square miles has been fully appreciated but only partially exploited. The radar meteorologist has been faced with great difficulties in relating the radar observation to surface phenomena. These difficulties are due principally to the fact that radar is essentially a mesometeorological instrument and has far outstripped the capabilities of its surrounding synoptic or larger scale network for delineating the detail of weather patterns. Indeed, only two complete surface networks, the Florida and Ohio Thunderstorm networks, have ever approached the quality of a radar in relating the detail of mesoscale systems.

As stated previously, the purpose of this report is to design a network capable of resolving mesoscale systems in time and space. The position which radar will hold in this design is basic and fundamental.

1. TYPES OF RADAR

The type of radar in a mesometeorological network should be determined principally by the role it is to perform. The K, X, C, S, and L-band radars (1, 3, 5, 10, and 20-centimeter wave lengths) vary widely in their detection capabilities, which depend on, among other things, the wave length of the set.

This can be illustrated through reference to the following equation:

$$K = \frac{\bar{P}_r}{P_{r(min)}} = \frac{\pi^5}{72}\left(\frac{P_t \theta \phi h A_p^2}{\lambda^6 P_{r(min)}}\right)|K|^2 \frac{Z}{r^2} F \qquad \text{II.C.1}$$

where $\bar{P}_r$ is the received average power of each echo pulse; $P_{r(min)}$, the minimum detectable power, P_t, the transmitted pulse power; A_p^2, the apertural area of the antenna; θ and ϕ, the horizontal and vertical widths of the focused beam; λ, the wave length of the radiation; h, the pulse length; $|K|^2$, a dimensionless function of the complex refractive index of the scatterer; r, the range of the target; Z, the "reflectivity factor", denoting the density within the reflecting volume of the diameter of the reflecting particles to the sixth power; and F, the attenuation factor.

All terms within the parentheses are characteristic of a particular radar. Examples of the characteristics of two radars, the AN/FPS-41 and the AN/CPS-9, are shown in Table II.C.1.

	AN/FPS-41	AN/CPS-9
P_t (w)	5.0×10^5	2.5×10^5
λ (cm)	10.0	3.2
h (μ sec)	1/2 or 4	1/2 or 5
PRF	800 or 200	931 or 186
Antenna shape	circular	circular
Antenna diameter (m)	3.7	2.36
θ	1.8	1.0
ϕ	1.8	1.0
Minimum detectable P_r	10^{-13} to 10^{-15}	1.6×10^{-13} or 1.6×10^{-14}

Table II.C.1. From Battan, Radar Meteorology (3).

These two 10 and 3 cm sets are similar in pulse length, h; pulse repetition frequency, PRF; antenna shape; and minimum detectable power return, $P_{r(min)}$.

Their major difference is in the operating wave length, other differences being the transmitted power, P_t, and the size of the antennas and their corresponding beam widths.

Using the Rayleigh approximation to the Mie backscattering theory for spherical particles, it can be shown that the 3 cm set is capable of detecting particles about three orders of magnitude smaller than those detectable with the 10 cm set. By the same token, however, it can be shown that the precipitation attenuation of the radiated beam is greater for the 3 than for the 10 cm set. It might be stated at this time that, aside from the initial purpose of studying meso-systems, the network could play a vital role in assessing the quantitative results produced by various instruments in the detection of the same phenomena. Because of its past proven performance, narrow beam width, and mobility, the 3 cm set would prove extremely valuable to the mesometeorology network. At the same time, the use of a 10 cm set during periods of heavy rainfall would provide an independent check on the attenuation problem.

In addition to the above radars there is also need in a mesometeorology network for two other types: (a) one capable of rapidly scanning a precipitating storm system and displaying and recording three-dimensional data, such as the U. S. Army Signal Research and Development Laboratory modified AN/MPG-1, and (b), a radar system (Doppler) capable of rapidly determining the three-dimensional velocity distribution in a precipitating volume.

2. DISPLAY

There are several types of radar display that are suitable for analysis and data collection (4). The PPI or plan-position-indicator is fundamental to the display function of a radar. The qualitative information obtained from the PPI scope of an uncalibrated radar can be made quantitative in several ways.

In the first method (stepped gain or stepped sensitivity), the received signal is reduced by fixed amounts between consecutive sweeps of the antenna, thereby eliminating the weaker returns and isolating the stronger. Analyses of echoes

obtained in this manner are illustrated in Fig. II.C.1. The intensities of different echoes are still difficult to relate because of range attenuation. A solution to this problem is to incorporate a circuit in the radar that will attenuate the returning signal in a manner inversely proportional to the square of the range of the echo.

This method appears to be preferable both to iso-echo contouring, that is the alternate deletion of backscattered power within certain limits so that alternate or concentric bands of return are presented on the scope; and to stepped gray scaling, that is, the indication of stronger intensities by deeper shades of gray.

Another method, consisting of elevating the radar antenna through a series of angular steps until all echoes are eliminated, indicates intensities indirectly by determining echo tops. An example is shown in Figs. II.C.2 and 3. Time of observation is shown on the clock in the upper right of each photograph; also shown is the date, range marker interval (in this case, 25 miles), sensitivity time control on or off (on in all photos except the first), and frame number. The PPI scope contains concentric rings representing range, azimuth angles representing degrees from true north, a mark indicating the elevation angle, and the precipitation echoes themselves. It is clear that the last echo disappeared between an antenna elevation angle of 13 and 14 degrees. The time taken to complete a cycle depends on the rotation rate of the antenna, the number of angular steps taken, and the maximum height of the cells nearest the radar. In this case approximately five minutes elapsed. The angular variation also serves to determine and eliminate ground clutter or permanent echoes. Figure II.C.4 shows photographs taken at various elevation and depression angles of a radar situated in Montana. The corresponding topographic chart is given in Fig. II.C.5.

Other useful methods of displaying precipitation echoes include RHI (range-height-indicator), off-center PPI, A and R scope. For a vertically scanning 1 cm radar set, THI presentation on a facsimile chart or on a moving film should be used.

3. METHODS OF RECORDING RADAR OBSERVATIONS

The most suitable method of recording radar observations for subsequent analysis is photography. Consideration must be given to the timing of the photographs,

the size of film for recording purposes, the data panel, and the use of repeater tubes.

A separate display tube for each radar in operation is necessary in order to allow the operator freedom to manipulate range settings while maintaining consistency in photography. The photographed display tube should be equipped with a data panel indicating the date, time, station, pulse length, range, receiver, gain, elevation angle of the antenna, and a digital counter indicating the frame number of the exposure. Some automatic indication of the azimuth of the radar during RHI operation would be extremely helpful to the analyst. In the construction of the data panel, care should be taken not to overlook the main purpose of placing as large a representation of the radar echoes on the film as possible. If a satisfactory balance can be obtained, the recording of data on 16 mm film might achieve the necessary results with an economy of storage and of initial and subsequent expenses involved in developing, analysis, and projection. If, however, preliminary tests indicate that the quality of the record would suffer, 35 mm film should be utilized. In addition to the automatic time-lapse recording of the scope, a more nearly instantaneous method of obtaining data through the use of a Polaroid Land camera should be available.

4. NUMBER OF RADARS TO BE USED

For most small mesoscale studies the use of a single radar has proved to be satisfactory; for a network on the order of 300 x 400 miles, however, it becomes necessary to consider more than one radar. Ligda, et. al. (6) and Fujita (7) have clearly demonstrated the value of synoptic data from numerous radars. Figures II. C. 6 and 7 show a composite study made by Fujita using four radars. The upper figure shows the echoes obtained by the individual radar sets; and the lower figure illustrates the resulting composite which has accounted, as much as possible, for the finite beam width effect at large ranges.

A combination of six radars--either a 1, a 10, and two 3 cm sets, or a 1, a 3, and two 10 cm sets, plus two additional research radars--is recommended for the network. Two sets (3 and 10 cm) should be located at one site at a distance of 80-100 miles from the other set (3 or 10 cm). The sites should be chosen so that

the β network lies equidistant between them. The 1 cm set should be located at the center of the β network (an area of cloud camera surveillance) and operated as a vertically pointing cloud-height-time instrument. The 3 and 10 cm radar sets should be synchronized to the extent that during a selected period all sweep at the same rpm and go through the same variable elevation or stepped-gain program. In addition, provision should be made to locate the two research radars--one to provide three-dimensional data, the other to provide three-dimensional velocity data--down wind of the β network.

5. RESEARCH POTENTIAL

The research potential of radar is being realized by numerous groups throughout the country. Until the present time, however, no adequate surface or upper-air network has existed within range of the radars. It seems quite likely that the full potential of radar will never be realized until this inadequacy has been eliminated.

As an example of the type of problem that should be handled by the meso-meteorological network and could be solved by it, a study (8) was made of radar echoes that we believe to be caused by abrupt refractive index gradients along a zone separating thunderstorm-modified air from maritime tropical air (9; 10).

The radar data for this case were supplied by the Radar Meteorology Section of the A. and M. College of Texas. The main objective was to gather as much data as possible from the surrounding area in order to determine at least the surface weather changes accompanying the "thin lines" and the station spacing that might be necessary to study them fully. The surrounding network, illustrated in Fig. II. C. 8, consists of recording microbarographs, hygrothermographs, raingauges, and wind velocity equipment. The ground clutter pattern at an antenna elevation angle of 1 degree is shown extending out to the 25-mile range.

The data were taken from four days in August, 1958. Only two days will be discussed here; a more complete description is given in (8). Figures II. C. 9 and 10 show the radar photographs on August 4. At 1600 C there is a thin line west of the

echo group 40 miles southeast of the radar site. Another thin line can be detected to the northeast at about 55 miles. These thin lines moved to the west and southwest, respectively. The thunderstorm echoes apparently associated with them dissipated in the meantime. It can be seen that new thunderstorms formed along the intersection of the lines from 1629 C to 1730 C. Range height observations taken at 1615 C along an azimuth of 65 degrees revealed that the thin line had a vertical extent of 6000-8000 feet.

On the following three days, August 5-7, thunderstorms and thin lines were again observed. Figure II.C.11 shows the sequence of events on the 7th. With close scrutiny, two apparently different thin lines can be detected at 1700 C: one almost coincident with the thunderstorm cells 40 miles to the east and southeast, the other with no cells 45-50 miles to the southeast. It is not unusual to detect thin lines first at the 50-mile range, for their low height makes them invisible at greater distances even to a radar at a zero antenna setting. By 1732 C the thin lines had moved farther to the west and northwest approaching the radar site, the northern line breaking away from the thunderstorms and finally moving into the ground clutter pattern.

A method of analysing individual echo motion and development has been described by Fujita (5) and Fujita and Brown (11). Figure II.C.12 illustrates the procedure, a simple geometrical calculation which consists of determining the displacement of an echo over a given period of time. At the same time (through stepped-gain pictures) it is possible to determine the intensity changes of the echo, or if variable elevation angle photographs are available, the height variation.

The echoes of the 4th and 7th of August were subjected to this type of analysis, with the results shown in Figs. II.C.13, 14, and 15. The stippled areas are thunderstorm echoes. The thin lines are shown as thin broken or solid lines in an attempt to represent them as realistically as possible. The radar site may or may not appear on the center time line, depending on the size of the radar surveillance sector used in the construction. Time is adjusted along the center line, however, so that all echoes can be related to the radar site. For example, in Fig. II.C.13, the radar site at 1600 C is located at the large circle at the top of the north-south line. The thin line is joined to the station circle by a straight line. By 1702 C,

reconstruction of this straight line from the radar site to the original thin line position shows the motion of the thin line to the south and west. This thin line passed only two network stations: raingauge station no. 15 between 1646 and 1702 C (which, incidentally indicated no rain at the time of passage), and Brenham (BRN), a microbarograph-hygrothermograph-raingauge station. Another radar time section constructed to the northeast-southwest (Fig. II. C. 14) shows the passage of the thin line at Madisonville (MAD) between 1717 and 1730 C. Huntsville (HNT) was behind the thin line at the time of its first appearance on the radar scope at 1646 C.

The situation on August 7 (Fig. II. C. 15) was extremely interesting because it indicated what appears to be the amalgamation of cellular mesosystems into larger scale mesosystems as described in (12). At 1700 and 1720 C the cellular structure of the thin lines is quite obvious. Reference should be made to Figs. II. C. 2 and 3, which show photographs between these two times. A nomograph (Fig. II. C. 16) was used to solve for echo tops (5000-70, 000 feet) in terms of range and elevation angle of disappearance. The cell heights ranged from 20, 000 feet for the small isolated echoes to the north and east, through 45, 000 feet for the northern cell of the thin line group and the cell far to the south-southeast, to 53, 000 feet for the cell 70 miles southeast of the station. The thin lines continued to move west and northwest into the ground clutter pattern. Continued movement at the same speed indicates that they would have passed the radar site at Texas A. and M. at approximately 1900 C and Brenham (BRN) at about 1820 C.

The changes that occurred at the relatively few stations passed by a thin line on these two days can be seen in Figs. II. C. 17 and 18. On August 4 at 1730 C, the change in temperature, humidity, and pressure at Madisonville was not accompanied by rainfall at the thin line passage, although a precipitation cell was in the neighborhood. Changes at Huntsville and Brenham were not so dramatic, probably because of the age of the thin line and the small pressure variation that would in any case be expected to accompany it.

On August 7, some slight changes were apparent at Madisonville (MAD) at 1700 C, and much more striking changes were apparent at Brenham (BRN) and

Texas A. and M. The times of these changes in pressure, temperature, humidity, and wind direction and speed coincide quite well with the passage of the thin line.

It has become very apparent from this study that a mesonetwork, with station spacing and time and space resolution consistent with the previous recommendations, would be equipped to solve problems of this or a similar nature, e.g., sea breeze circulations, space and time changes of inversions, cloudless or dry cold fronts, turbulent layers, or the many problems associated with the three-dimensional space and time variation of squall line mesosystems. The utilization of a sferics network (13) within the mesonetwork, together with current methods of presenting observations rapidly and visually (14), would prove a valuable tool to the mesoanalyst for locating lightning within and surrounding the network.

REFERENCES

1. Ligda, M. G. H., 1951: Radar storm observation, Compendium of Meteor., AMS, Boston, 1265-1282.

2. Swingle, D. M., and L. Rosenberg, 1953: Mesometeorological analysis of cold front passage using radar weather data, Proc., Conf. on Radio Meteor., Univ. of Texas, Austin, p. XI.5.

3. Battan, L., 1959: Radar meteorology. Univ. of Chicago Press, 161 pp.

4. Jones, R. F., et.al., 1959: Use of ground-based radar in meteorology. Tech. Note No. 27, WMO, Geneva.

5. Fujita, T., 1958: Mesoanalysis of the Illinois tornadoes of 9 April 1953, J. Meteor., 15, 288-296.

6. Ligda, M. G. H., et.al., 1957: Middle latitude precipitation patterns as observed by radar (A collection of composite radar observations). Texas A. & M. Sci. Rep. No. 1, Contract AF 19(604)-1564.

7. Fujita, T., 1959: Study of mesosystems associated with stationary radar echoes, J. Meteor., 16, 38-52.

8. Brown, H. A., 1960: Report on radar thin lines, Proc. 8th Wea. Radar Conf., San Francisco.

9. Ligda, M. G. H., and S. G. Bigler, 1959: Radar echoes from a cloudless cold front, J. Meteor., 15, 494-501.

10. Luckenbach, G., 1959: Some non-precipitation radar echoes as observed by CPS-9 radar. Unpub. thesis, Texas A. & M.

11. Fujita, T., and H. A. Brown, 1958: A study of mesosystems and their radar echoes, BAMS, 39, 538-554.

12. Fujita, T., H. A. Brown, and Y. Omoto, 1959: Design of a three-dimensional meso-meteorological network. First Quarterly Tech. Rep. to USASRDL, Contract No. DA-36-039 SC-78901.

13. Wanta, R. C., 1951: Sferics, Compendium of Meteor., AMS, Boston, 1297-1300.

14. 1960: New weather warning system under test, Weatherwise, 13, 63.

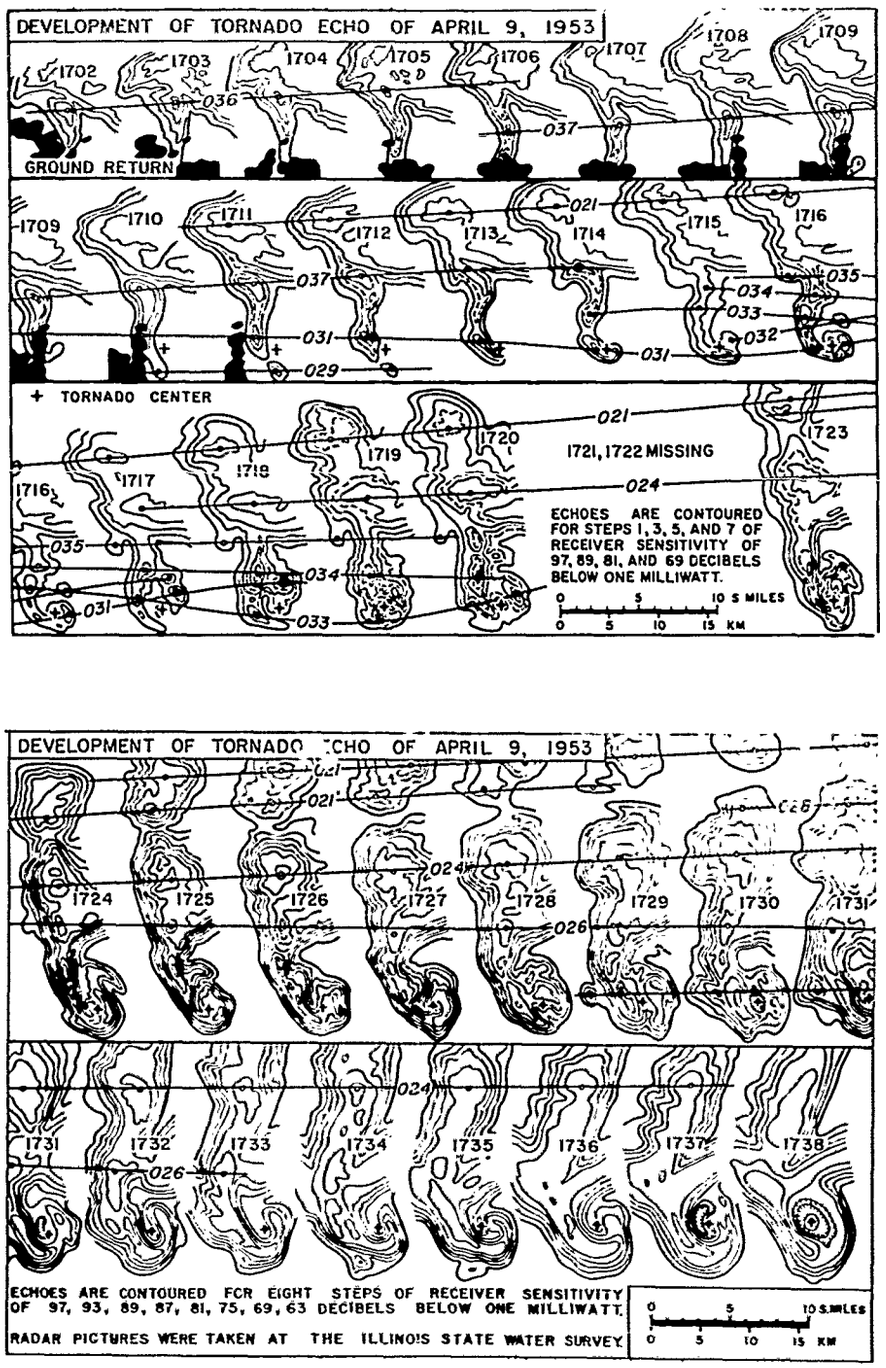

Fig. II.C.1. Development of pendant echo of the Champaign tornado from 1702-1738 CST. From Fujita (5).

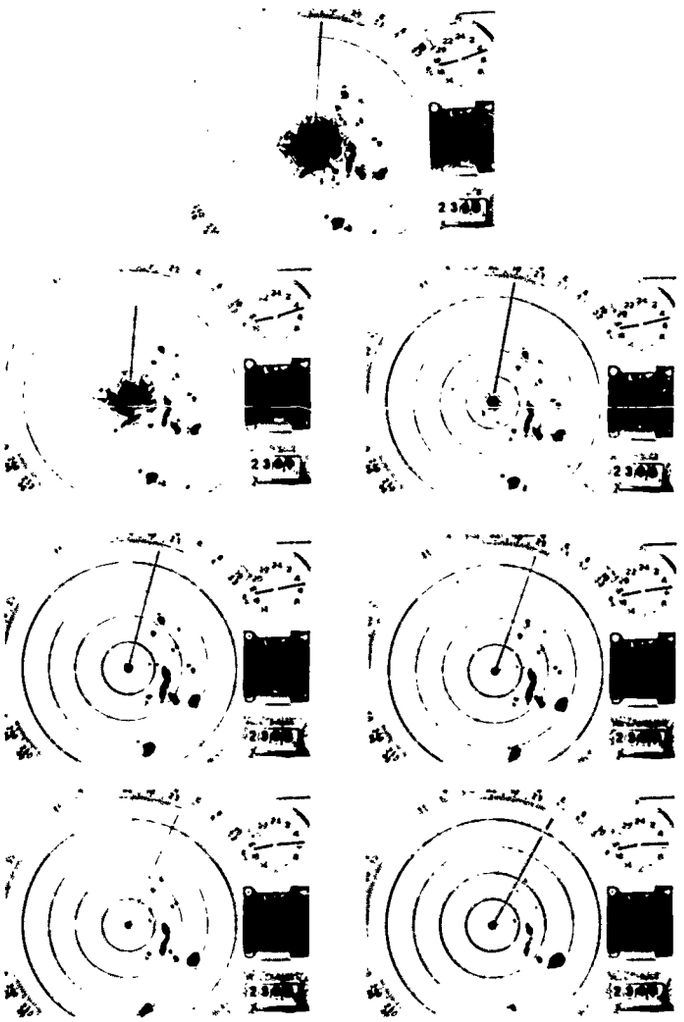

Fig. II.C.2. Variation of Texas A & M CPS-9 radar antenna elevation angle (1^{o}-6^{o}) on August 7, 1958.

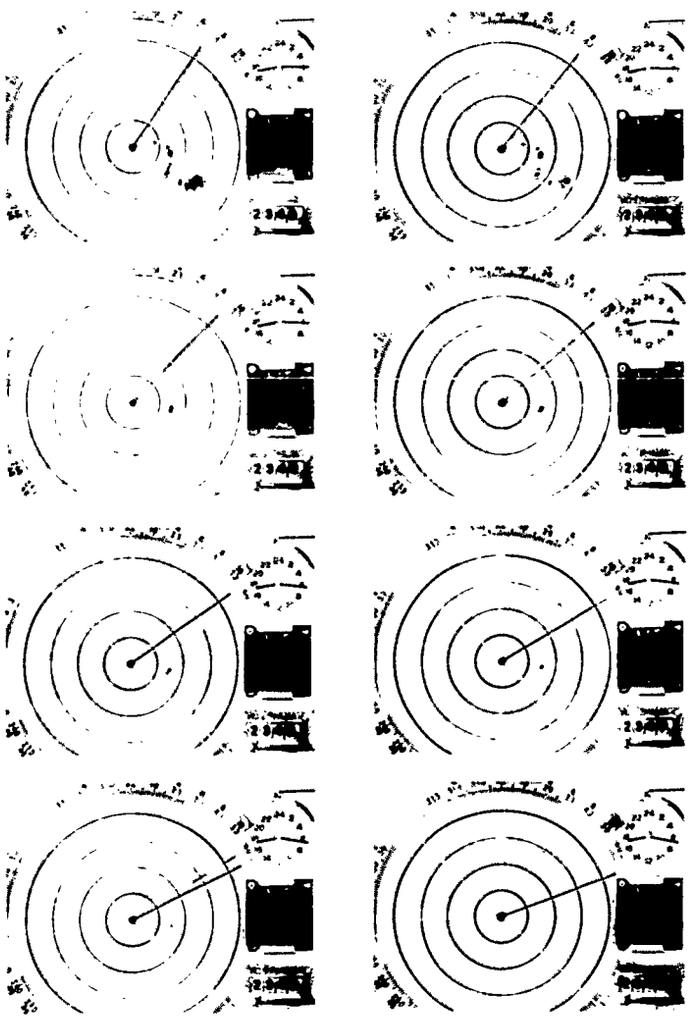

Fig. II.C.3. Variation of Texas A & M CPS-9 radar antenna elevation angle (7^{o}-14^{o}) on August 7, 1958.

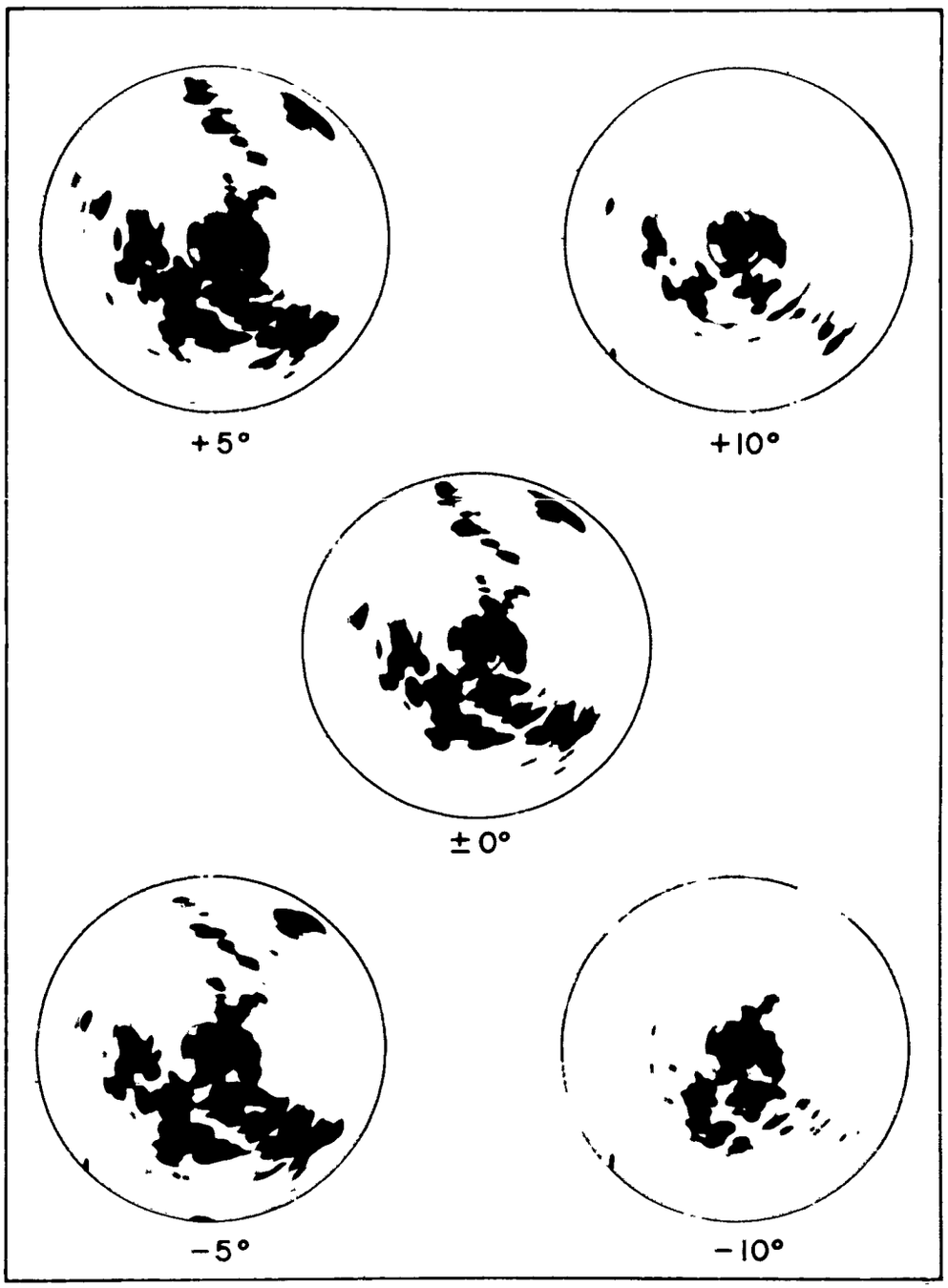

Fig. II.C.4. Ground clutter of Marpeak radar, Montana.

Fig. II.C.5. Topography inside the area of effective radar range.

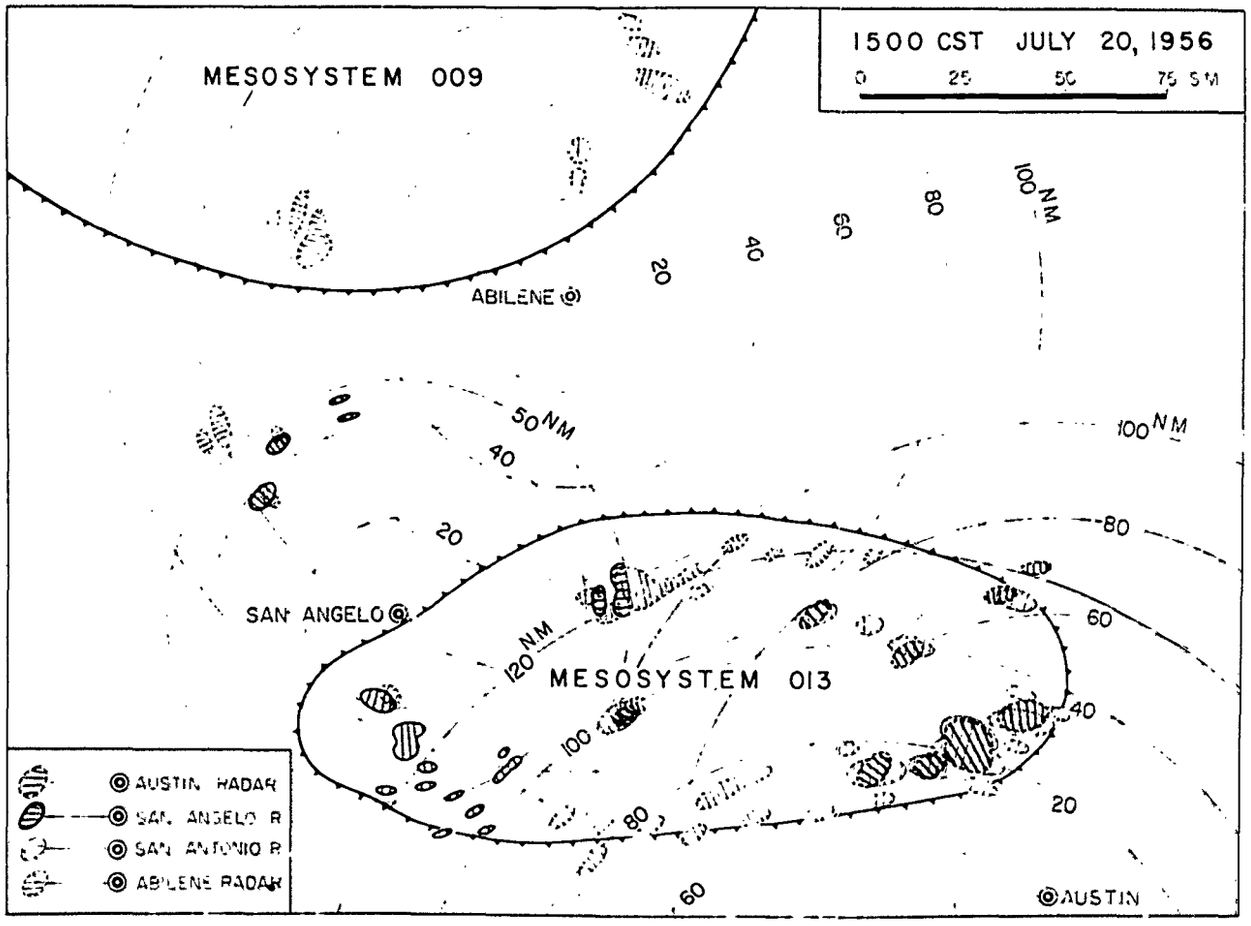

Fig. II.C.6. Construction of composite radar echo chart. Hatched lines converge to radar site.

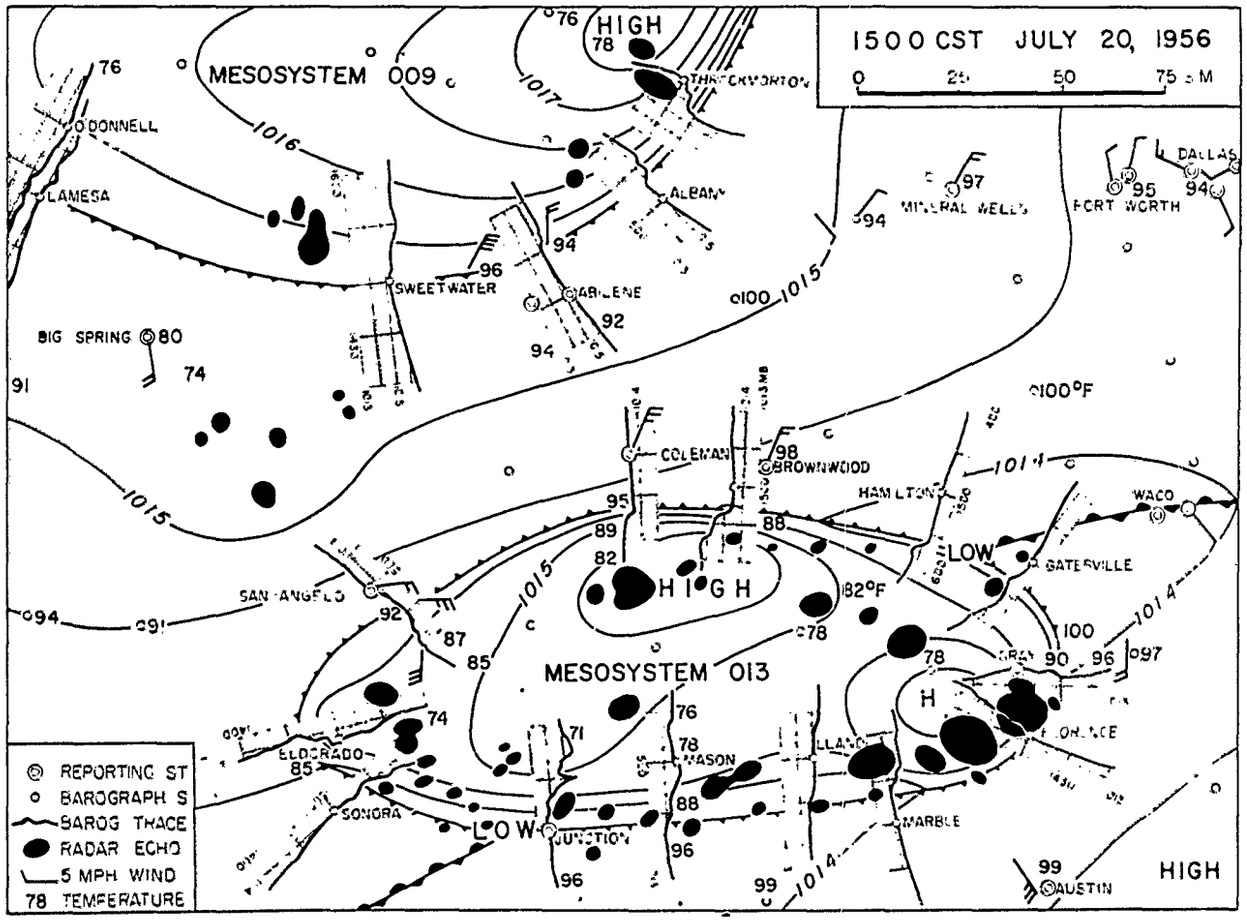

Fig. II.C.7. Mesoanalysis of same area. Time sections are converted to space sections along vectors perpendicular to system boundary. Composite echoes in black. From Fujita (7).

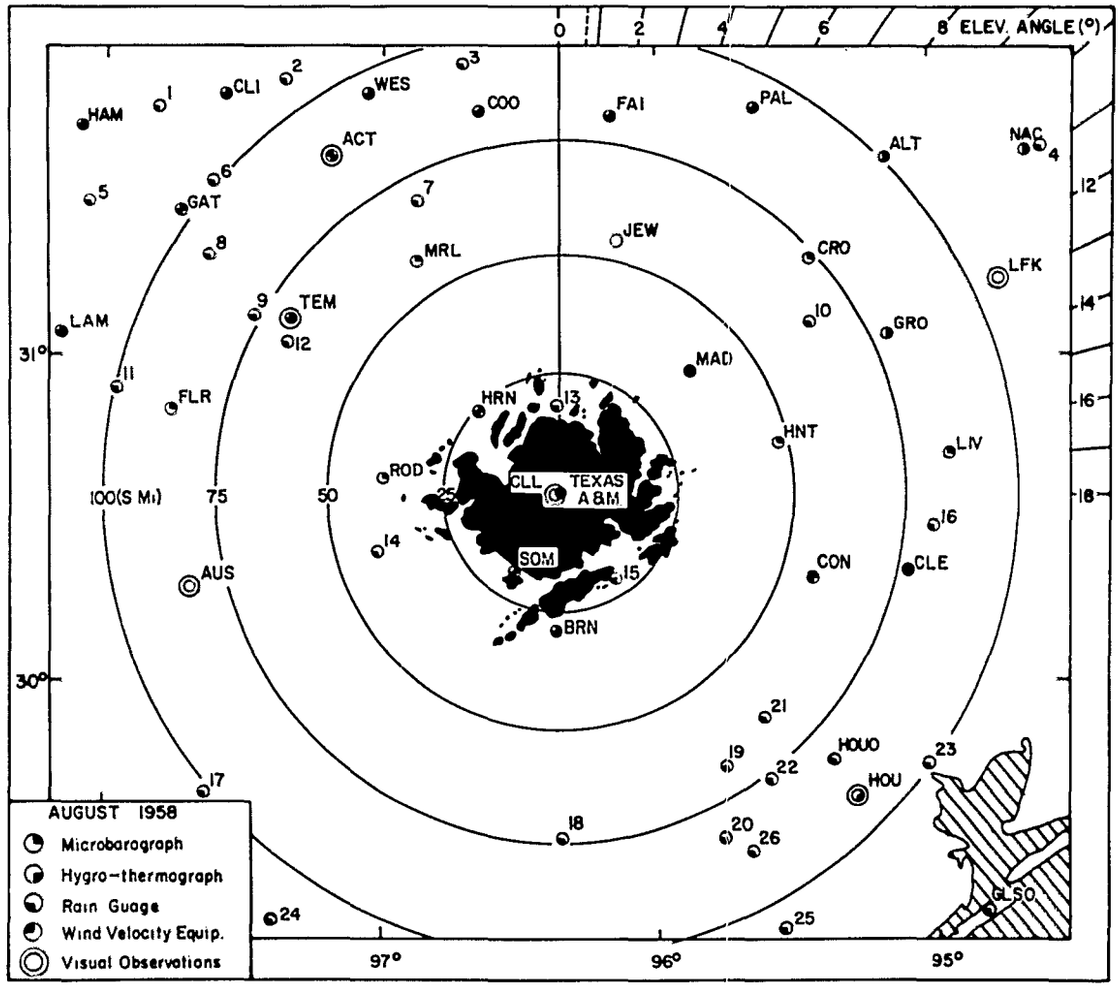

Fig. II.C.8. Surface network surrounding Texas A & M CPS-9 radar.

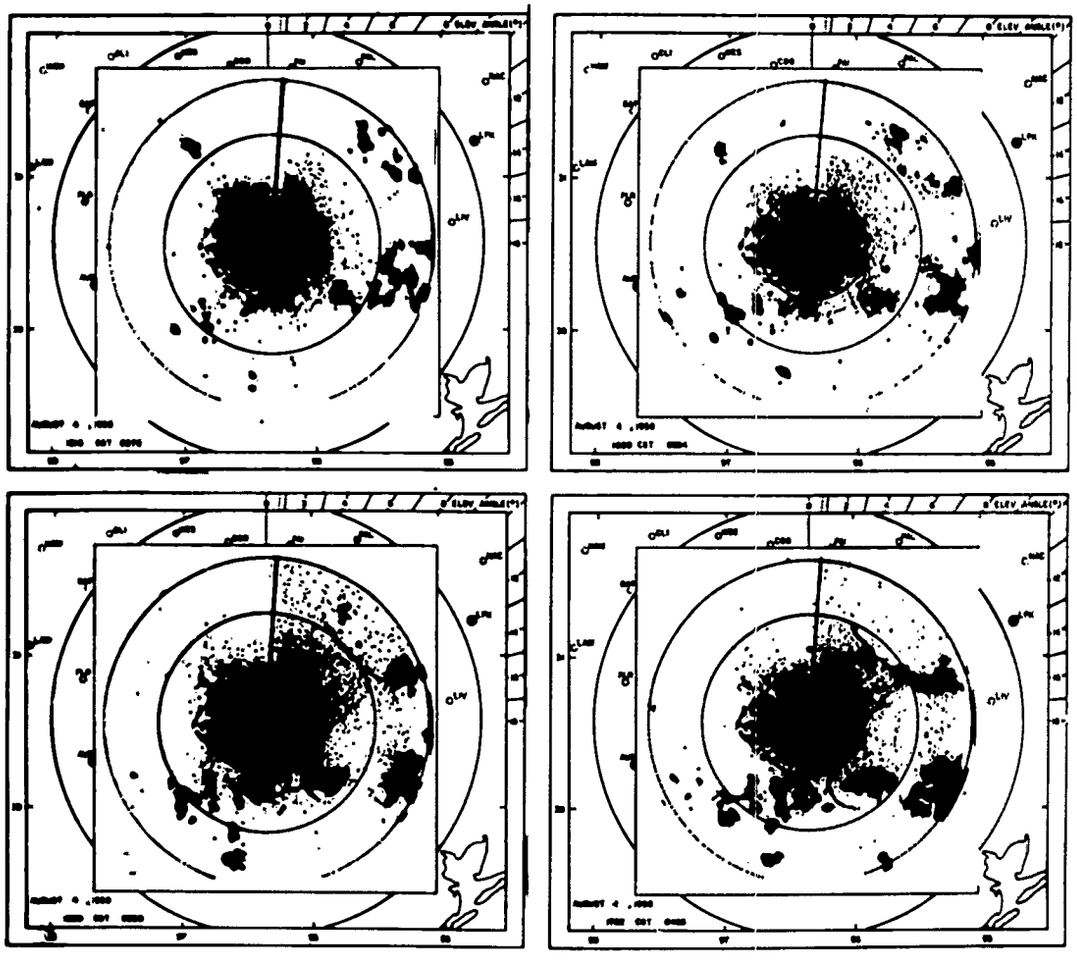

Fig. II.C.9. Radar echoes on August 4, 1958, 1515-1702 C.

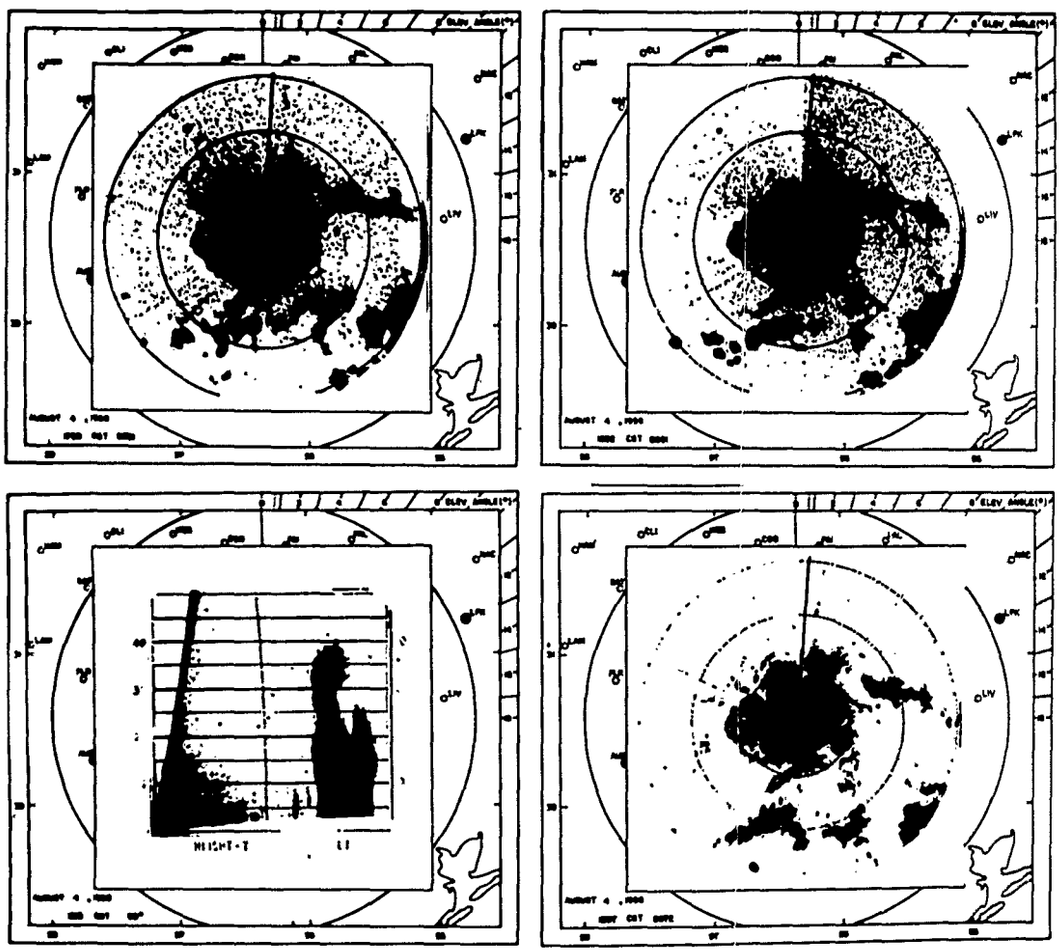

Fig. II.C.10. Radar echoes on August 4, 1958, 1730-1837 C.

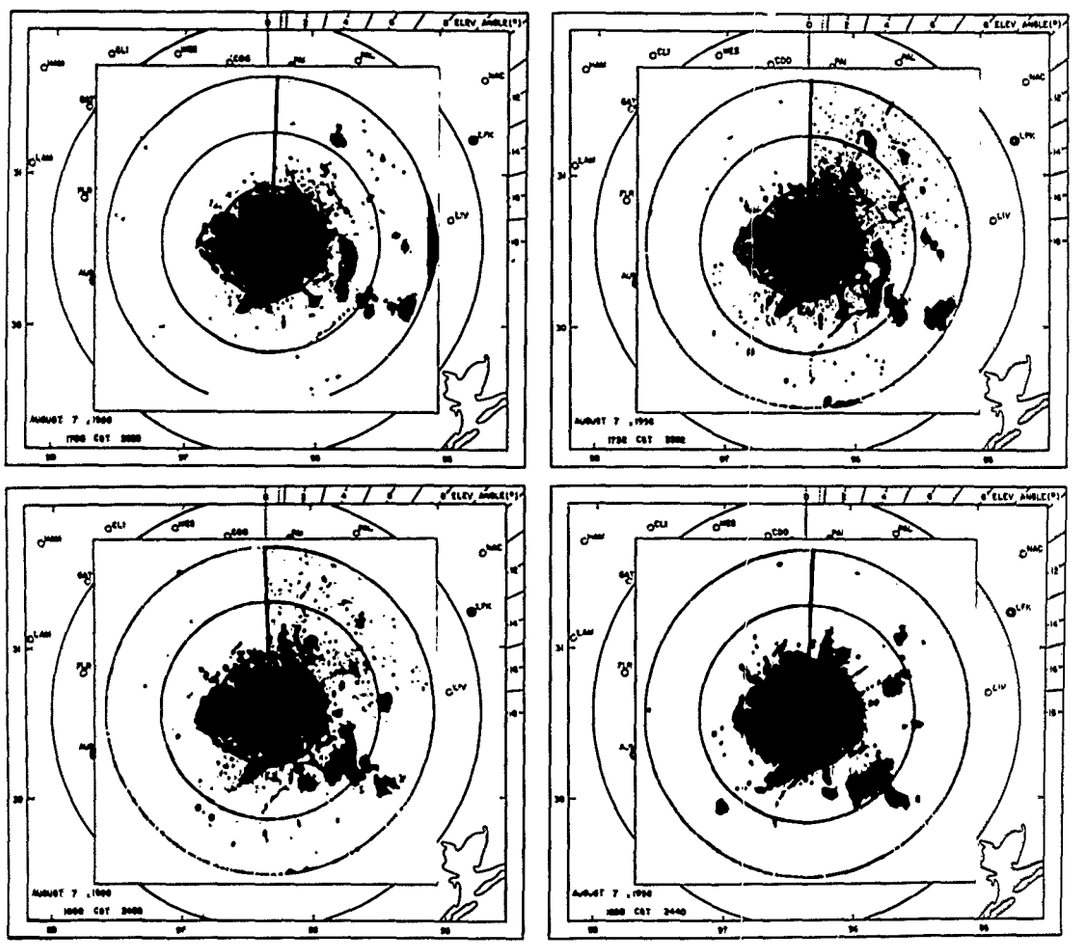

Fig. II.C.11. Radar echoes on August 7, 1958, 1700-1830 C.

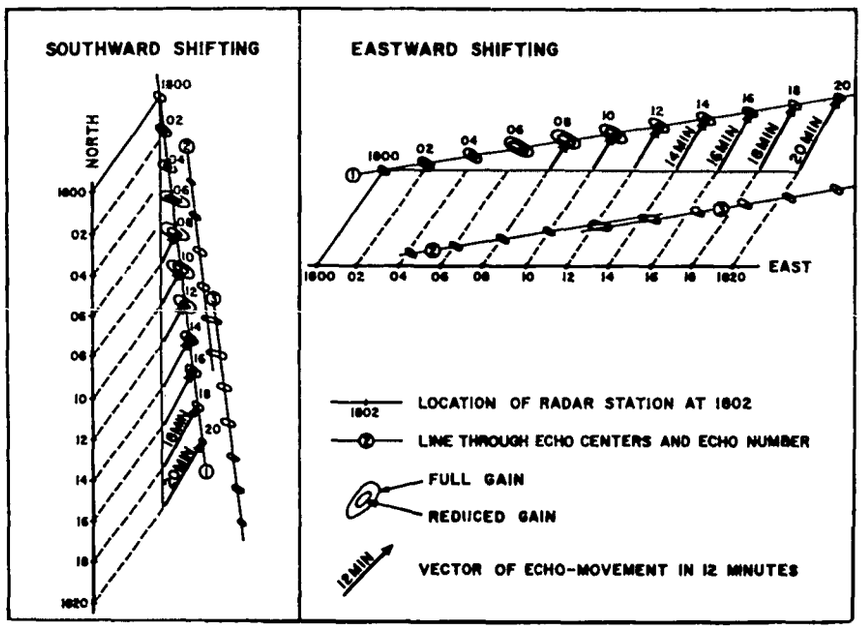

Fig. II.C.12. Technique for obtaining velocity and intensity change of radar echoes. From Fujita (5).

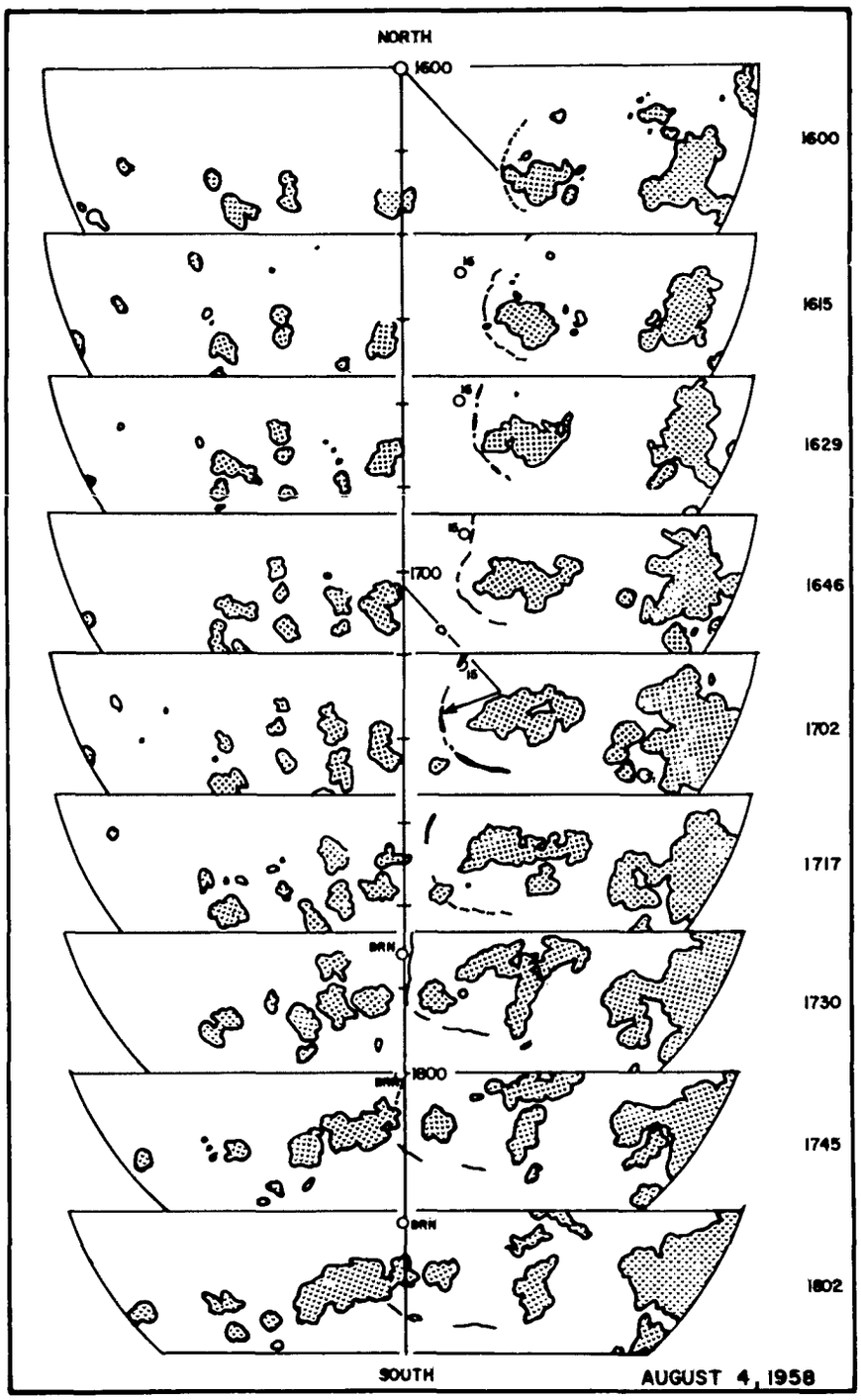

Fig. II.C.13. North-south radar time section, August 4, 1958, 1600-1802 C.

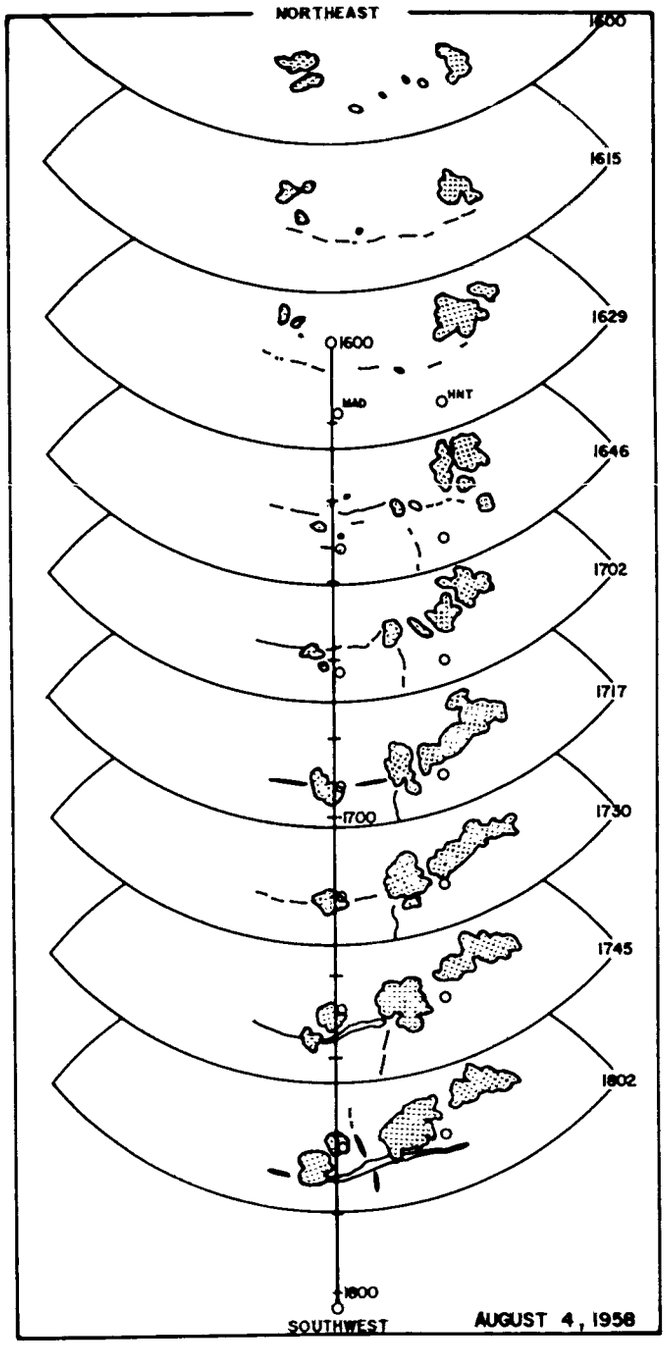

Fig. II.C.14. Northeast-southwest radar time section, August 4, 1958, 1600-1802 C.

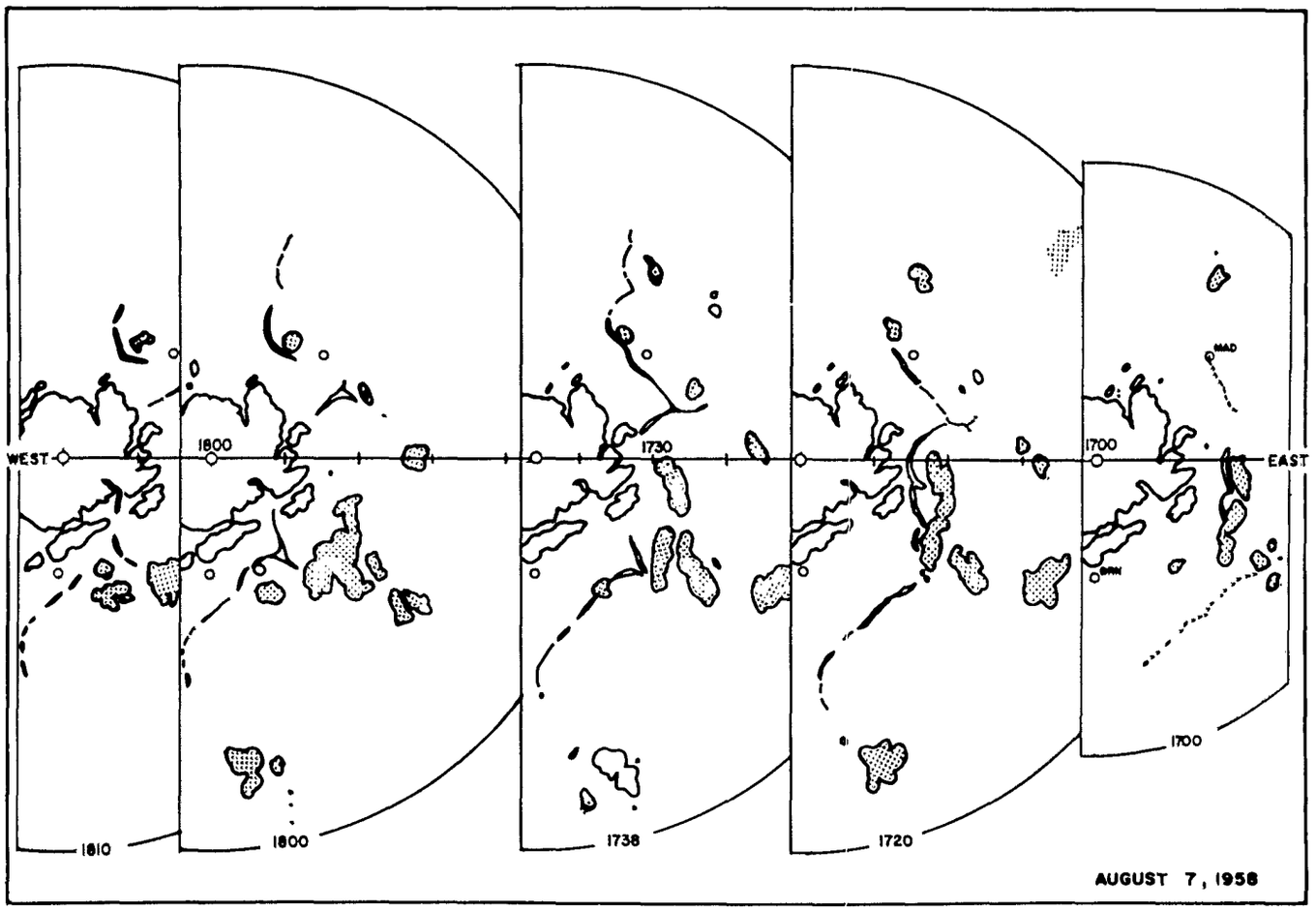

Fig. II.C.15. East-west radar time section, August 7, 1958, 1700-1810 C.

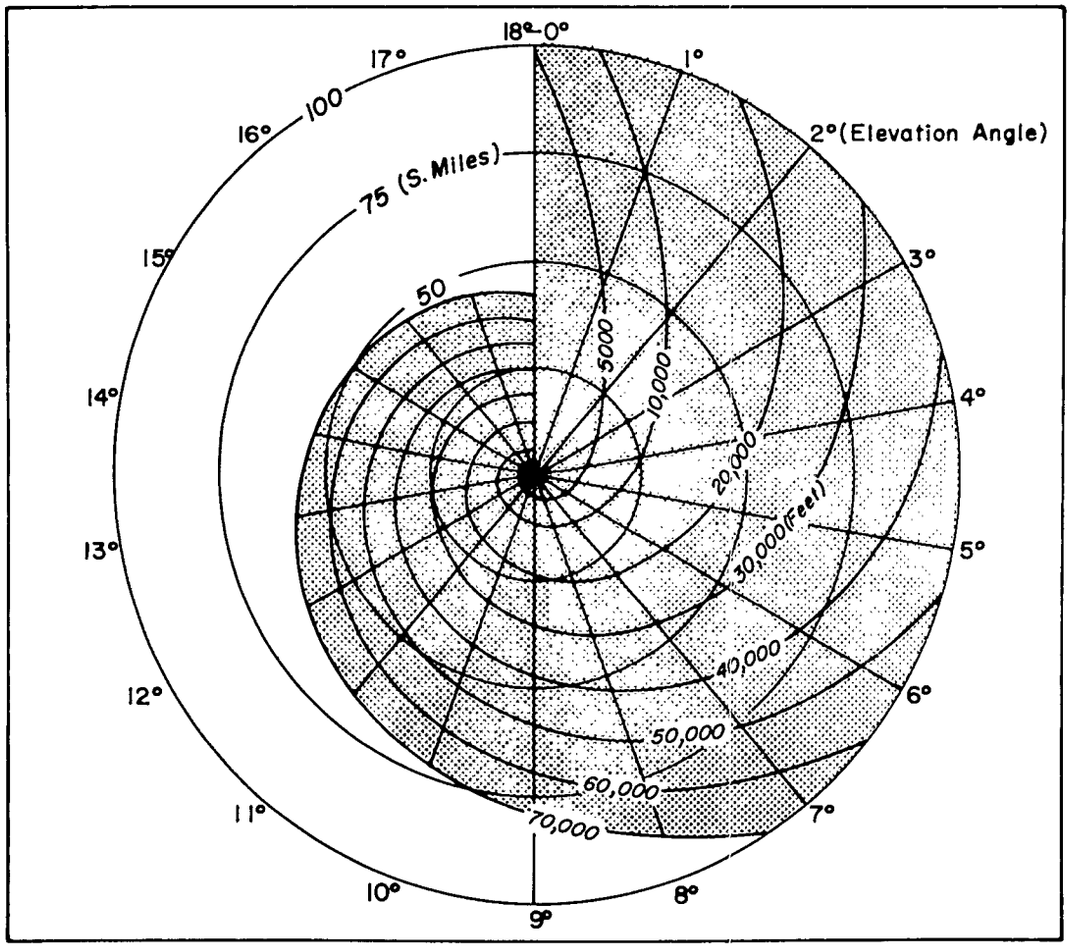

Fig. II.C.16. Nomograph for obtaining echo tops from elevation angle and range.

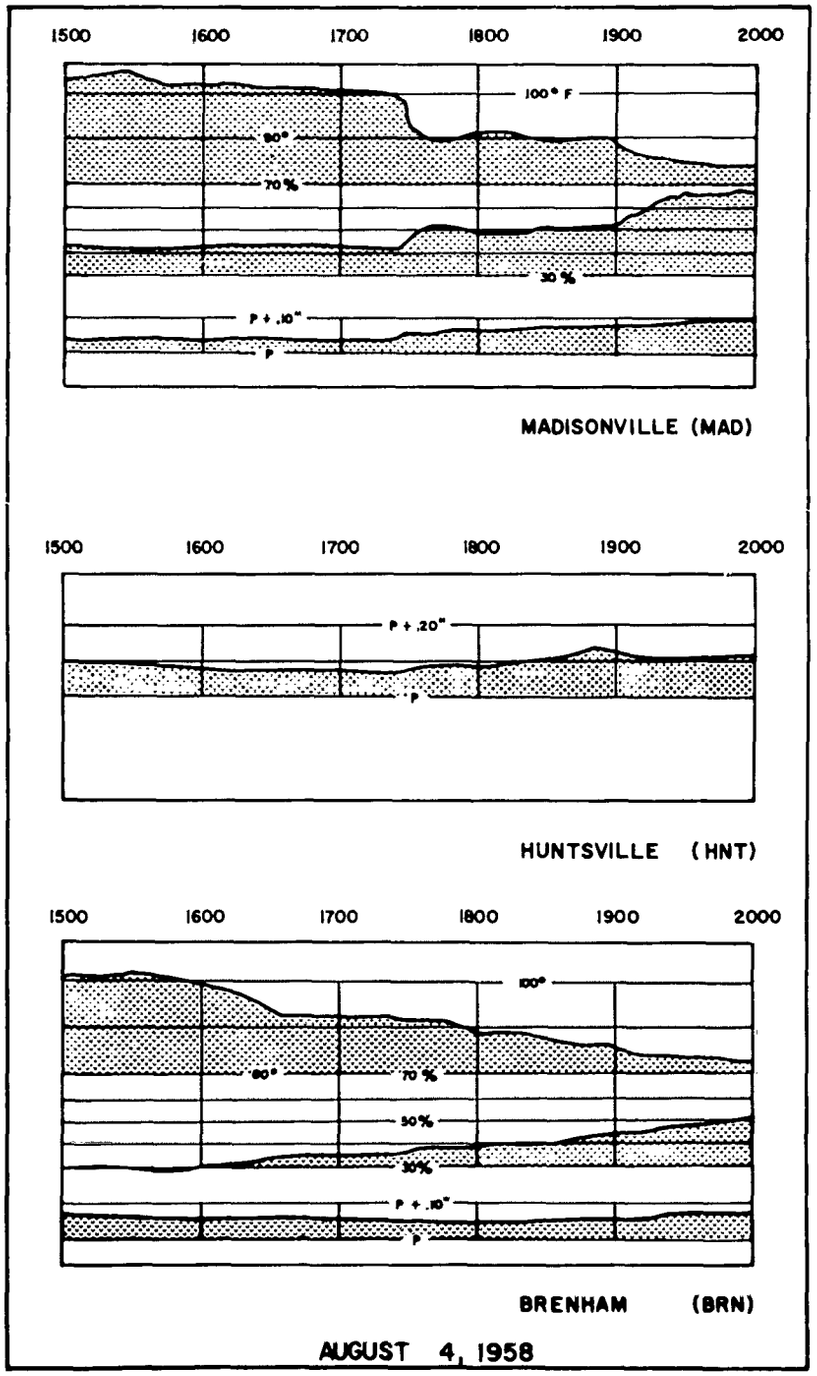

Fig. II.C.17. Meteorological time sections, August 4, 1958.

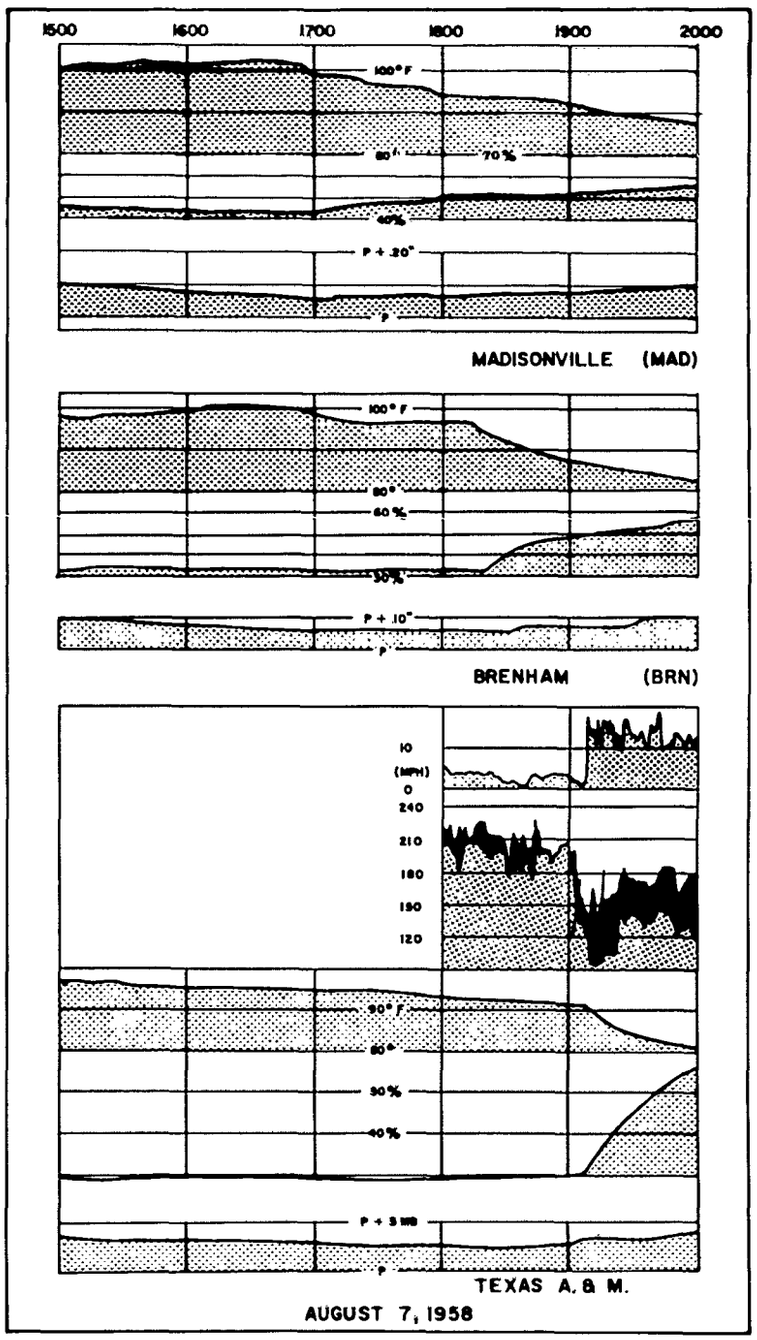

Fig. II.C.18. Meteorological time sections, August 7, 1958.

D. CAMERA

Cloud photographs taken inside the area of a mesometeorological network have potential value in obtaining important information about the dynamical and physical structure of the atmosphere. These photographs may be taken by cameras fixed on the ground or aboard moving vehicles such as aircraft, high-level balloons, rockets, etc.; they must, however, be analysed properly in conjunction with the other network data.

1. GROUND PHOTOGRAPHS

Time-lapse cloud photographs, widely used at present in cloud physics, can also be utilized in mesometeorological studies of the atmosphere. With a picture field of up to 90 degrees, wide-angle cameras are very useful for investigating single clouds or small groups of clouds, but their coverage is insufficient for mapping clouds distributed throughout the area of a mesometeorological network. Despite an inferior resolution of photographs, the use of whole-sky cameras capable of taking time-lapse cloud pictures is recommended, in order that clouds in all directions can be photographed in each frame. Figure II.D.1 shows examples of whole-sky photographs enlarged from 16 mm color time-lapse movie film taken by the U. S. Forest Service, Missoula, Montana.

Geometry of Whole-Sky Camera System

One type of whole-sky camera commonly used for meteorological purposes consists of a spherical surface mirror and a regular time-lapse camera (Fig. II.D.2). The camera is mounted on a tripod in such a way that its optical axis exactly coincides with the perpendicular passing through the center of the spherical mirror resting flat on a rigid board. When the camera is properly fixed, the azimuths

of actual clouds theoretically remain the same as those of photographed clouds. In the figure, the elevation angle ϕ of each cloud viewed from the mirror varies according to the height and distance of the cloud base.

Let d be the horizontal distance of line LP at the level of the mirror top measured from the center line OZ in the figure: θ, the inclination of the perpendicular to the mirror at P, the point of reflection; α, the angle of reflected cloud image viewed from the camera lens; H, the height of the camera above the mirror; and R, the radius of curvature of the mirror. The following relations then exist:

$$\frac{d}{R} = \frac{H}{H + R(1-\cos\theta)}$$

$$\theta = \frac{\pi}{2} - (\alpha + 2\theta)$$

$$\alpha = \tan^{-1} \frac{R \sin\theta}{H + R(1-\cos\theta)} \qquad \text{II.D.1}$$

From these equations, values of d/R were computed as a function of ϕ, changing H as a parameter. Figure II.D.3 represents the result with four values of H: R, 2R, 4R, and infinity. It will be seen that the descending characteristics of the four curves are very similar, suggesting that the values of ϕ plotted against the ratio

$$\frac{d}{R} \Big/ \frac{d_o}{R} = \frac{d}{d_o} \qquad \text{II.D.2}$$

would lie on a single curve irrespective of H, the height of the camera. The following table reveals that what is thus postulated is, with great accuracy, true.

H \ ϕ	90°	80°	70°	60°	50°	40°	30°	20°	10°	0°	-10°	-20°
∞	0.00	0.12	0.25	0.37	0.49	0.60	0.71	0.81	0.91	1.00	1.08	1.16
4R	0.00	0.13	0.26	0.38	0.50	0.61	0.72	0.82	0.91	1.00	1.08	1.14
2R	0.00	0.13	0.25	0.38	0.50	0.61	0.72	0.82	0.91	1.00	1.08	1.14
R	0.00	0.13	0.25	0.37	0.49	0.61	0.72	0.82	0.92	1.00	1.08	1.13

Table II.D.1. Ratio d/d_o tabulated as a function of H and ϕ.

As shown in Fig. II.D.2, d_o can be considered as the radius of the horizon circle appearing on whole-sky photographs, and d, the radius of a circle of ϕ degree elevation angle. Thus the process of determining, for example, the circle of a 10-degree interval elevation angle becomes extremely simple. No information about the camera lens, camera height, or radius of mirror curvature is needed. If the camera is mounted properly when the photographs are made, azimuths and circles of any elevation angle can be determined on photographs.

Figure II.D.4 represents concentric circles of 10-degree interval elevation angles. These circles, when adjusted to the size of given whole-sky photographs, give the elevation angles for each photograph.

The above discussion assumes that spherical mirrors are geometrically accurate. As measured by Conover (1) however, an error of as much as ± 0.8 degree in the elevation angle was made with the use of an imperfect mirror. We do not yet know the extent to which mirror irregularities affect actual measurements in mesometeorological research.

Accuracy of Triangulation

For mapping clouds accurately, whole-sky pictures must be made by two or more cameras in simultaneous operation. Photographs thus obtained are enlarged to a size adequate for carrying out the process of triangulation described in Fig. II.D.5. Let the angle ACB in the figure be β , and the distance of two cameras be b; the expected accuracy of the triangulation depends on both b and β . For the purpose of easy identification and triangulation of individual clouds appearing in two simultaneous photographs, it is preferable to limit β within the following angles:

$$90^\circ > \beta > 10^\circ$$

This is true because a large β makes it extremely difficult to identify clouds which might be photographed from opposite directions. On the other hand, a small results in an appreciable error in triangulation. The area which can be triangulated under the above conditions is shown in Fig. II.D.5, which indicates (1) a maximum range of triangulation extending to a distance about six times larger than b, the

distance of cameras and (2), two directions of restricted triangulation.

Three cameras placed at the vertices of an equilateral triangle would be ideal for unrestricted triangulation in all directions. Experience shows, however, that the third camera is not absolutely necessary, since it is usually possible to estimate the height of clouds which lie in the direction of restricted triangulation.

The next problem is to determine a reasonable value of b, the distance of cameras. So far, we know by the previous discussion the maximum range of triangulation to be:

$$r_{max} \fallingdotseq 6b \qquad \text{II.D.3}$$

There are, however, other factors which should be taken into consideration: (1) the decreased resolution of a picture when the elevation angle of a cloud is lower than 10 degrees, and (2), visibility, which varies according to the time and location of field operation.

In order to photograph the cloud within the limits of satisfactory resolution, the maximum range must be:

$$r_{max} = h_c \cot 10^{o} \qquad \text{II.D.4}$$

where h_c is the height of the cloud to be triangulated.

Assuming unrestricted visibility, we combine equations II.D.3 and 4, obtaining

$$6b = h_c \cot 10^{o}, \text{ or } b = h_c \qquad \text{II.D.5}$$

That is to say, the distance of two whole-sky cameras should preferably be the height of the cloud to be studied. For cumulus studies, a camera distance of two miles is recommended.

Technique and Example of Cloud Mapping

Using whole-sky photographs made by the U. S. Forest Service, Missoula, Montana (2; 3), a mapping of cumuli in the mountainous region was made. During

the summer of 1958 there were two whole-sky cameras in operation at Garden Point (6100 feet) and Wagon Mountain (5500 feet), which are about 2.7 miles apart in a SSW-NNE direction. A set of simultaneous photographs taken at these two points is shown in Fig. II.D.6.

Figure II.D.7 reveals the result of cloud triangulation completed by using the photographs shown in the previous figure. Circles in the figure give the isolines of equal to 10, 20, 30, 50, and 90 degrees. The height of the cumulus base above Wagon Mountain was computed to be 9610 feet--that is, 15,400 feet above sea level.

It is of extreme interest to investigate the origin of these cumuli. As seen in the figure, there were two or more cloud streaks drifting into the area of operation. Figure II.D.8 shows the definite relationship between orography and these streaks. The west-northwest extension of the northernmost streak leads to an unnamed peak (7750 feet), the second streak to Crater Mountain (7700 feet), and the third to other peaks. Areas above 7000 feet, stippled in the chart, behaved like points sticking up into the sky to produce cumuli. After formation, the small cumuli drifted over complicated orography as far as 30 miles or more, producing remarkable cumulus streaks. From the time-lapse whole-sky movie, it is evident that the orientation of these streaks changed according to the change in general flow pattern.

There is no doubt that a whole-sky camera network can solve important mesometeorological problems as yet unknown and unmeasured.

2. AERIAL PHOTOGRAPHS

There is a disadvantage in using aerial photographs in that they are usually taken from a moving platform, which does not permit photographing time changes of visible activity. However, they have a tremendous advantage in covering a large area which otherwise could not be photographed.

Aircraft Photographs

Uncertainty about the position of an aircraft and the direction of its camera has limited the use of aircraft photographs. To overcome this difficulty, Fujita (3) is developing techniques for computing cloud distribution and height from a single aircraft photograph and for determining cloud movements from two or more photographs. The results so far have been fruitful.

An example of cumulus mapping using an oblique photograph taken by Cunningham (4) from 31,000 feet appears in Fig. II.D.9. The base of these cumuli was about 14,500 feet above sea level. No relation was found between cloud distribution and rolling surface topography.

Balloon Photographs

Due to the maximum altitude and comparatively slow movement of high-level balloons, their photographs can be extremely useful for studying changes in the shapes of individual clouds ranging from small cumulus to cumulo-nimbus.

An example of balloon photographs taken at 115,000 feet on August 21, 1956, supplied by Vonnegut (5) of Arthur D. Little, Inc., is shown in Fig. II.D.10. These photographs are printed from every 10th frame of a 16 mm movie taken at 10 frames per minute. The prints thus show one-minute interval balloon pictures. The picture field covers an area of about seven by nine miles. The balloon was moving at about 30 miles per hour.

Using these balloon photographs it is possible to detect the cloud distribution above the surface. It is recommended that a 90-degree wide-angle lens be used in order to photograph a much larger area. If a 10 mm lens is used for a 16 mm movie, the resulting photograph would cover almost 20 x 25 miles from a 120,000-foot altitude.

Rocket Photographs

There is no doubt that rocket or satellite photographs will become popular in meso to macroscale meteorological research in the near future. For such studies, it is recommended that several rocketborne wide-angle or panoramic cameras

capable of photographing cloud patterns and geographic features of the earth be used. These rockets would be fired in daytime before, during, and after convective activities. After their recovery, rocket photographs can be carefully analysed by proper techniques to obtain cloud patterns over much larger areas than would otherwise be photographed.

An example of rocketborne photograph analysis is shown in Fig. II.D.11. The photograph used in constructing this cloud chart appears in articles by Petterssen (6) and Wexler (7).

REFERENCES

1. Conover, J. H., 1959: Cloud patterns and related air motions derived by photographs. Final Rep. for Contract No. AF 19(604)-1589.

2. U. S. Forest Service, 1958: Time-lapse 16 mm movie films. Garden Point and Wagon Mountain sites.

3. Fujita, T., 1960: Analysis techniques for aerial photographs. Tech. Rep. to U. S. Weather Bureau, Contract Cwb 9762 (to be completed in Sept. 1960).

4. Cunningham, R., 1958: T-11 photograph series made by C-130 airborne cameras.

5. Vonnegut, B., 1956: Time-lapse 16 mm movie film. Stratosphere balloon flight from South St. Paul, Minn.

6. Petterssen, S., 1960: 1959--a year of growth, Weatherwise, 13, 3-6.

7. Wexler, H., 1960: Satellites and meteorology, WMO Bull., 9, 1-7.

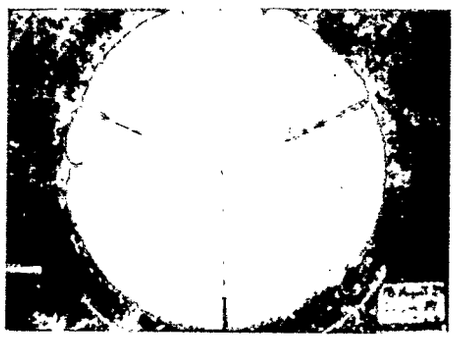

RAIN

CUMULO NIMBUS

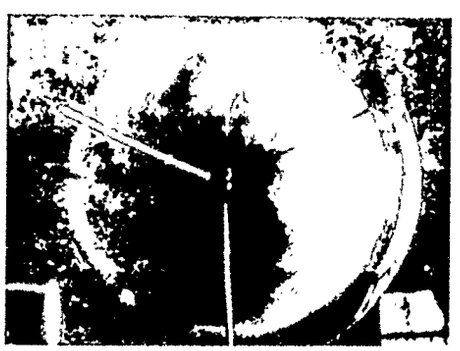

CIRRUS

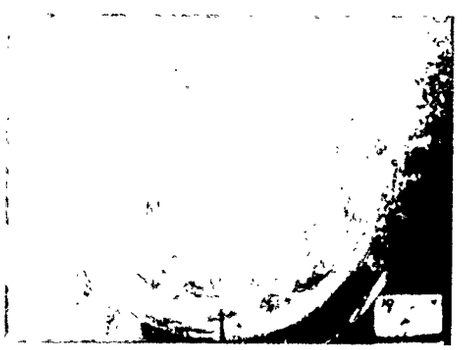

ALTO STRATUS

STRATO CUMULUS

CB BASE

Fig. II.D.1. Examples of whole-sky photographs taken by U. S. Forest Service, Missoula, Montana.

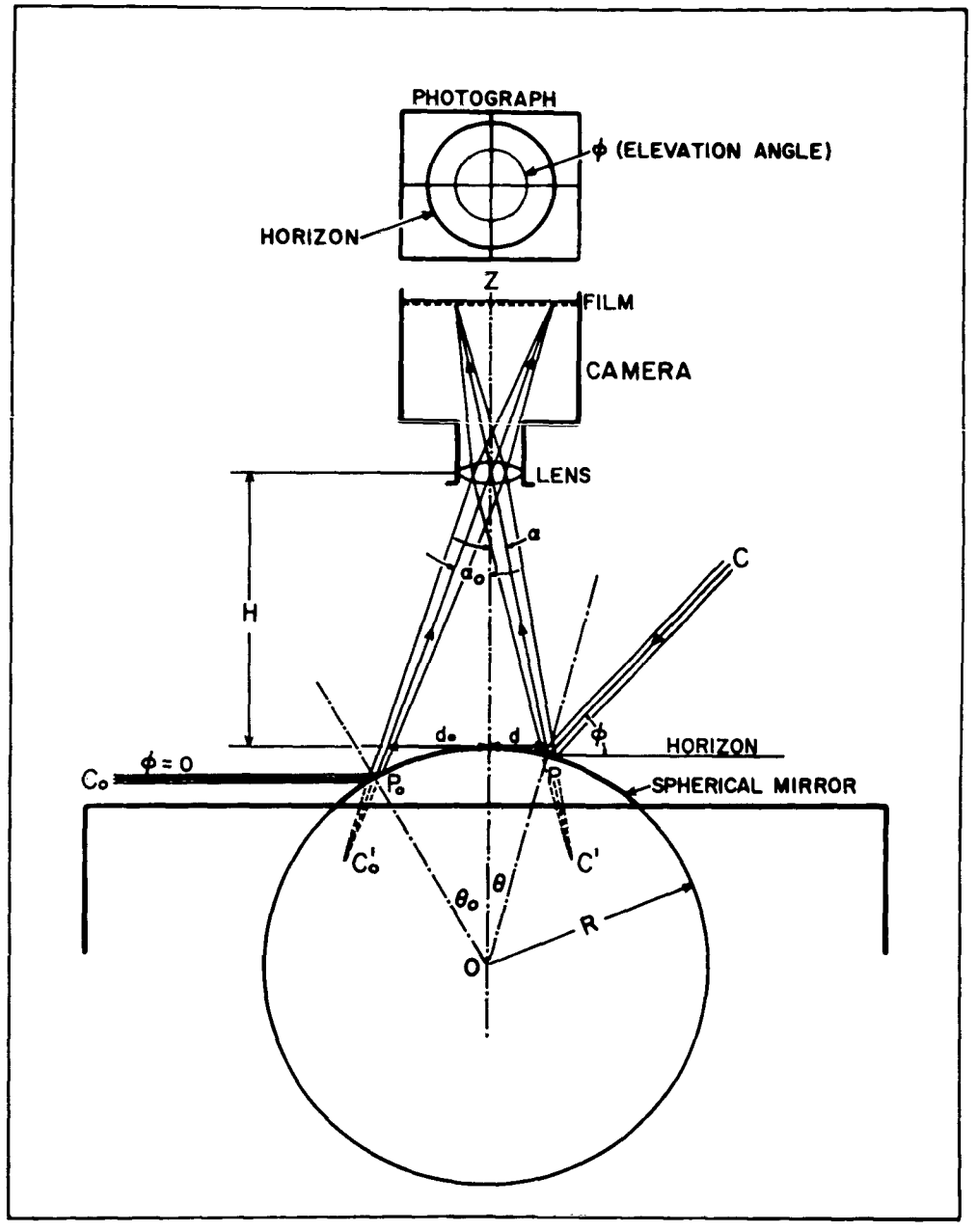

Fig. II.D.2. Schematic diagram showing principles of whole-sky camera system.

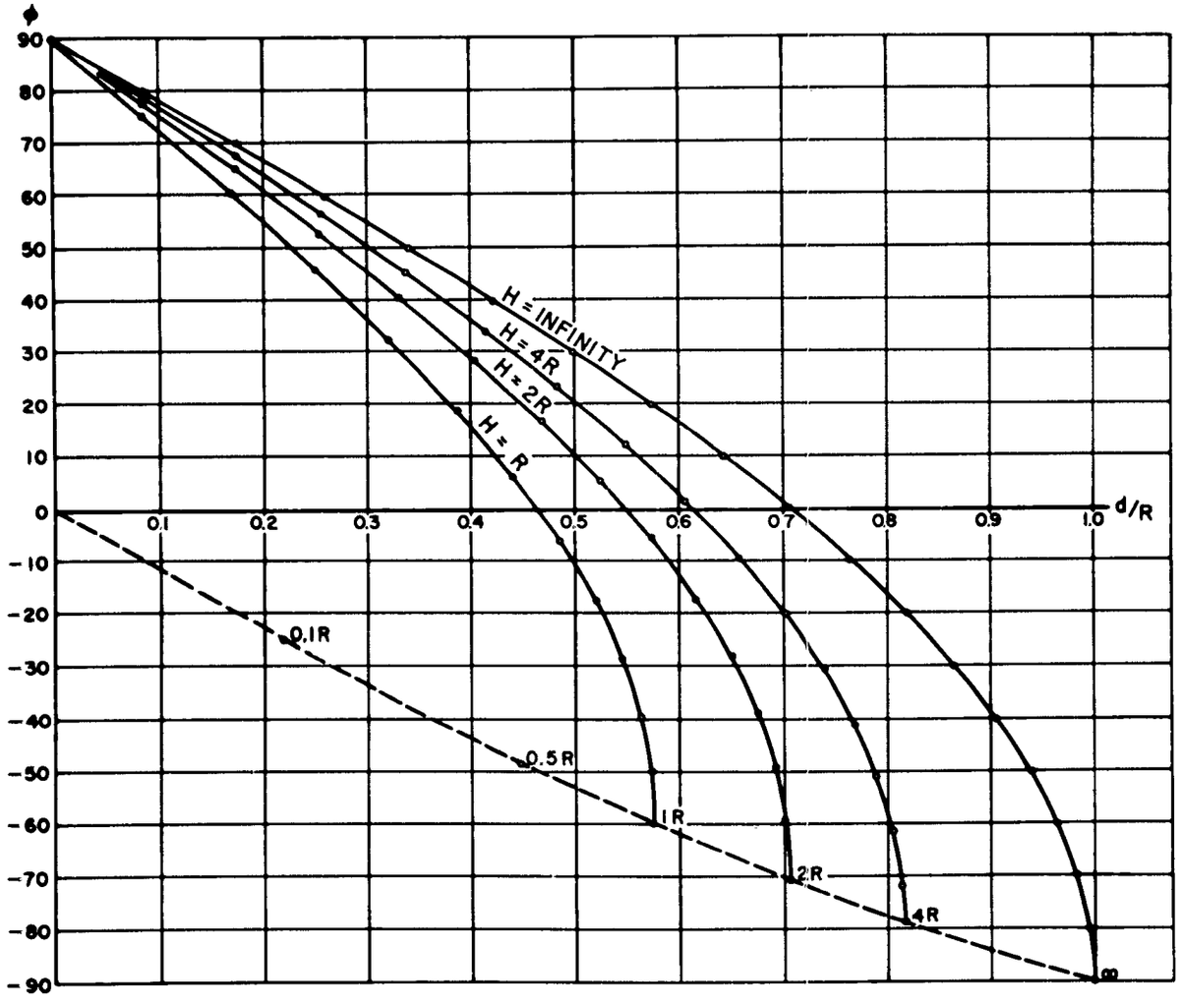

Fig. II.D.3. Elevation angle plotted against d/R, the radius of equi-elevation angle circle.

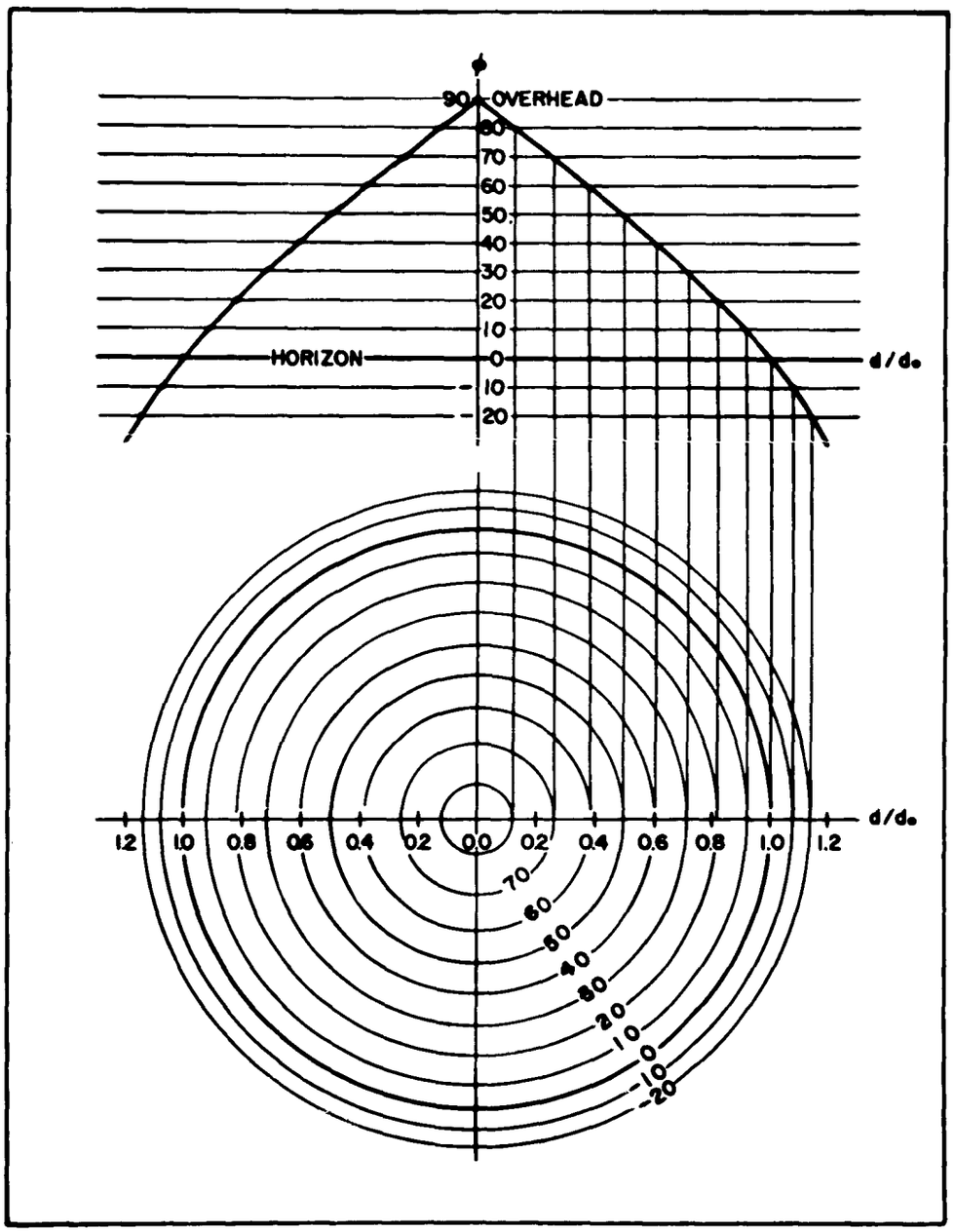

Fig. II.D.4. Diameters of concentric circles representing lines of equi-elevation angles as they would appear on a whole-sky photograph.

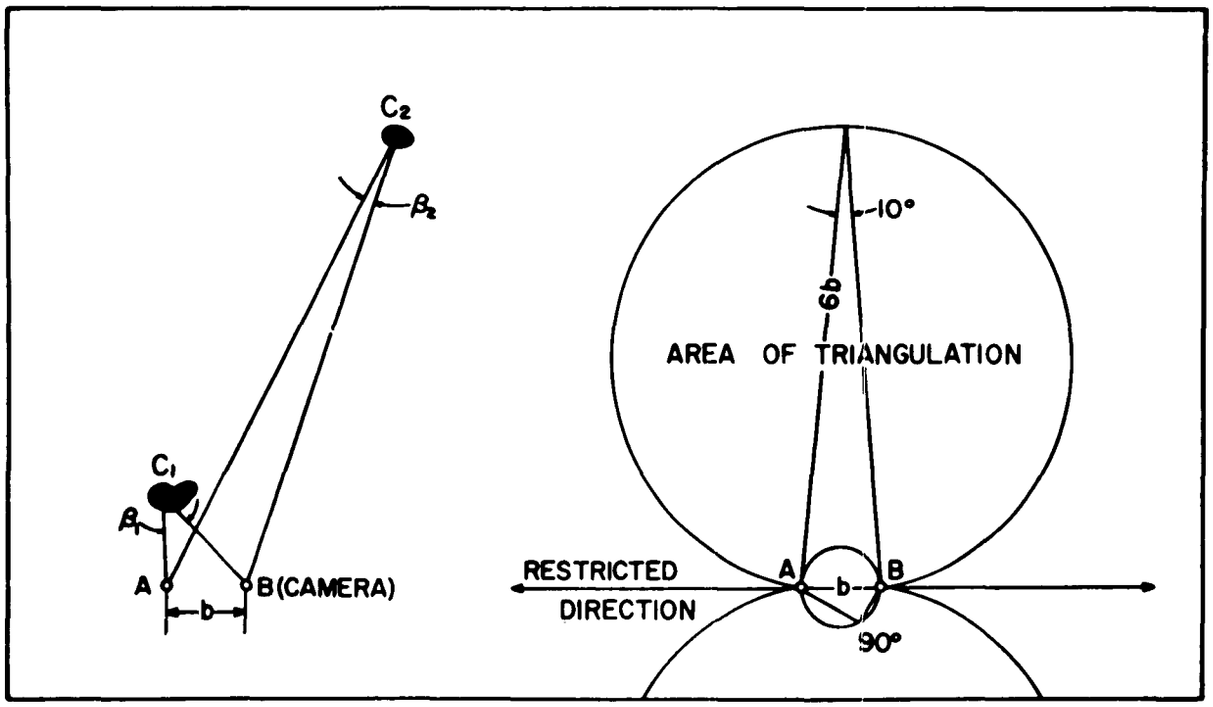

Fig. II.D.5. Triangulation of clouds using two whole-sky photographs taken simultaneously at two camera sites.

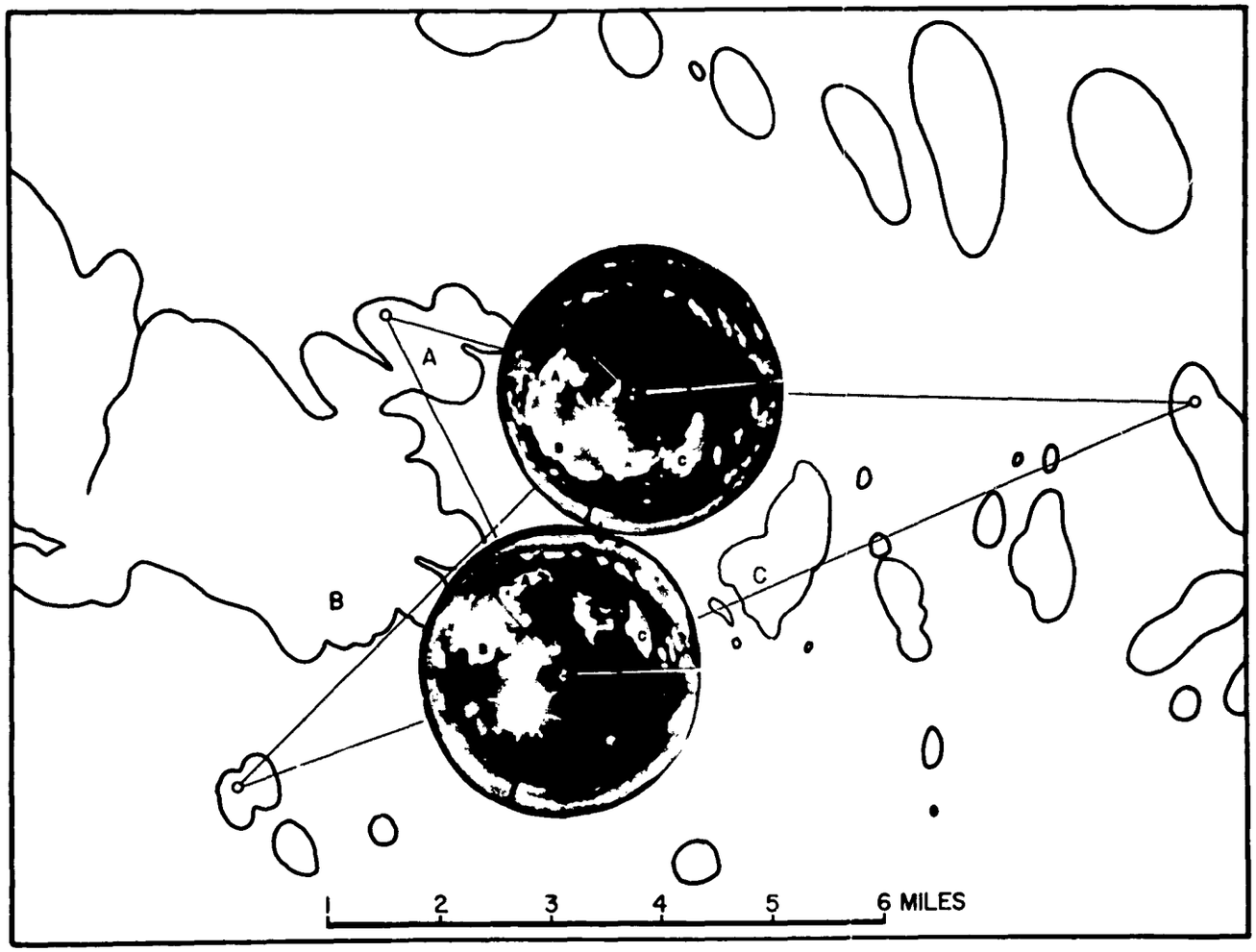

Fig. II.D.6. Whole-sky photographs taken at 1350 MST, August 19, 1958, by U. S. Forest Service, Missoula, Montana. Cameras were located at Garden Point and Wagon Mountain, a separation of 2.7 miles.

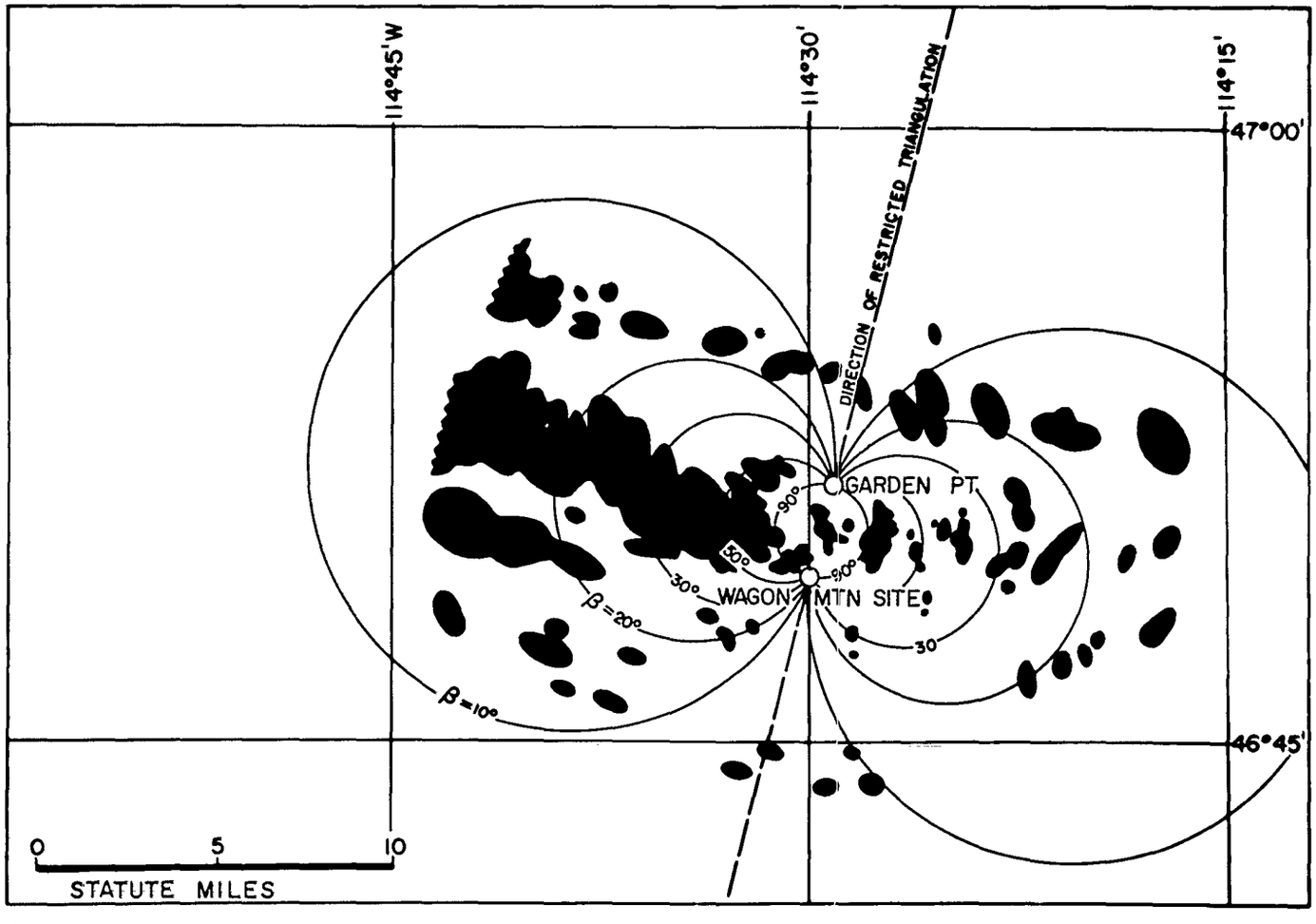

Fig. II.D.7. Result of cumulus triangulation using pictures in Fig. II.D.6.

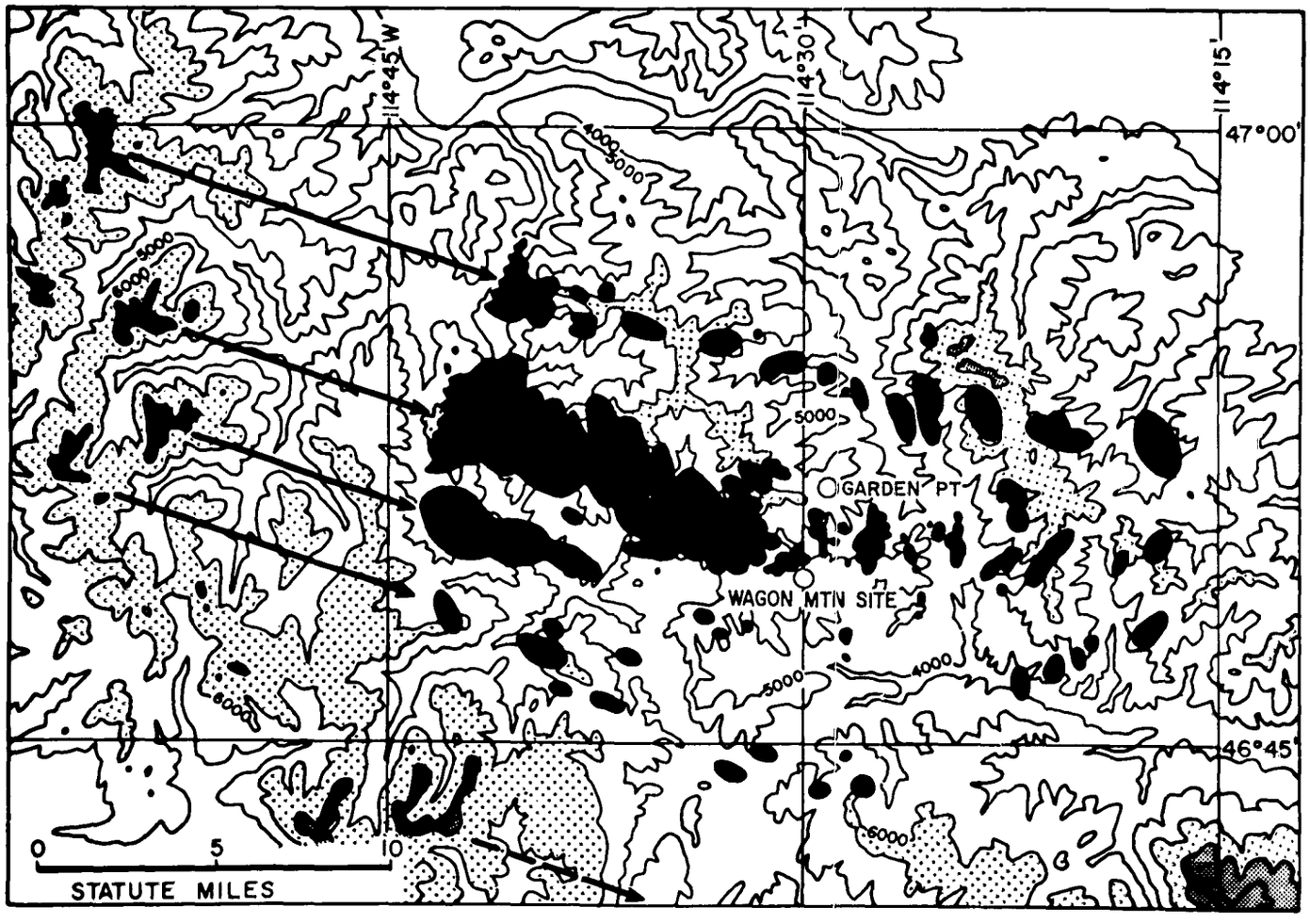

Fig. II.D.8. Relation between triangulated cumuli and orography southwest of Missoula, Montana.

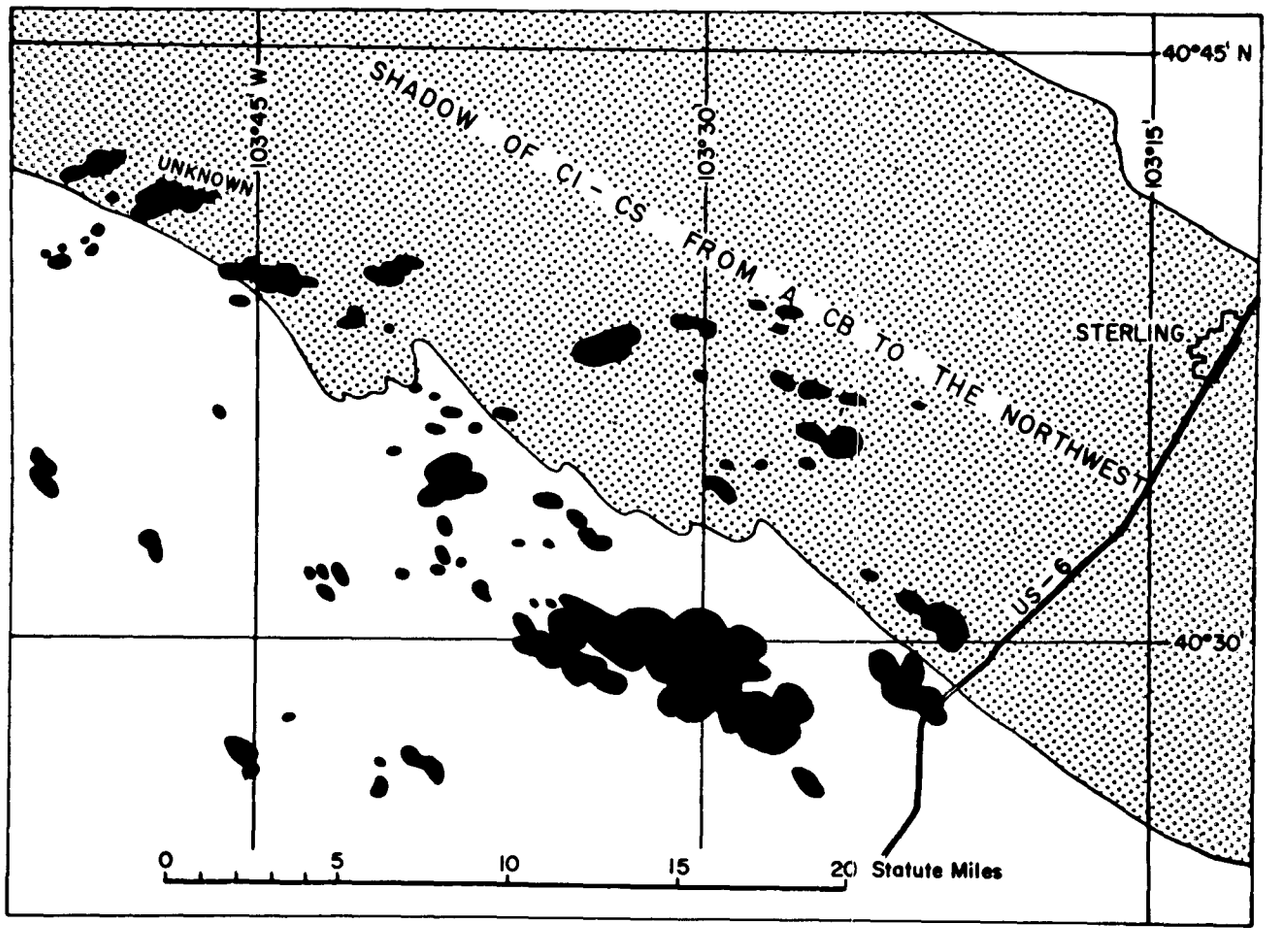

Fig. II.D.9. Cumulus distribution obtained by Air Force C-130 using a T-11 camera at 31,000 feet (September 11, 1958).

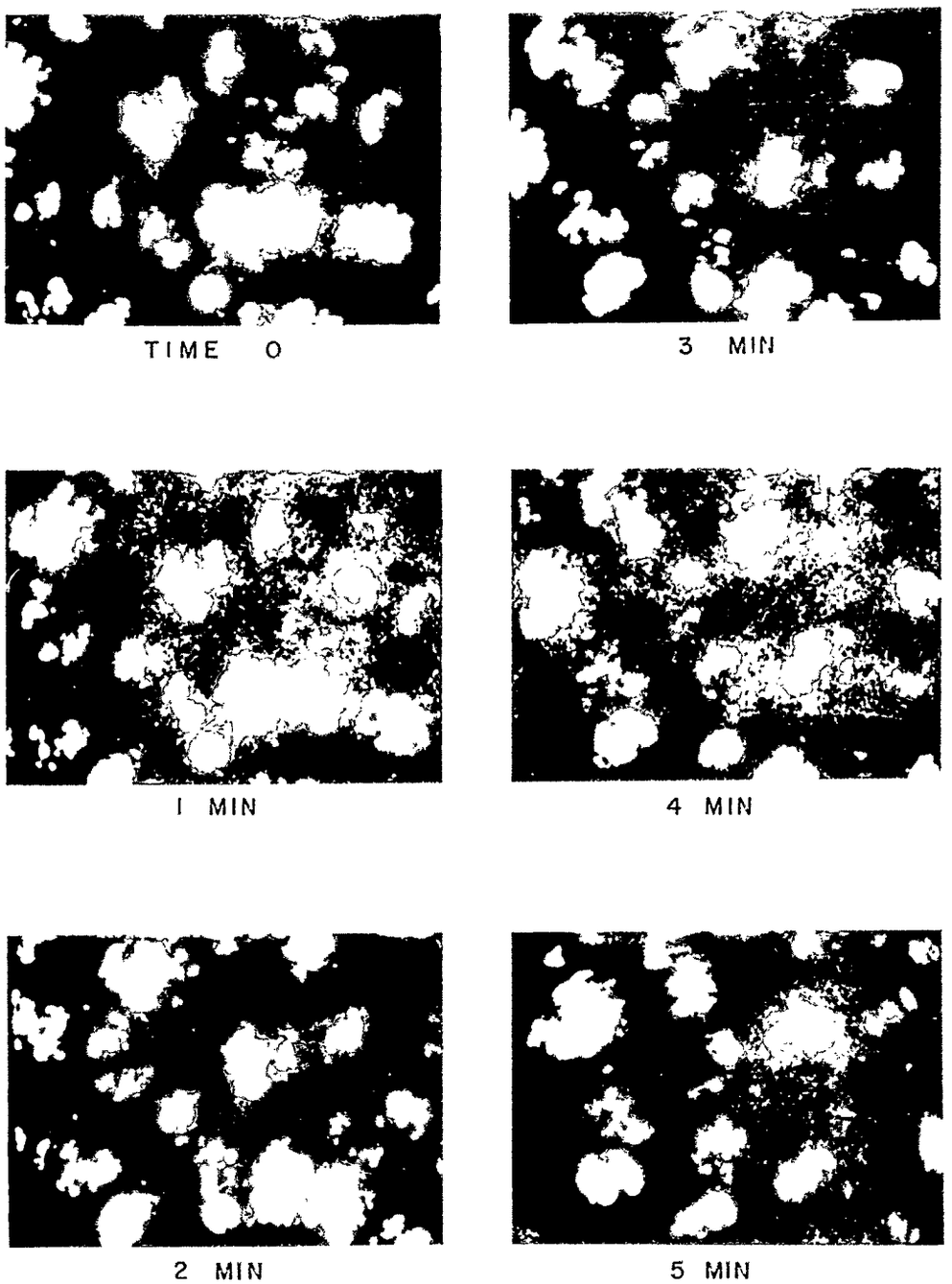

Fig. II.D.10. One-minute interval photographs taken August 21, 1956, from balloon at 115,000 ft. Picture covers 7 x 9 mile area. From Vonnegut (5).

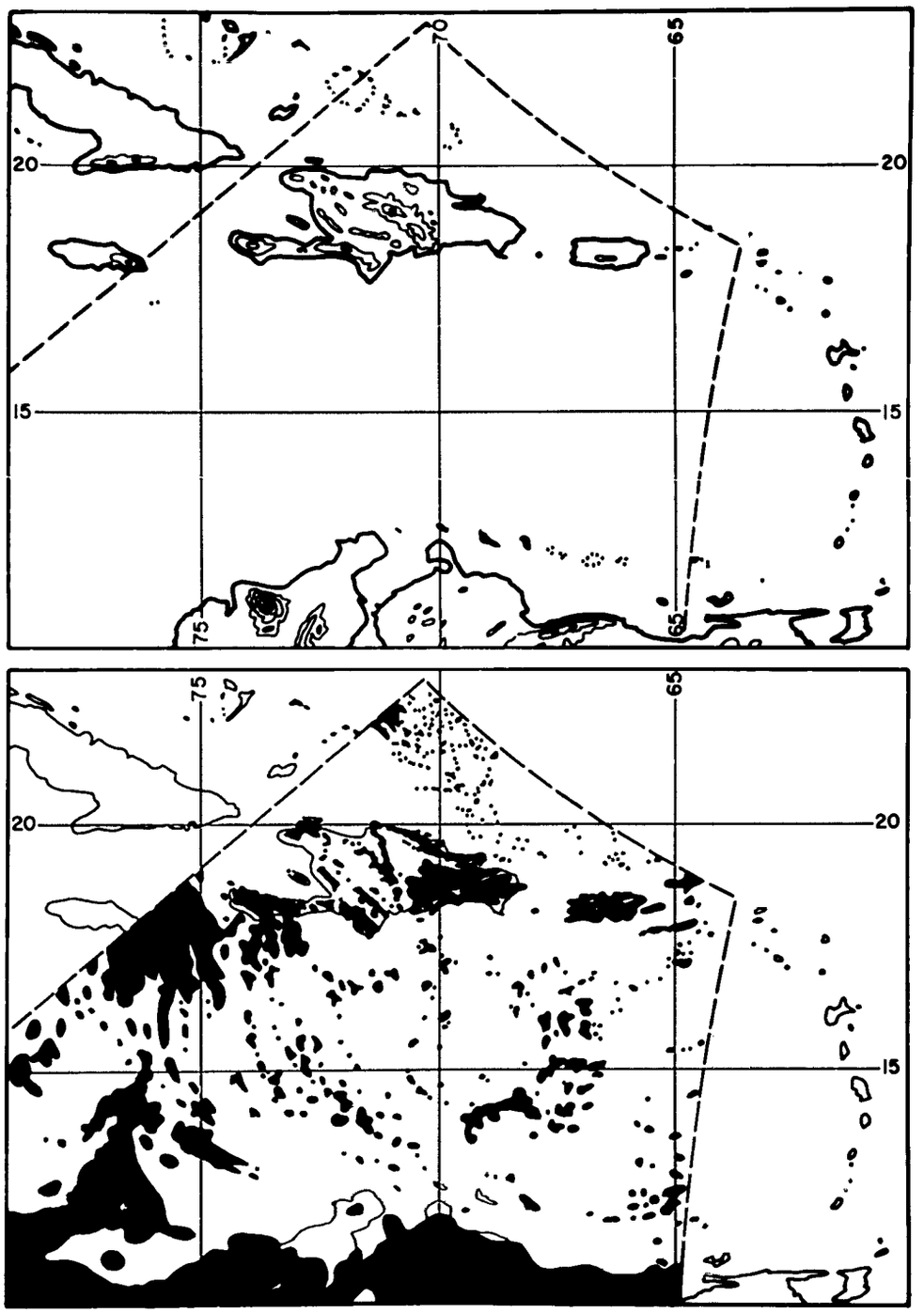

Fig. II.D.11. Analysis of Atlas missile photograph showing cloud distribution over the Carribean. Photographed from a point 400 miles above the Atlantic Ocean.

III. A MODEL THREE-DIMENSIONAL MESOMETEOROLOGICAL NETWORK

Four major categories of instruments necessary for a three-dimensional mesometeorological network were discussed in the previous chapter. Consideration will now be given to the combination of these categories in a model network.

The network, consisting of 121 surface stations covering an area of 300 x 400 miles, is shown in Fig. III.1. The station separation of 30 x 40 miles will suffice to represent mesosystems in the area. The network is oriented so that its major axis coincides with the vector movement of the mesosystems to be studied. The network would contain those instruments for measuring those elements referred to in Chapter II.A, i.e., pressure, temperature, relative humidity, wind, precipitation, and others that may be required for specialized studies. Frequency of measurement depends on the phenomena to be studied.

The network consists of 81 surface stations spaced at 5 x 7.5-mile intervals. The major axis is oriented to coincide with the vector movement of individual or component parts of the mesosystems. The network would contain the instruments recommended in Chapter II.A.

The radar (3 and 10 cm) stations are situated at the two locations shown in Fig. II.1, with a separation of 80 miles. The vertically pointing 1 cm radar is located at the center station of the network. The 80-mile separation is necessary for a number of reasons. It is small enough to allow for a comparative surveillance of the network from the two sites, yet large enough to allow complete surveillance of the network and to place the network outside the two ground clutter patterns. The radars are also close enough together to allow simultaneous observations of phenomena of a limited vertical extent. As mentioned in Chapter II.C, the radars would be synchronized to the extent that all of them would maintain the same observing cycles at a given time.

The whole-sky cloud cameras are located at nine stations with a separation of 15 to 23 miles. With an observation radius of 12 miles, cloud coverage over the β network can be determined with sufficient overlap to maintain cloud continuity.

Upper air observations have been recommended at 57 sites within the α and β networks as shown in Fig. III. 1. Station separation of 60 to 80 miles in the outlying portion of the network decreases to 25 to 30 miles in the central portion of the network. The center of the upper air network is shifted upwind of the movement of group and individual mesosystem vectors. This will insure a maximum coverage of the upper levels over the β network.

It should be emphasized that the primary concern of this report has been the design of a research network. Although instantaneous collection at a central location of various types of data from numerous outlying points is of the utmost importance to an operational network, it is not absolutely essential for the successful operation of a research network, where detailed and more prolonged evaluation of the original data is necessary. This does not imply, however, that a command station is dispensable. A control point should be located at one of the radar sites with communication facilities to the other radars, to the upper air sites, and to any aircraft that may be operating as mobile observational platforms. This will guarantee a time consistency and uniformity of purpose in a particular operation and allow for schedule changes to fit a mesoscale weather pattern.

Considering the results of previous and present analyses of mesosystems as determined from a variety of networks, this basic design will be most suitable for determining the three-dimensional and time variation of medium-scale weather systems.

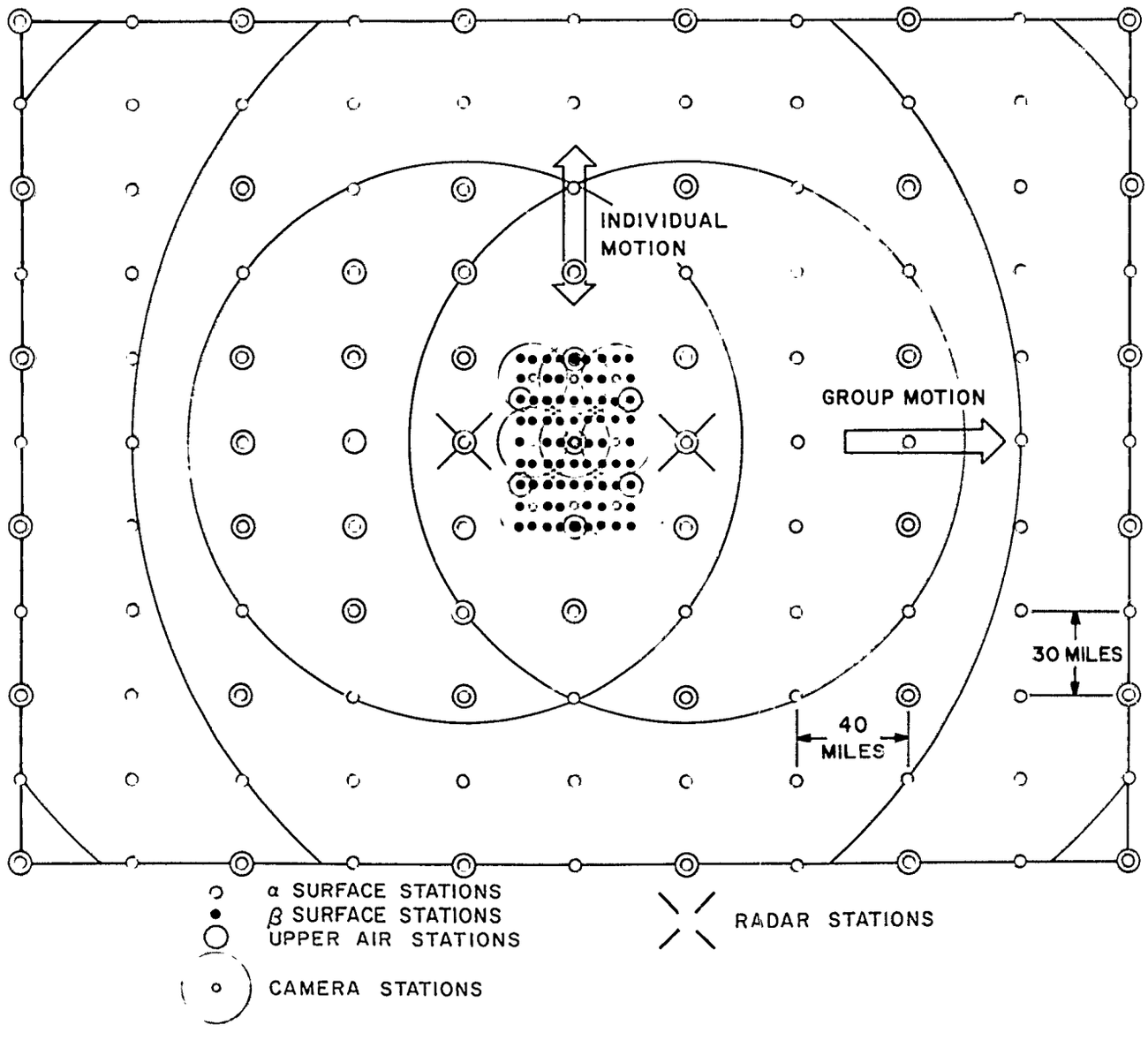

FIG. III.1 PROPOSED MODEL NETWORK

IV. PRACTICAL DESIGNS OF THREE-DIMENSIONAL MESOMETEOROLOGICAL NETWORKS

The previous chapters have dealt with the role of various network instruments and the design of a model network. Since the surface of the earth is far from ideal, varying both in roughness and form, the model design will of necessity be modified to fit various terrains and locations. It is also most likely that the scale of mesosystems will vary with latitude and climatological location. In this respect, since all of the networks examined were located in middle latitudes, it must be expected that the design of the model network is biased. A network in tropical or polar areas, therefore, would have to be modified on the basis of either experience or analysis of available tropical or polar network data.

Following are designs for networks in three different middle-latitude locations in the United States: the first along the east coast; the second, a plains or midwestern area; and the third, a mountainous region. In addition, future plans include the consideration of a possible network in the White Sands, New Mexico, area, and in the Fort Huachuca-Yuma area, the latter using the U. S. Army Engineering Proving Grounds' "Electronic Environmental Test Facility".

For consistency, the three networks have been designed to contain the same number and types of equipment. The basic network and personnel will then be the same for all three areas. In addition, all station locations have been selected at normally accessible sites. The need for automatic weather stations, seaworthy and rugged for ground and water drops, will certainly arise with the need for obtaining data of a mesoscale nature over oceans and inaccessible terrain. The present design does not include this equipment, because the operation of the proposed research networks will provide the surface and upper air data necessary to bring the radar to its ultimate usefulness as an instrument for rapidly interpreting "visible" mesoscale systems over large areas. The automatic instruments would then be most valuable as a specialized aid for the description of those mesofeatures that are "invisible" to the radar.

A. COASTAL AREA

The coastal area selected for a network design is shown in Fig. IV.A.1. The first overlay illustrates the α network, bounded on the east by the Atlantic Ocean and extending from Erie, Pennsylvania, in the northwest to Langley Field, Virginia, in the southeast, and from Pulaski, Virginia, in the southwest to Pittsfield, Massachusetts, in the northeast. Table IV.A.1 gives station names and elevations, obtained from World Aeronautical (U. S. Coast and Geodetic Survey), U. S. Geological Survey, and Army Map Service charts. In all possible cases the locations refer to an airport near the town. The almost square shape of the α network reflects the results obtained in previous analyses and reported in the First and Third Quarterly Technical Reports under this contract.

Bounded by Philadelphia, Newark, and Allentown, the β network is situated in the eastern section of the α network, its major axis oriented southwest-northeast. The β stations are distributed, at the given distances, along highways around the periphery and in the interior of the network. Here again, as many sites as possible were chosen at airports or in small towns, the remainder at crossroads or along the highways. The β network is thus bounded on the south by U. S. Highway 422, on the east by U. S. Highway 1, and on the north and west by interconnecting state highways.

The top overlay of Fig. IV.A.1 shows the distribution of the upper air stations and the cloud camera and radar sites. A circle of radius 12 miles is drawn around the cloud camera stations; circles of 100 and 200 miles are drawn around the radar sites. The upper air stations are concentrated to the south and west of the β network. The radar sites are located at Belmar (Evans Area-Signal Corps Engineering Laboratories) and Reading, and the cameras are located at selected stations in the β network.

Table IV.A.1. network stations for Coastal Area. (Connecticut, Delaware, Maryland, Massachusetts, New Jersey, New York, Ohio, Pennsylvania, Virginia, West Virginia)

Sta. No.	Elev.	Name	Sta. No.	Elev.	Name
1	985	Jefferson, O.	41	600	Trinca, N. J.
2	732	Erie, Pa.	42	7	Teterboro, N. J.
3	620	Fredonia, N. Y.	43	98	MacArthur, N. Y.
4	2580	Olean, N. Y.	44	1280	Sunset, O.
5	662	Dansville, N. Y.	45	1168	Pittsburgh, Pa.
6	460	Watkins Glen, N. Y.	46	960	Leechburg, Pa.
7	1180	Cortland, N. Y.	47	2100	Edensburg, Pa.
8	1012	Sidney, N. Y.	48	730	Stitt, Pa.
9	1245	Cooperstown, N. Y.	49	---	Liverpool, Pa.
10	105	Catskill, N. Y.	50	582	Grimes, Pa.
11	1170	Pittsfield, Mass.	51	391	Allentown, Pa.
12	1400	Meadville, Pa.	52	195	Solberg, N. J.
13	1100	Warren, Pa.	53	12	Idlewild, N. Y.
14	2142	Bradford, Pa.	54	640	Glendale, W. Va.
15	2330	Cherry Springs, Pa.	55	1183	Washington, Pa.
16	1900	Grand Canyon, Pa.	56	1144	Latrobe, Pa.
17	700	Towanda, Pa.	57	1100	Bedford, Pa.
18	880	Hallstead, Pa.	58	560	Mt. Union, Pa.
19	1440	Livingston, N. Y.	59	347	Harrisburg, Pa.
20	260	Anderson Acres, N. Y.	60	403	Lancaster, Pa.
21	843	Waterbury, Conn.	61	311	Pottstown, Pa.
22	1196	Youngstown, O.	62	213	Trer n, N. J.
23	1540	Franklin, Pa.	63	---	Belmar, N. J. (Evans Area-SCEL)
24	1600	Benninger, Pa.	64	---	New Martinsville, W. Va.
25	1911	St. Mary's, Pa.	65	1256	Morgantown, W. Va.
26	---	Renovo, Pa.	66	2550	Bowman, Md.
27	528	Williamsport, Pa.	67	780	Cumberland, Md.
28	1179	Scranton, Pa.	68	704	Hagerstown, Md.
29	920	Honesdale, Pa.	69	590	Hanover, Pa.
30	450	Port Jervis, Pa.	70	520	Oxford, Pa.
31	471	Stewart AFB, N. Y.	71	185	Wilmington, Del.
32	9	Bridgeport, C.	72	100	Clementon, N. J.
33	1300	Koons, O.	73	12	Forked River, N. J.
34	1340	Butler, Pa.	74	---	West Union, W. Va.
35	---	New Bethlehem, Pa.	75	1209	Clarksburg, W. Va.
36	1220	Clearfield, Pa.	76	---	Thomas, W. Va.
37	1200	State College, Pa.	77	700	Winchester, Va.
38	480	Lewisburg, Pa.	78	556	Martinsburg, W. Va.
39	620	Berwick, Pa.	79	---	Gaithersburg, Md.
40	1925	Mt. Pocono, Pa.	80	14	Baltimore, Md.

Table IV.A.1 (con't.)

Sta. No.	Elev.	Name
81	20	Smyrna, Del.
82	87	Millville, N. J.
83	11	Atlantic City, N. J.
84	1264	Sutton, W. Va.
85	1987	Elkins, W. Va.
86	945	Petersburg, W. Va.
87	---	Woodstock, Va.
88	600	Wilson, Va.
89	15	Washington, D. C.
90	66	Easton, Md.
91	35	Milford, Del.
92	22	Cape May, N. J.
93	1840	Summersville, W. Va.
94	---	Marlinton, W. Va.
95	2100	Franklin, W. Va.
96	950	Shenandoah, Va.
97	---	Culpeper, Va.
98	20	Dahlgren, Va.
99	38	Patuxent, Va.
100	52	Salisbury, Md.
101	1520	Hinton, W. Va.
102	1600	Covington, Va.
103	1450	Waynesboro, Va.
104	300	Charlottesville, Va.
105	---	Pendleton, Va.
106	---	Tappahannock, Va.
107	25	DuPont, Del.
108	38	Chincoteague, Va.
109	1174	Roanoke, Va.
110	942	Lynchburg, Va.
111	---	Buckingham, Va.
112	400	Plainview, Va.
113	167	Richmond, Va.
114	85	Harcum, Va.
115	2200	Pulaski, Va.
116	---	Rocky Mount, Va.
117	---	Alta Vista, Va.
118	600	Keysville, Va.
119	436	Blackstone, Va.
120	115	Waverly, Va.
121	10	Langley, Va.

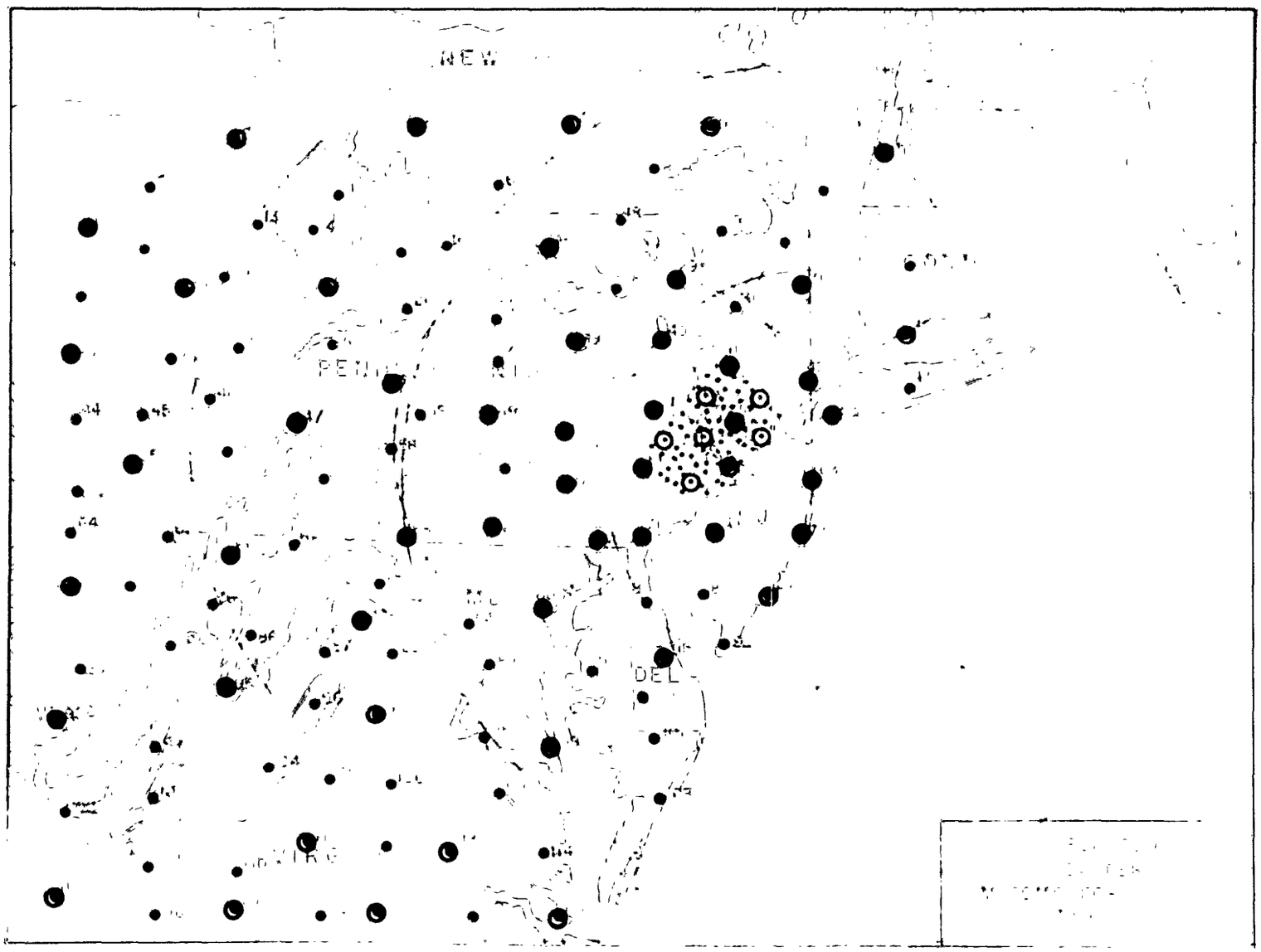
NEW
PEN
DEL

B. PLAINS AREA

The plains area chosen for a network design is shown in Fig. IV.B.1. The topography shows a gradual increase in height to the north and west. The choice of this area for the study of mesosystems is supported by a wealth of analyses and statistics. In fact, it can be said that the techniques of mesoanalysis were developed during the investigation of weather systems in this area.

The network (121 stations--Table IV.B.1), seen in the first overlay of Fig. IV.B.1, is oriented so that its major axis points northwest-southeast in order to contain the average mesosystem for a maximum amount of time. It ranges from Dodge City in the north to Waco in the south, and from Amarillo in the west to Fort Smith in the east, almost covering the state of Oklahoma.

The network (81 stations), shown in the center of the network, lies between the Red River to the south and the Washita River to the north. To the west is Fort Sill (61) and the Wichita Mountains (seen in Fig. II.B.2), and to the southeast, Ardmore (62) and Lake Texoma. The major axis of the network is oriented north-south rather than the preferred southwest-northeast because of the restriction placed on instrument location by the number and orientation of roads in the area.

The network is bounded on the south by U. S. Highway 70 and on the north by State Highway 39 and U. S. Highway 62. U. S. Highway 81 traverses the center of the network and branching roads connect the other portions.

The top overlay in Fig. IV.B.1 shows the proposed upper air, camera, and radar networks. Density of the upper air stations is greatest to the south and west of the β network. Nine camera sites are distributed throughout the β network. Radar sites are at Chattanooga, Oklahoma, just southwest of Fort Sill (in order to clear the Wichita Mountains as much as possible), at Ardmore (62) to the east, and the 1 cm set at Duncan (β 46).

Table IV.B.1. $\mathcal{A}$ network stations for Plains Area (Arkansas, Kansas, Oklahoma, Texas).

Sta. No.	Elev,	Name	Sta. No.	Elev,	Name
1	2594	Dodge City, Kan.	41	1008	Ada, Okla.
2	2230	Greensburg, Kan.	42	---	Kiowa, Okla.
3	1520	Medicine Lodge, Kan.	43	---	Antlers, Okla.
4	1340	Anthony, Kan.	44	---	Broken Bow, Okla.
5	1094	Medford, Okla.	45	3104	Spearman, Tex.
6	1014	Ponca City, Okla.	46	---	Canadian, Tex.
7	715	Bartlesville, Okla.	47	---	Cheyenne, Okla.
8	674	Tulsa, Okla.	48	1580	Cordell, Okla.
9	623	Muskogee, Okla.	49	---	Carnegie, Okla.
10	750	Sallisaw, Okla.	50	1286	Anadacko, Okla.
11	468	Fort Smith, Ark.	51	967	Pauls Valley, Okla.
12	2528	Meade, Kan.	52	640	Tishomingo, Okla.
13	1940	Ashland, Kan.	53	703	Durant, Okla.
14	1820	Tegarden, Okla.	54	547	Paris, Tex.
15	1300	Cherokee, Okla.	55	---	Clarksville, Tex.
16	1172	Enid, Okla.	56	---	Stinnett, Tex.
17	985	Stillwater, Okla.	57	3275	Pampa, Tex.
18	883	Stroud, Okla.	58	2323	Shamrock, Tex.
19	715	Okmulgee, Okla.	59	1937	Sayre, Okla.
20	---	Eufala, Okla.	60	1562	Hobart, Okla.
21	513	Poteau, Okla.	61	1187	Fort Sill, Okla.
22	---	Waldron, Ark.	62	875	Ardmore, Okla.
23	2888	Liberal, Kan.	63	---	Marietta, Okla.
24	---	Laverne, Okla.	64	749	Sherman, Tex.
25	2187	Woodward, Okla.	65	550	Commerce, Tex.
26	1300	Fairview, Okla.	66	416	Mt. Pleasant, Tex.
27	1067	Kingfisher, Okla.	67	3604	Amarillo, Tex.
28	1074	Guthrie, Okla.	68	---	Groom, Tex.
29	1080	Shawnee, Okla.	69	2010	Wellington, Tex.
30	864	Holdenville, Okla.	70	1605	Gould, Okla.
31	770	McAlester, Okla.	71	1233	Frederick, Okla.
32	725	Talihina, Okla.	72	1140	Chattanooga, Okla.
33	1069	Mena, Ark.	73	1334	Nocona, Tex.
34	---	Gray, Okla.	74	833	Gainesville, Tex.
35	---	Darrouzett, Tex.	75	---	McKinney, Tex.
36	---	Arnett, Okla.	76	544	Greenville, Tex.
37	---	Putnam, Okla.	77	440	Quitman, Tex.
38	---	Geary, Okla.	78	---	Canyon, Tex.
39	1284	Oklahoma City, Okla.	79	---	Clarendon, Tex.
40	---	Purcell, Okla.	80	1952	Childress, Tex.

Table IV.B.1. (con't).

Sta. No.	Elev.	Name
81	1602	Quanah, Tex.
82	1261	Vernon, Tex.
83	1029	Wichita Falls, Tex.
84	1100	Bowie, Tex.
85	1059	Decatur, Tex.
86	644	Addison, Tex.
87	479	Terrell, Tex.
88	---	Canton, Tex.
89	4100	Hereford, Tex.
90	---	Silverton, Tex.
91	2350	Turkey, Tex.
92	1740	Triangle Ranch, Tex.
93	1400	Arledge Ranch, Tex.
94	1274	Olney, Tex.
95	1560	Graham, Tex.
96	1122	Weatherford, Tex.
97	---	Cedar Hill, Tex.
98	---	Ennis, Tex.
99	422	Palestine, Tex.
100	3840	Dimmit, Tex.
101	3372	Plainview, Tex.
102	2600	Matador, Tex.
103	1760	Guthrie, Tex.
104	---	Knox City, Tex.
105	---	Throckmorton, Tex.
106	1282	Breckenridge, Tex.
107	---	Granbury, Tex.
108	700	Itasca, Tex.
109	---	Hubbard, Tex.
110	---	Fairfield, Tex.
111	3600	Littlefield, Tex.
112	3256	Lubbock, Tex.
113	2700	Post, Tex.
114	---	Jayton, Tex.
115	1545	Stanford, Tex.
116	1429	Albany, Tex.
117	1468	Eastland, Tex.
118	1310	Stephenville, Tex.
119	---	Meridian, Tex.
120	470	Waco, Tex.
121	---	Thornton, Tex.

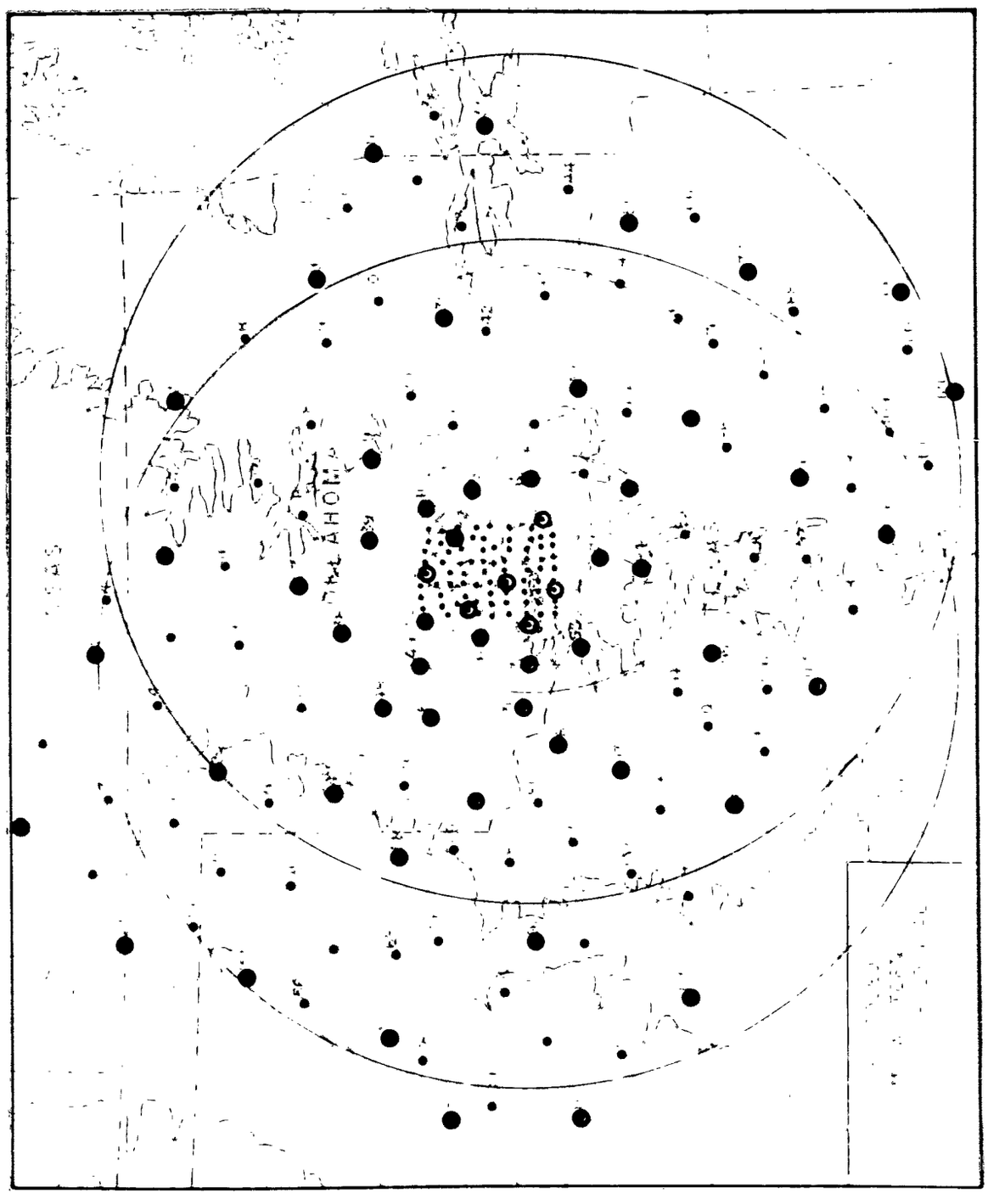

C. MOUNTAIN AREA

The mountainous area considered for design is located in Idaho and Montana (base map of Fig. IV.C.1). The blacked-out areas represent regions which are at a higher elevation than the radar sites.

The $\mathcal{K}$ network, with an elongation from west to east, ranges from Hanford, Washington (50), in the west to Bozeman, Montana (77), in the east and from Kalispell, Montana (13), in the north to Anderson, Idaho (121), in the south. Heights of stations range from 402 feet at Richland (51) to 9500 feet at Odell (95).

The $\mathcal{B}$ network, with major axis east-west, is located just south of Missoula (42). Sites have been chosen mainly along valleys and on accessible ridge lines.

The upper air, radar, and camera networks are shown in the top overlay of Fig. IV.C.1. The greatest density of upper air stations is to the west. The whole-sky cameras are located at ridge-line sites where possible and the radars are located at the highest accessible elevations. Lookout Tower (42), located 10 miles north of Missoula at an elevation of 6900 feet, and Anderson Mountain (93), at 8100 feet six miles south of Lost Trail Path, are best suited for the 3 and 10 cm radar sets, while Stevensville (64) is a central location for the vertically pointing 1 cm radar.

Table IV.C.1. α network stations for Mountain Area.

Sta. No.	Elev.	Name	Sta. No.	Elev.	Name
1	1013	Scott	41	5200	Double Arrow
2	1303	Omak	42	6900	Missoula Tv-Mt
3	5943	Graves Pk	43	3203	Missoula
4	1300	Hunters	44	7200	Falls Pt
5	5740	Chewelah	45	4118	Augusta
6	6185	North Baldy	46	4900	Lincoln
7	5520	Gisborne Mt	47	3580	Gordon
8	2081	Clark Fk	48	3671	Great Falls
9	1900	Troy	49	8852	Helena Hogbk
10	4336	Big Swede	50	500	Hanford
11	5300	Sex Peak	51	402	Richland
12	7493	Baldy Mt	52	1491	La Crosse
13	2935	Kalispell	53	800	Starbuck
14	6370	Desert Mt	54	1205	Walla Walla
15	4900	Big Prairie	55	2549	Pullman
16	5350	Gate Park	56	1438	Lewiston
17	3863	Cut Bank	57	1005	Orofino
18	3945	Choteau	58	2900	Elk River
19	3350	Woods	59	1900	Canyon RS
20	3167	Chester	60	3500	Kelley Cr
21	2888	Fort Benton	61	6000	Hemlock Bt
22	2270	Mansfield	62	4600	Jay Pt
23	1258	Ephrata	63	6930	Coldwater
24	1200	Moses Lake	64	3310	Stevensville
25	2175	Wilbur	65	7700	Slide Rock
26	1725	Odessa	66	3830	Darby
27	1478	Lind	67	7282	Deer Mt.
28	2372	Geiger	68	4245	Drummond
29	2000	Sprague	69	5900	Anaconda
30	2503	Willard	70	4800	Avon
31	4400	Coeur D'Alene	71	8852	Haystack
32	5330	Bald Mt	72	5554	Butte
33	4800	Mullan Path	73	3882	Helena
34	2900	Avery	74	4674	Whitehall
35	6800	Simmons Pk	75	4060	Three Fk
36	2700	St. Regis	76	3900	Townsend
37	2700	Round Butte	77	4750	Bozeman
38	3100	Nine-Mile	78	350	Peterson
39	5380	Williams	79	1493	Pendleton
40	3900	Condon	80	1650	Lexington

Table IV.C.1 (con't.)

Sta. No.	Elev.	Name
81	2713	LaGrange
82	2400	Elgin
83	3900	Paradise
84	3800	Enterprise
85	6888	Horse Mt
86	6925	Cold Springs
87	3295	Grangeville
88	7235	Green Mt.
89	5800	Dixie
90	5912	Warren
91	8154	Long Tom
92	4800	West Fk
93	8100	Anderson Mt
94	4045	Salmon
95	9500	Odell
96	6000	Grant
97	5238	Dillon
98	4985	Sportsmans
99	3200	Hardman
100	1500	Spray
101	2400	Dayville
102	3400	Ukiah
103	3900	Long Creek
104	3090	John Day
105	3350	Baker
106	3800	Ironside
107	2700	Richland
108	7000	Russel Mt
109	2120	Weiser
110	4860	Donnelly
111	6539	Stibnite
112	3000	Garden Valley
113	6500	Silva Ranch
114	5085	Challis
115	6000	Ima Mines
116	6114	Dell
117	6700	Chilly
118	6700	Lakeview
119	5123	Dubois
120	6654	West Yellowstone
121	5520	Anderson

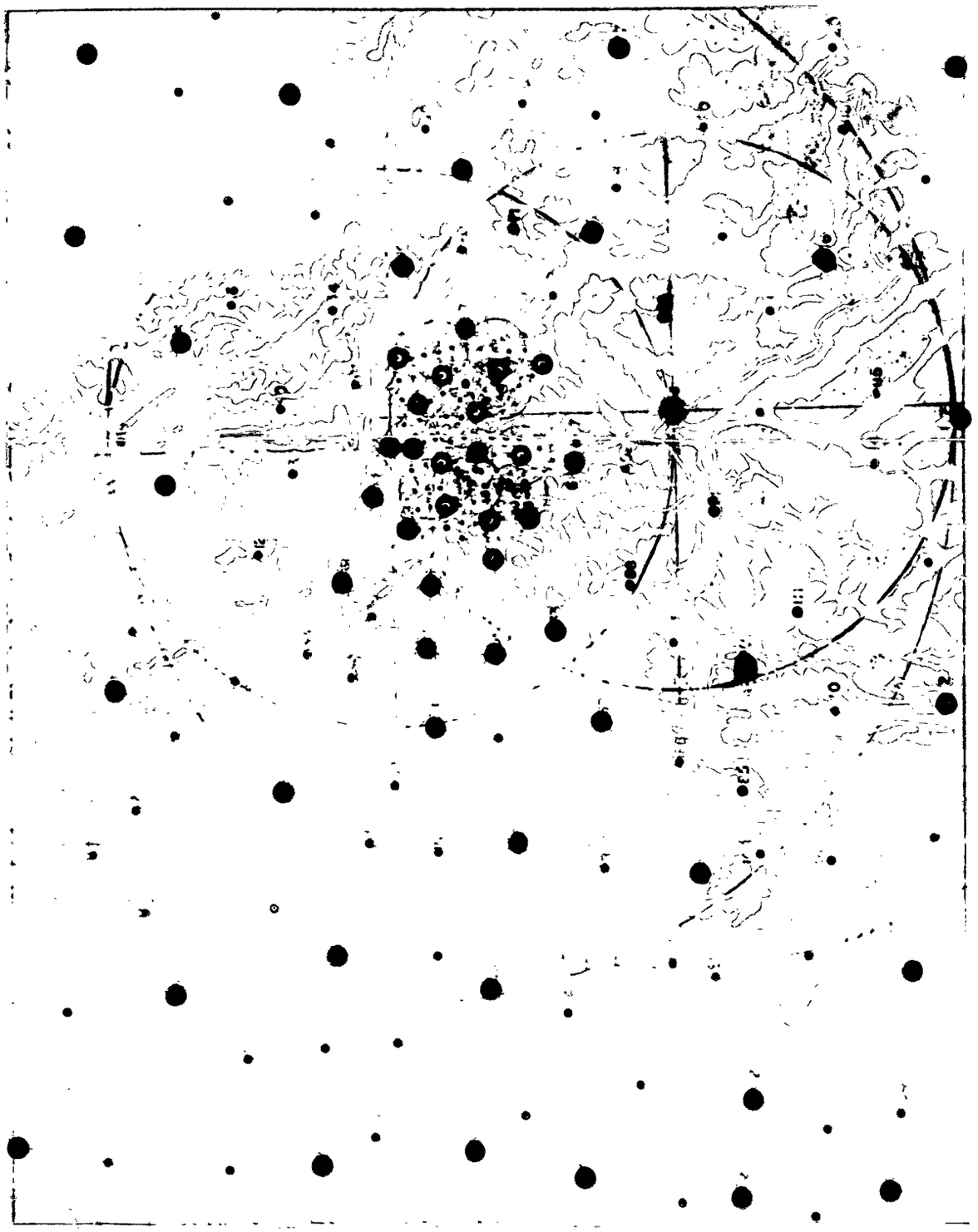

PROGRAM FOR NEXT QUARTER

Research during the next quarter will be performed in two phases. The first phase will consist of selecting case studies from the New Jersey and the Texas-Oklahoma area to be analysed in conjunction with the New Jersey Microbarograph Network and the specialized instrumentation that is to be installed and operated in the area of Cedar Hills, Texas. These data will be augmented as quickly as possible with surrounding data from the regular U. S. Weather Bureau synoptic network in both regions and from the Severe Local Storms Research Network in Texas, Oklahoma, and Kansas.

The second phase will consist of the completion of the previously selected cases in the areas of New Jersey, Utah, and Arizona.

PERSONNEL

Hours Worked by Project Personnel

Fujita	Principal Investigator	555	
Brown	Associate Director	680	
Omoto	Meteorologist	140	terminated 2/3/60
Osawa	Meteorologist	510	
Styber	Meteorologist	0	terminated 12/31/59
Auxer	Meteorological Aide	220	terminated 2/19/60
Bram	Meteorological Aide	190	began 1/4/60
Butterfield	Meteorological Aide	200	began 1/4/60
Geisel	Meteorological Aide	205	began 1/4/60
Kirwan	Meteorological Aide	160	
Ritz	Meteorological Aide	440	
Shaw	Meteorological Aide	360	began 1/18/60
Battino	Secretary	640	(nee Ridinger)

DISTRIBUTION LIST

Address	No. of Copies
Corps of Engineers Liaison Office, U. S. Army Signal Research & Development Laboratory, Fort Monmouth, New Jersey, ATTN: SIGRA/SL-LNF	1
ARDC Liaison Office, U. S. Army Signal Research & Development Laboratory, Fort Monmouth, New Jersey, ATTN: SIGRA/SL-LNA	1
U. S. Navy Electronics Liaison Office, U. S. Army Signal Research & Development Laboratory, Fort Monmouth, New Jersey, ATTN: SIGRA/SL-LNS	1
Marine Corps Liaison Office, U. S. Army Signal Research & Development Laboratory, Fort Monmouth, New Jersey, ATTN: SIGRA/SL-LNR	1
Commanding Officer, U. S. Army Signal Research & Development Laboratory, Fort Monmouth, New Jersey, ATTN: SIGRA/SL-DR	1
Commanding Officer, U. S. Army Signal Research & Development Laboratory, Fort Monmouth, New Jersey, ATTN: SIGRA/SL-ADT	1
Commanding Officer, U. S. Army Signal Research & Development Laboratory, Fort Monmouth, New Jersey, ATTN: SIGRA/SL-ADJ (Responsible File & Record Unit)	1
Commanding Officer, U. S. Army Signal Research & Development Laboratory, Fort Monmouth, New Jersey, ATTN: SIGRA/SL-TNR	5
Commanding Officer, U. S. Army Signal Research & Development Laboratory, Fort Monmouth, New Jersey, ATTN: SIGRA/SL-SMA	5
OASD (R&E), Rm 3E1065, The Pentagon, Washington 25, D. C., ATTN: Technical Library	1
Chief of Research and Development, OCS, Dept of the Army, Washington 25, D. C.	1
Chief Signal Officer, Department of the Army, Washington 25, D. C., ATTN: SIGRD	1

Address	No. of Copies
Director, U. S. Naval Research Laboratory, Washington 25, D. C., ATTN: Code 2027	1
Commanding Officer and Director, U. S. Navy Electronics Laboratory, San Diego, 52, California	1
Commander, Air Force Command & Control Development Division, Air Research & Development Command, USAF, ATTN: CROTL Laurence Hanscom Field, Bedford, Massachusetts	1
Commanding General, U. S. Army Electronic Proving Ground, Fort Huachuca, Arizona	1
Commander, Armed Services Technical Information Agency, Arlington Hall Station, Arlington 12, Virginia, ATTN: TIPDR	10
Chairman, U. S. Army Chemical Corps Meteorological Committee Ft. Detrick, Frederick, Maryland	1
Chief, Meteorology Division, U. S. Army Chemical Corps Proving Ground, Dugway Proving Ground, Utah	1
Chemical Research & Development Laboratories, Technical Library Army Chemical Center, Edgewood, Maryland	1
Director, Atmospheric Sciences Programs, National Science Foundation, Washington 25, D. C.	1
Director, Bureau of Research & Development, Federal Aviation Agency, Washington 25, D. C.	1
Chief, Fallout Studies Branch, Division of Biology and Medicine, Atomic Energy Commission, Washington 25, D. C.	1
Officer-in-Charge, Meteorological Curriculum, U. S. Naval Post Graduate School, Monterey, California	1
Chief of Naval Operations (OP 07), U. S. Navy Department, Washington 25, D. C.	1
Office of Naval Research, U. S. Navy Department, Washington 25, D. C.	1

Address	No. of Copies
Director, U. S. Naval Weather Service, U. S. Naval Station, Washington 25, D. C.	1
Officer-in-Charge, U. S. Naval Weather Research Facility, U. S. Naval Air Station, Bldg. R48, Norfolk, Virginia	1
U. S. Army Corps of Engineers, Snow, Ice and Permafrost Research Establishment, 1215 Washington Ave., Wilmette, Illinois	1
U. S. Army Corps of Engineers, Waterways Experiment Station, P. O. Box 631, Vicksburg, Mississippi	1
Office of the Chief of Ordinance, Department of the Army, Washington 25, D. C.	1
Commanding Officer, U. S. Army Signal Missile Support Agency White Sands Missile Range, New Mexico, ATTN: Missile Geophysics Division	1
Chief, West Coast Office, U. S. Army Research & Development Laboratory, 75 South Grand Ave., Bldg. 6, Pasadena 2, California	1
The University of Texas, Electrical Engineering Research Laboratory, Austin, Texas, ATTN: Mr. Gerhardt	1
American Meteorological Society, 45 Beacon Street, Boston 8, Massachusetts, ATTN: Mr. K. Spengler	1
Commanding Officer, U. S. Army Signal Materiel Support Agency Fort Monmouth, New Jersey, ATTN: SIGFM/ES-ADJ	1
Commander, WADD (WCOSI-3), Wright-Patterson Air Force Base, Ohio	2
Commander, Rome Air Development Center, Air Research and Development Command, Griffiss Air Force Base, New York, ATTN: RCSSLD	1
Commander, Air Force Command & Control Development Division, Air Research & Development Command, USAF, ATTN: CRZC, Dr. M. R. Nagel, Laurence Hanscom Field, Bedford, Massachusetts	1

Address	No. of Copies
Chief, Bureau of Naval Weapons (FAME), U. S. Navy Department, Washington 25, D. C.	1
U. S. Naval Research Laboratory (Code 7110), Washington 25, D. C.	1
Chief, Aerophysics Branch, Aeroballistics Laboratory, Army Ballistic Missile Agency, Redstone Arsenal, Alabama	1

AD________________ Accession No.________

THE UNIVERSITY OF CHICAGO DEPARTMENT OF METEOROLOGY

Design of a Three-Dimensional Meso-Meteorological Network--Tetsuya Fujita and Henry A. Brown

Quarterly Report #4, 1 January 1960 to 30 April 1960, 63 pp., 60 illustrations

Contract Nr. DA-36-039 SC-78901 DA Project Nr. 3A99-07-001-04-01--UNCLASSIFIED

Results of analyses of case studies of numerous networks in various locations are combined in a discussion of the observations necessary for the operation of a three-dimensional meso-meteorological network. Four observational categories are considered: (1) surface, (2) upper air, (3) radar, and (4) photography. Each category is discussed in terms of the elements measured, optimum time and space resolution, accuracy required, and techniques for analysis.

A model network design incorporating the above results is then proposed. This is followed by a proposed practical design for three different areas in the United States characterized by coastal, plains, and mountainous environments.

UNCLASSIFIED

1. Mesometeorology
2. Network Analysis
3. Network Design
4. SC Contract DA-36-039 SC-78901

AD________________ Accession No.________

THE UNIVERSITY OF CHICAGO DEPARTMENT OF METEOROLOGY

Design of a Three-Dimensional Meso-Meteorological Network--Tetsuya Fujita and Henry A. Brown

Quarterly Report #4, 1 January 1960 to 30 April 1960, 63 pp., 60 illustrations

Contract Nr. DA-36-039 SC-78901 DA Project Nr. 3A99-07-001-04-01--UNCLASSIFIED

Results of analyses of case studies of numerous networks in various locations are combined in a discussion of the observations necessary for the operation of a three-dimensional meso-meteorological network. Four observational categories are considered: (1) surface, (2) upper air, (3) radar, and (4) photography. Each category is discussed in terms of the elements measured, optimum time and space resolution, accuracy required, and techniques for analysis.

A model network design incorporating the above results is then proposed. This is followed by a proposed practical design for three different areas in the United States characterized by coastal, plains, and mountainous environments.

UNCLASSIFIED

1. Mesometeorology
2. Network Analysis
3. Network Design
4. SC Contract DA-36-039 SC-78901

AD________________ Accession No.________

THE UNIVERSITY OF CHICAGO DEPARTMENT OF METEOROLOGY

Design of a Three-Dimensional Meso-Meteorological Network--Tetsuya Fujita and Henry A. Brown

Quarterly Report #4, 1 January 1960 to 30 April 1960, 63 pp., 60 illustrations

Contract Nr. DA-36-039 SC-78901 DA Project Nr. 3A99-07-001-04-01--UNCLASSIFIED

Results of analyses of case studies of numerous networks in various locations are combined in a discussion of the observations necessary for the operation of a three-dimensional meso-meteorological network. Four observational categories are considered: (1) surface, (2) upper air, (3) radar, and (4) photography. Each category is discussed in terms of the elements measured, optimum time and space resolution, accuracy required, and techniques for analysis.

A model network design incorporating the above results is then proposed. This is followed by a proposed practical design for three different areas in the United States characterized by coastal, plains, and mountainous environments.

UNCLASSIFIED

1. Mesometeorology
2. Network Analysis
3. Network Design
4. SC Contract DA-36-039 SC-78901

AD________________ Accession No.________

THE UNIVERSITY OF CHICAGO DEPARTMENT OF METEOROLOGY

Design of a Three-Dimensional Meso-Meteorological Network--Tetsuya Fujita and Henry A. Brown

Quarterly Report #4, 1 January 1960 to 30 April 1960, 63 pp., 60 illustrations

Contract Nr. DA-36-039 SC-78901 DA Project Nr. 3A99-07-001-04-01--UNCLASSIFIED

Results of analyses of case studies of numerous networks in various locations are combined in a discussion of the observations necessary for the operation of a three-dimensional meso-meteorological network. Four observational categories are considered: (1) surface, (2) upper air, (3) radar, and (4) photography. Each category is discussed in terms of the elements measured, optimum time and space resolution, accuracy required, and techniques for analysis.

A model network design incorporating the above results is then proposed. This is followed by a proposed practical design for three different areas in the United States characterized by coastal, plains, and mountainous environments.

UNCLASSIFIED

1. Mesometeorology
2. Network Analysis
3. Network Design
4. SC Contract DA-36-039 SC-78901